Synthesis of Modular and Pipelineable Wave Digital Filters

by

Victor Wai Tak Cheng

A Thesis
Presented to the Faculty of Graduate Studies
in Partial Fulfillment of the Requirements
for the Degree

MASTER OF SCIENCE

Department of Electrical and Computer Engineering
University of Manitoba
Winnipeg, Manitoba

ISBN 0-315-78055-X

Canada

SYNTHESIS OF MODULAR AND PIPELINEABLE WAVE DIGITAL FILTERS

BY

VICTOR WAI TAK CHENG

A Thesis submitted to the Faculty of Graduate Studies of the University of Manitoba in partial fulfillment of the requirements for the degree of

MASTER OF SCIENCE

I hereby declare that I am the sole author of this thesis.

I authorize the University of Manitoba to lend this thesis to other institutions or individuals for the purpose of scholarly research.

Victor W. T. Cheng

I further authorize the University of Manitoba to reporduce this thesis by photocopying or by other means, in total or in part, at the request of other institutions or individuals for the purpose of scholarly research.

Victor W. T. Cheng

ABSTRACT

Two simple decomposition algorithms are presented for the synthesis of modular, pipelineable, complex wave (unitary) digital filters (CWDFs), namely the PU synthesis algorithm and the cascade synthesis algorithm. The main features of the PU synthesis algorithm are the following:

1. The PU structure has built-in pipelineability;
2. Requires only six basic rotations per order of the filter;
3. Requires only one basic building block, which makes the overall structure modular and easy to implement.

For the pipelineable cascade algorithm, the main features are the following:

1. The extraction step obviates coefficient-form polynomial arithmetic and zero-finding operations by using an alternative (sample) representation of the canonic polynomials that describe the lossless two-port - an idea that was first introduced for real two-ports in [13];
2. First-order sections that effect pipelineability are treated like any other section (they realize a transmission zero at $z^{-1} = 0$), thus eliminating the need for special treatment;
3. A fully general 1st-order complex section is derived that can realize a "transmission zero" anywhere in the z-plane and is the only section required for the cascade decomposition. It requires six basic rotations per order.
4. Each transmission zero in the cascade realization can be fine tuned individually because each cascade section realizes a distinct transmission zero.
5. This algorithm can also be used to synthesize real two-port networks; equivalences are given between a cascade of two complex sections with $ke^{\pm j\omega_0}$ transmission zeros and a 2nd-order real section.

A method to obtain the frequency response for investigation of coefficient quantization effects directly in the z-domain is given for both structures and the merits of each synthesis algorithm are discussed.

ACKNOWLEDGMENTS

The author wishes to express his sincere appreciation to Professor G.O. Martens for his always-available, and ever-helpful guidance throughout the course of this work. Also special thanks to M.R. Jarmasz for his untiring, ever-patient discussions on most of the theory and programming work related to this thesis, and the proof reading of it. Many helpful discussions with G. Scarth are also appreciated.

Special thanks to the author's parents, family and friends for their support.

TABLE OF CONTENTS

CHAPTER I

INTRODUCTION

Digital filters have advantages compared to analog filters because they are easily reprogrammed, their responses are not affected by temperature variations and aging, and they can be readily implemented using cost-effective digital signal processors (DSPs). Due to the steady technological advances in the signal processor design, what used to be an unbridgeable gap in the computational efficiencies of real and complex digital circuits has largely disappeared over the years. The criteria used in evaluating the various digital circuits have also changed. The total number of multiplications and delays, and the maximum bits allowed for multiplier quantization are no longer as critical as, for example, pipelineability [18][25] (different instances of the algorithm are executed simultaneously), or modularity, having only one basic building block repeated throughout the structure. Other important properties such as numerical robustness, availability of a simple schemes that ensure nonlinear stability, and low-passband-sensitivity circuits can be carried over to the complex-domain as long as the resulting circuit is internally passive [17], i.e., it is a complex wave digital (CWD) circuit.

Acha and Torres [16] realize a complex transfer function as the reflectance of a lossless two-port with the restriction that all the attenuation zeros must be located on the unit circle; otherwise, the reflectance must be scaled with a passive multiplier to force a reflection one on the unit-circle. In this thesis, we present two CWD structures that are modular, pipelineable, and have no restrictions on the location of either the transmission or attenuation zeros.

The first CWD structure is the pipelineable, complex, lossless (unitary), two-port network that will be referred to as the pipelinable unitary (PU) structure. The derivation of the circuit is based on iteratively interchanging the h and f polynomials [9]. The synthesis algorithm for real two-port networks was first introduced by Rao and Kailath [10] and modified by Fettweis [9] using a network theory approach. We extend this to the complex two-port networks using only one additional two-port element, the unimodular multiplier section. Three forms of polynomial representation can be used in the synthesis algorithm, namely the coefficient-form, DFT-form, and the zero-form, with the second one being the easiest to implementation. A unitary 1st-order complex circuit was derived using the PU structure that can realize a transmission zero anywhere

in the z-plane and consists of only six real planar rotations and two real delays. This section is derived such that one of the unimodular multiplier is used to directly control the location of the unit-circle transmission zero. It is used as the basic building block in the second CWD structure.

The second CWD structure is the cascade (chain) decomposition of complex two-ports. Again, there are no restrictions on the location of either the transmission or attenuation zeros, and the designer has the option of having a given (real or complex) transfer function realized as a transmittance or a reflectance of a lossless and internally-passive two-port. To make the decomposition algorithm very simple and easy to program, we make use of an observation from the real two-port decomposition [13] and the PU structure above that a noncanonic (called sample) representation of the polynomials is used. This eliminates the need for handling either coefficient or zero-form polynomials, thus avoiding the explicit derivation of order-reduced remainder polynomials. In contrast to real circuits, the lossless complex cascade require only one elementary section, which leads to a very modular configuration.

Although the development is entirely in the z-domain, we chose to use terms and concepts from the classical scattering domain for the simple reason that all the analytic properties of scattering coefficients (such as passivity of the reflection coefficient [5], reflection-free ports [1], etc.) can be carried over to the z-domain. Because the resulting CWD filters are internally passive, one can always derive an equivalent analog circuit, although such a circuit may have little practical value and its implementation maybe difficult.

CHAPTER II

ANALOG AND DIGITAL COMPLEX LOSSLESS TWO-PORT NETWORKS

This chapter presents the basic building blocks for the decomposition of complex lossless two-port networks together with their analog equivalents. We will also discuss the characterization of lossless two-port networks using scattering parameters.

2.1 Characterization of Analog and Digital Two-Port Networks

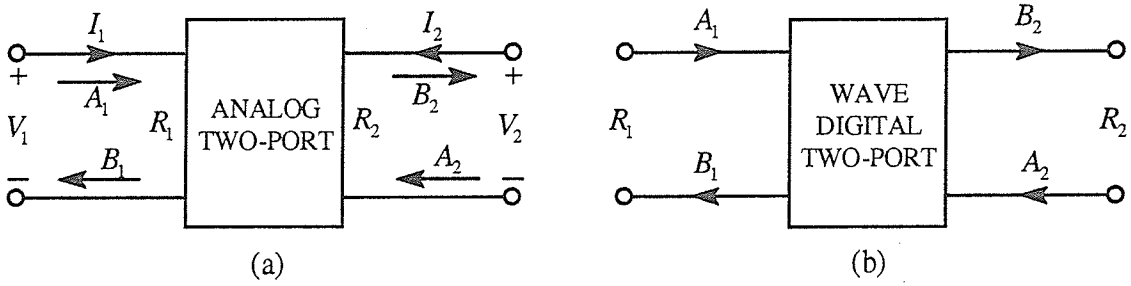

Figure 2.1 Analog and Digital two-port network.

Consider the two-port network shown in Fig. 2.1a; we can characterize the two-port using the chain (transmission) matrix:

$$\begin{bmatrix} V_1 \\ I_1 \end{bmatrix} = \mathbf{K} \begin{bmatrix} V_2 \\ -I_2 \end{bmatrix} \tag{2.1}$$

Alternatively, a two-port can be characterized using scattering variables, i.e., for each port i, the incident and reflected voltage waves are defined by [1]

$$A_i = V_i + R_i I_i \quad , \quad B_i = V_i - R_i I_i \tag{2.2}$$

respectively, where R_i is an arbitrary positive port reference. From Eq. (2.1) and Eq. (2.2), we can write

$$\begin{bmatrix} B_1 \\ A_1 \end{bmatrix} = \begin{bmatrix} 1 & -R_1 \\ 1 & R_1 \end{bmatrix} \begin{bmatrix} V_1 \\ I_1 \end{bmatrix} = \begin{bmatrix} 1 & -R_1 \\ 1 & R_1 \end{bmatrix} \mathbf{K} \begin{bmatrix} V_2 \\ -I_2 \end{bmatrix}$$
$$= \begin{bmatrix} 1 & -R_1 \\ 1 & R_1 \end{bmatrix} \mathbf{K} \frac{1}{2R_2} \begin{bmatrix} R_2 & R_2 \\ -1 & 1 \end{bmatrix} \begin{bmatrix} 1 & -R_2 \\ 1 & R_2 \end{bmatrix} \begin{bmatrix} V_2 \\ -I_2 \end{bmatrix}$$
$$= \begin{bmatrix} 1 & -R_1 \\ 1 & R_1 \end{bmatrix} \mathbf{K} \frac{1}{2R_2} \begin{bmatrix} R_2 & R_2 \\ -1 & 1 \end{bmatrix} \begin{bmatrix} A_2 \\ B_2 \end{bmatrix} \tag{2.3}$$

Eq. (2.3) defines the scattering transfer matrix for the two-port network in Fig. 2.1a, which is

$$\begin{bmatrix} B_1 \\ A_1 \end{bmatrix} = \mathbf{T} \begin{bmatrix} A_2 \\ B_2 \end{bmatrix} \quad \text{where} \quad \mathbf{T} = \begin{bmatrix} 1 & -R_1 \\ 1 & R_1 \end{bmatrix} \mathbf{K} \frac{1}{2R_2} \begin{bmatrix} R_2 & R_2 \\ -1 & 1 \end{bmatrix} \tag{2.4}$$

For normalized two-port networks, we have $R_1 = R_2 = 1$. It follows that the chain and transfer matrices are related by a similarity transformation:

$$\mathbf{T} = \mathbf{PKP}^{-1} \qquad \text{where} \quad \mathbf{P} = \begin{bmatrix} 1 & -1 \\ 1 & 1 \end{bmatrix} \tag{2.5}$$

An alternative grouping of the scattering variables is given below [3]

$$\begin{bmatrix} B_1 \\ B_2 \end{bmatrix} = \begin{bmatrix} S_{11} & S_{12} \\ S_{21} & S_{22} \end{bmatrix} \begin{bmatrix} A_1 \\ A_2 \end{bmatrix} = \frac{1}{T_{22}} \begin{bmatrix} T_{12} & T_{11}T_{12} - T_{12}T_{21} \\ 1 & -T_{21} \end{bmatrix} \begin{bmatrix} A_1 \\ A_2 \end{bmatrix} = \mathbf{S} \begin{bmatrix} A_1 \\ A_2 \end{bmatrix} \tag{2.6a}$$

$$\begin{bmatrix} B_1 \\ A_1 \end{bmatrix} = \begin{bmatrix} T_{11} & T_{12} \\ T_{21} & T_{22} \end{bmatrix} \begin{bmatrix} A_2 \\ B_2 \end{bmatrix} = \frac{1}{S_{21}} \begin{bmatrix} S_{12}S_{21} - S_{11}S_{12} & S_{11} \\ S_{22} & 1 \end{bmatrix} \begin{bmatrix} A_2 \\ B_2 \end{bmatrix} = \mathbf{T} \begin{bmatrix} A_2 \\ B_2 \end{bmatrix} \tag{2.6b}$$

where S is the scattering matrix [5].

A class of digital filters was introduced by Fettweis [1], called wave digital filters (WDFs), which has the same analytic properties (internal passivity) as analog filters. The term "wave" refers to the fact that, instead of voltage and current variables, incident and reflected wave quantities (see Eq. (2.2)) must be used to ensure computability (i.e. no delay-free loops). A wave digital two-port that corresponds to an analog two-port is shown in Fig. 2.1b.

2.2 The 2-port Adaptor – a Wave Digital Equivalent of an Ideal Transformer

In this section, we will derive the Wave Digital equivalent of an ideal transformer – the most basic and widely used zeroth-order two-port. An adaptor is the WD equivalent of an analog multi-port network which does not store or dissipate energy. Its main purpose is to ensure that Kirchhoff's voltage and current laws, as transcribed to the scattering domain, hold in WD domain. An ideal transformer and its chain matrix are shown in Fig. 2.2.

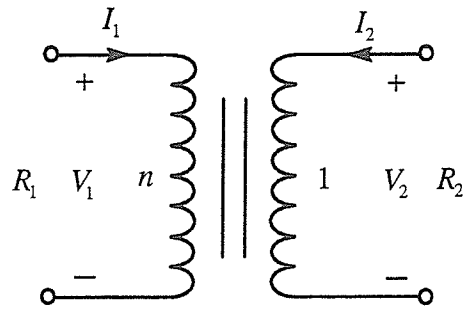

$$\begin{bmatrix} V_1 \\ I_1 \end{bmatrix} = \begin{bmatrix} n & 0 \\ 0 & 1/n \end{bmatrix} \begin{bmatrix} V_2 \\ -I_2 \end{bmatrix} = \mathbf{K} \begin{bmatrix} V_2 \\ -I_2 \end{bmatrix}$$

Figure 2.2 An ideal transformer and its chain matrix **K**.

From Eq. (2.4) and Eq. (2.6a), the corresponding voltage wave scattering and transfer matrices for the general port references R_1 and R_2 in Fig. 2.2 are given by

$$\begin{bmatrix} B_1 \\ A_1 \end{bmatrix} = \frac{1}{2n} \begin{bmatrix} n^2 + R_1/R_2 & n^2 - R_1/R_2 \\ n^2 - R_1/R_2 & n^2 + R_1/R_2 \end{bmatrix} \begin{bmatrix} A_2 \\ B_2 \end{bmatrix} = \mathbf{T} \begin{bmatrix} A_2 \\ B_2 \end{bmatrix} \tag{2.7a}$$

$$\begin{bmatrix} B_1 \\ B_2 \end{bmatrix} = \frac{1}{n^2 + R_1/R_2} \begin{bmatrix} n^2 - R_1/R_2 & 2nR_1/R_2 \\ 2n & R_1/R_2 - n^2 \end{bmatrix} \begin{bmatrix} A_1 \\ A_2 \end{bmatrix} = \mathbf{S} \begin{bmatrix} A_1 \\ A_2 \end{bmatrix} \tag{2.7b}$$

There are three cases of Eq. (2.7) that are of interest to us, which are shown in Table 2.1. The case $n = 1$ is simply an interconnection of 2 ports with different port references, R_1 and R_2, and the WD image is defined as the voltage wave 2-port adaptor. The second case, $R_1 = R_2 = 1$, defines the WD translation of the ideal transformer using power waves (normalized voltage waves), which is known as the normalized 2-port adaptor. Looking at the scattering and transfer matrices from Table 2.1, and by letting $\gamma = \cos\theta$ (i.e. $n^2 = R_2/R_1$), we can also write [3]

$$\mathbf{S}_\theta = \mathbf{P}^{-1}\mathbf{S}_\gamma\mathbf{P} \quad , \qquad \mathbf{T}_\theta = \mathbf{T}_\gamma\mathbf{T}_n = \mathbf{T}_n\mathbf{T}_\gamma \tag{2.8}$$

i.e., a normalized 2-port adaptor is equivalent to a voltage wave 2-port adaptor cascaded with a pair of inverse scaling multipliers. This is shown in Fig. 2.3.

Cases:	Scattering and Transfer Matrix	Symbolic representation & flowgraphs
$n=1$	2-port adaptor: $\mathbf{S}_\gamma=\begin{bmatrix}-\gamma & 1+\gamma\\ 1-\gamma & \gamma\end{bmatrix}$, $\mathbf{T}_\gamma=\frac{1}{1-\gamma}\begin{bmatrix}1 & -\gamma\\ -\gamma & 1\end{bmatrix}$ where $\gamma:=\frac{R_1-R_2}{R_1+R_2}$	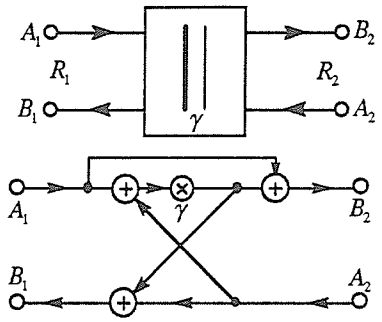
$R_1=R_2=1$	normalized 2-port adaptor: $\mathbf{S}_\theta=\begin{bmatrix}-\cos\theta & \sin\theta\\ \sin\theta & \cos\theta\end{bmatrix}$, $\mathbf{T}_\theta=\frac{1}{\sin\theta}\begin{bmatrix}1 & -\cos\theta\\ -\cos\theta & 1\end{bmatrix}$ where $\cos\theta=\frac{1-n^2}{1+n^2}$, $\sin\theta=\frac{2n}{1+n^2}$ $\Rightarrow$ $n=\tan\left(\frac{\theta}{2}\right)$	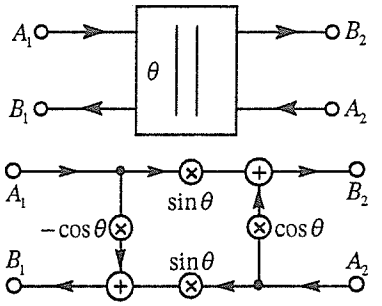
$n^2=\frac{R_1}{R_2}$	scaling multipliers: $\mathbf{S}_n=\begin{bmatrix}0 & n\\ 1/n & 0\end{bmatrix}=\mathbf{P}^{-1}\begin{bmatrix}0 & 1\\ 1 & 0\end{bmatrix}\mathbf{P}$, $\mathbf{P}=\begin{bmatrix}1 & 0\\ 0 & n\end{bmatrix}$, $\mathbf{T}_n=n\begin{bmatrix}1 & 0\\ 0 & 1\end{bmatrix}$	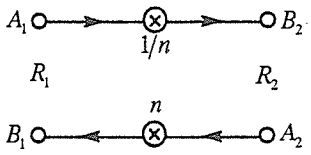

Table 2.1 Three special cases for the digital equivalent of an ideal transformer.

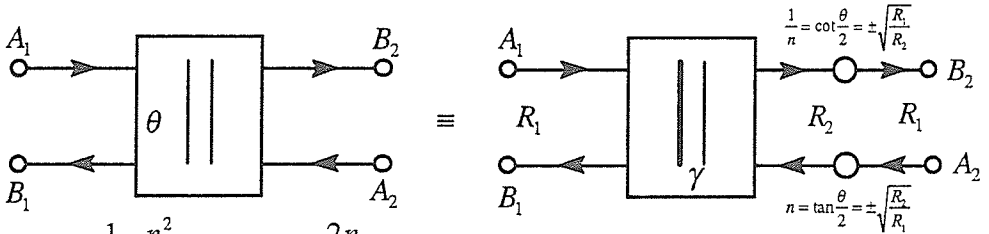

$$\cos\theta=\frac{1-n^2}{1+n^2}\ ,\ \sin\theta=\frac{2n}{1+n^2}$$

$$\Rightarrow\ n=\tan\left(\frac{\theta}{2}\right)$$

$$\gamma=\cos\theta=\frac{R_1-R_2}{R_1+R_2}$$

Figure 2.3 An equivalence between a normalized 2-port adaptor and a 2-port adaptor cascaded with a pair of inverse scaling multipliers.

Another zeroth-order two-port that is of interest is the gyrator, which is shown in Fig. 2.4 together with its WD equivalent. Again, using the chain matrix in Fig. 2.4, together with Eq. (2.4) and Eq. (2.6a), the corresponding voltage wave scattering and transfer matrices for the general port references R_1 and R_2 for the gyrator are given by

$$\begin{bmatrix} B_1 \\ A_1 \end{bmatrix} = \frac{1}{2RR_2}\begin{bmatrix} -(R_1R_2+R^2) & -(R_1R_2-R^2) \\ R_1R_2-R^2 & R_1R_2+R^2 \end{bmatrix}\begin{bmatrix} A_2 \\ B_2 \end{bmatrix} = \mathbf{T}\begin{bmatrix} A_2 \\ B_2 \end{bmatrix} \tag{2.9a}$$

$$\begin{bmatrix} B_1 \\ B_2 \end{bmatrix} = \frac{1}{R_1R_2+R^2}\begin{bmatrix} -(R_1R_2-R^2) & -2RR_2 \\ 2RR_2 & -(R_1R_2-R^2) \end{bmatrix}\begin{bmatrix} A_1 \\ A_2 \end{bmatrix} = \mathbf{S}\begin{bmatrix} A_1 \\ A_2 \end{bmatrix} \tag{2.9b}$$

For normalized case, we have $R_1 = R_2 = 1$, Eq. (2.9) reduces to the scattering and transfer matrices in Fig. 2.4.

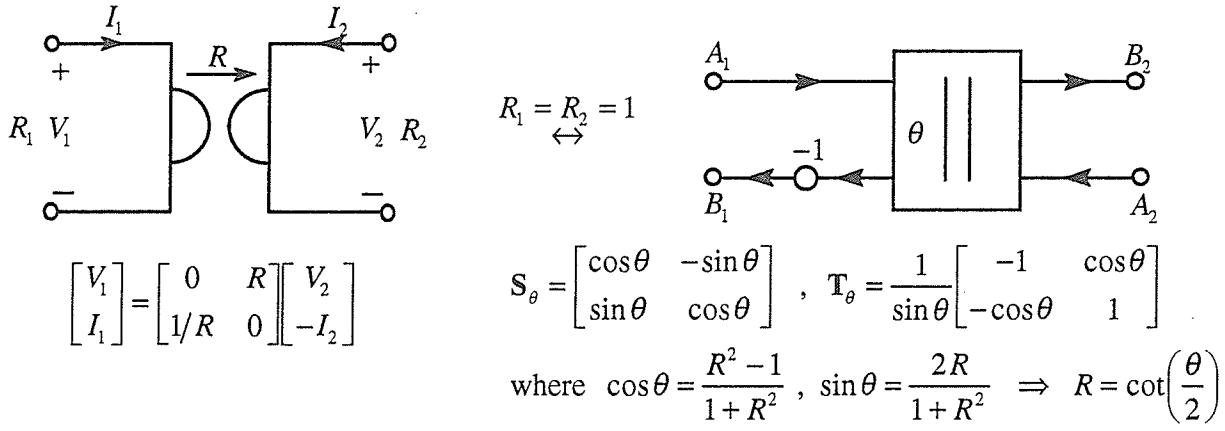

Figure 2.4 A gyrator and its WD image

We can see that the flowgraph of the gyrator is essentially the same as that of the ideal transformer except for the negation of B_1 in Fig. 2.4, and is equivalent to the rotation operator, also known as the Givens rotator [2].

For 2-port adaptors, we choose to label the rotation angle on port one. However, different orientation for the 2-port adaptor may be needed for convenience. Fig. 2.5 and Fig. 2.6 [3] show some of the equivalences between normalized 2-port adaptors.

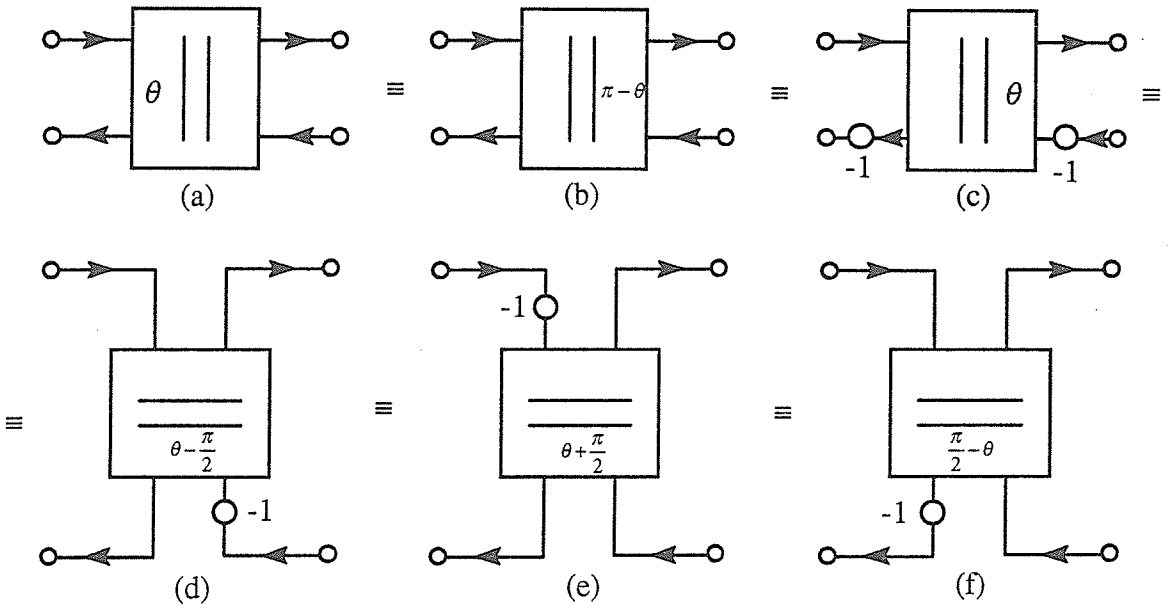

Figure 2.5 Normalized 2-port adaptor equivalences.

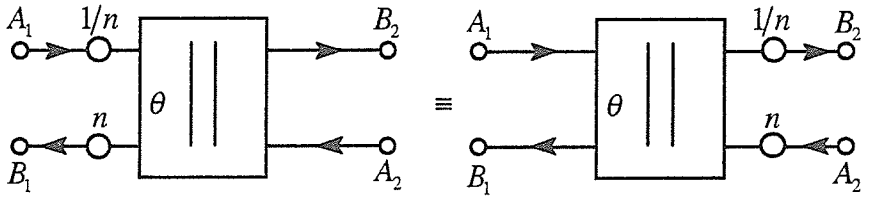

Figure 2.6 Shifting a pair of scaling multipliers through a normalized 2-port adaptor (n can be complex).

2.3 The unimodular multiplier section and its analog equivalent

The only additional two-port element that is required in extending real two-port networks to complex two-port is the unimodular multiplier element [4][2], as shown in Fig. 2.7. Here, we derive its analog equivalent in order to show that we are still dealing with WD circuits, i.e., the unimodular multiplier element has an analog equivalent circuit.

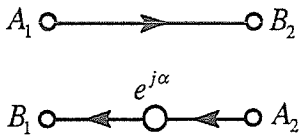

$$\mathbf{S}=\begin{bmatrix}0 & e^{j\alpha}\\ 1 & 0\end{bmatrix}\quad,\quad \mathbf{T}=\begin{bmatrix}e^{j\alpha} & 0\\ 0 & 1\end{bmatrix}$$

Figure 2.7 Unimodular multiplier section with its scattering and transfer matrices.

One approach is to obtain from the scattering matrix the corresponding two-port admittance parameters. Using the relation $\mathbf{Y}=2(\mathbf{I}+\mathbf{S})^{-1}-\mathbf{I}$, where $\mathbf{I}$ is the unit matrix, we obtain

$$\mathbf{Y}=\begin{bmatrix} j\cot\frac{\alpha}{2} & 1-j\cot\frac{\alpha}{2}\\ -1-j\cot\frac{\alpha}{2} & j\cot\frac{\alpha}{2}\end{bmatrix}=\begin{bmatrix} j\cot\frac{\alpha}{2} & -j\cot\frac{\alpha}{2}\\ -j\cot\frac{\alpha}{2} & j\cot\frac{\alpha}{2}\end{bmatrix}+\begin{bmatrix}0 & 1\\ -1 & 0\end{bmatrix}=\mathbf{Y}_1+\mathbf{Y}_2\quad,\quad \begin{bmatrix}I_1\\ I_2\end{bmatrix}=\mathbf{Y}\begin{bmatrix}V_1\\ V_2\end{bmatrix} \tag{2.10}$$

which is expressed as the sum of two admittance matrices, $\mathbf{Y}_1$ and $\mathbf{Y}_2$. These two admittance matrices correspond to a series connection of an imaginary resistance($\mathbf{Y}_1$) and a gyrator with $R=1(\mathbf{Y}_2)$ respectively, as shown in Fig. 2.8.

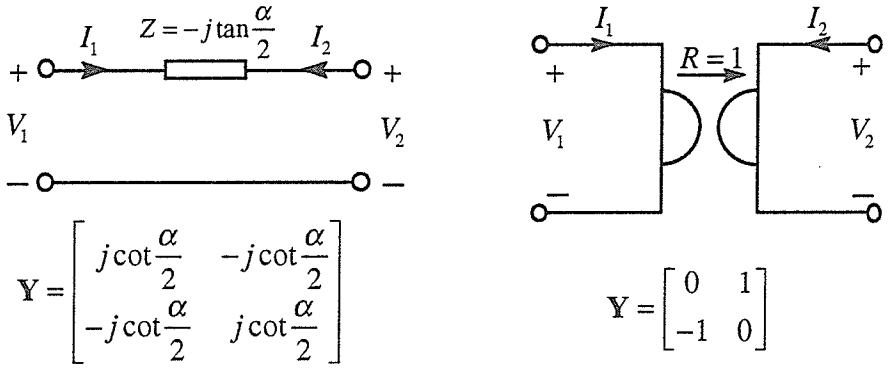

Figure 2.8 Admittance matrices for the imaginary resistance and the gyrator ($R=1$).

Therefore, the normalized unimodular multiplier section in Fig. 2.7 has an analog equivalence as shown in Fig. 2.9.

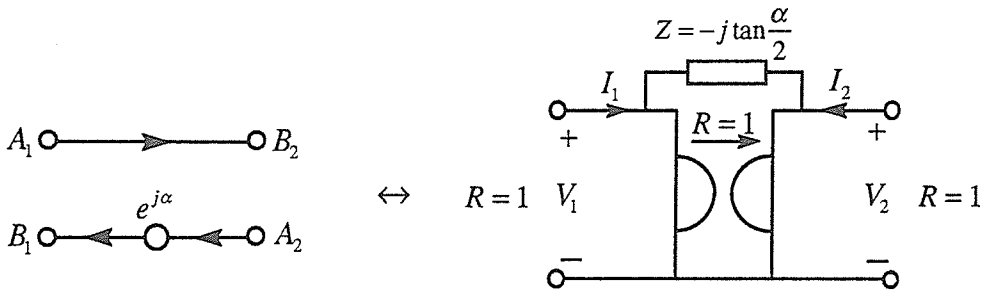

Figure 2.9 Unimodular multiplier section and its analog equivalence

If port #2 for the unimodular multiplier section is open-circuited (i.e. $A_2 = B_2$; $I_2 = 0$), the corresponding WD one-port terminator and its analog equivalent is shown in Fig. 2.10.

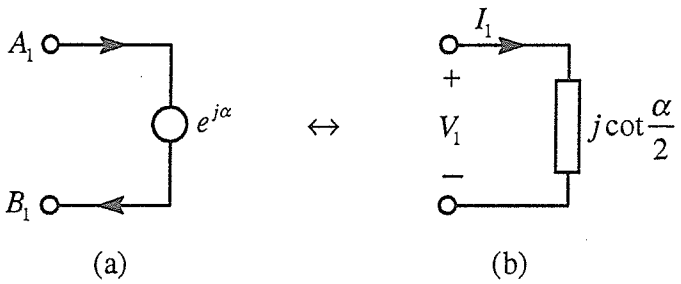

Figure 2.10 (a) One-port termination of an unimodular multiplier section with port #2 open-circuited; (b) its analog equivalent.

2.4 One-Port Dynamic Terminations

In this section, we derive a number of one-port terminations which are used in the synthesis process. Consider a section of uniform lossless transmission line with characteristic impedance R and a one-way delay of $\tau = T/2$ seconds, where T can be associated with the sampling frequency, as shown in Fig. 2.11 together with its wave digital image [1] [3]. The analog circuit in Fig. 2.11a is referred to as the unit element (UE).

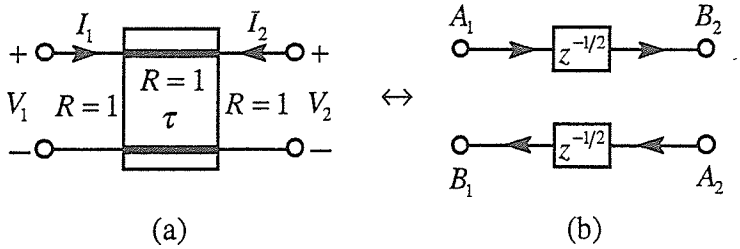

Figure 2.11 (a) Unit element; (b) its wave digital image.

The chain matrix for this section is given by

$$\begin{bmatrix} V_1 \\ I_1 \end{bmatrix} = \begin{bmatrix} \cosh(sT/2) & \sinh(sT/2) \\ \sinh(sT/2) & \cosh(sT/2) \end{bmatrix} \begin{bmatrix} V_2 \\ -I_2 \end{bmatrix} = \mathbf{K} \begin{bmatrix} V_2 \\ -I_2 \end{bmatrix} \tag{2.11}$$

Using the mapping $z = e^{sT}$, we obtain the WD equivalent as shown in Fig. 2.11b. To derive all the necessary one-port dynamic terminations that we are going to use in the following chapters, we terminate port #2 of Fig. 2.11a with an imaginary resistance of $j\cot(\alpha/2)$ (see Fig. 2.10b) as shown in Fig. 2.12a.

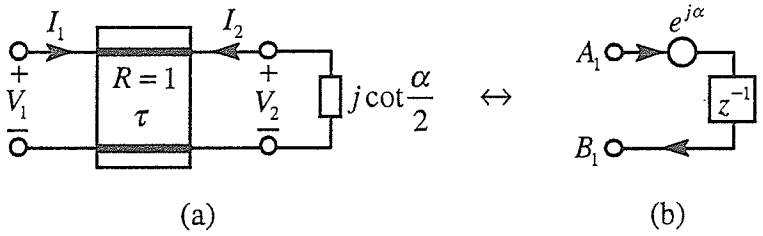

Figure 2.12 A one-port dynamic termination: (a) analog circuit; and (b) its WD equivalent.

From Eq. (2.11), the driving point impedance is given by

$$\frac{V_1}{I_1} = \frac{\cosh\left(s\frac{T}{2}\right)\frac{V_2}{-I_2} + \sinh\left(s\frac{T}{2}\right)}{\sinh\left(s\frac{T}{2}\right)\frac{V_2}{-I_2} + \cosh\left(s\frac{T}{2}\right)} \qquad \text{and} \qquad \frac{V_2}{-I_2} = j\cot\left(\frac{\alpha}{2}\right) \tag{2.12}$$

In the scattering domain, the corresponding reflection coefficient is given by

$$\frac{B_1}{A_1} = \frac{V_1/I_1 - 1}{V_1/I_1 + 1} = z^{-1}e^{j\alpha} \qquad \text{where} \qquad z = e^{sT} \tag{2.13}$$

The corresponding wave-flow diagram follows easily from Eq. (2.13) and is shown in Fig. 2.12b.

There are two special cases of interest for the circuit in Fig. 2.12a; viz. $\alpha = 0$ and $\alpha = \pi$. Using the complex frequency variable mapping defined by

$$\psi = \tanh\left(\frac{sT}{2}\right) = \frac{e^{sT}-1}{e^{sT}+1} = \frac{z-1}{z+1} \quad , \quad \tau = \frac{T}{2} \quad , \quad z = e^{sT} \tag{2.14}$$

where ψ is referred to as Richard's variable [6], the one-port complex dynamic termination reduces to two real cases, which also have lumped element equivalents, as shown in Fig. 2.13.

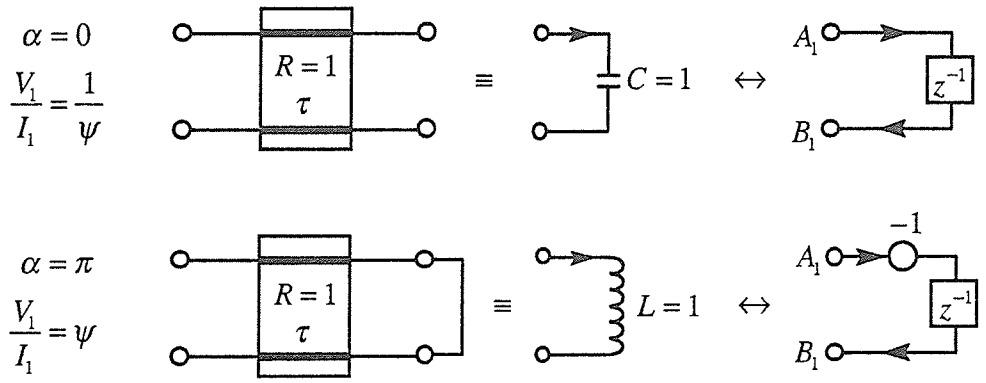

Figure 2.13 Real one-port dynamic terminations.

A two-port that is closely related to the UE is the quasi-reciprocal line (QUARL), which does not have the same delay in both transfer directions. However, the sum of the constant group delays is the same in the transmittance. Fig. 2.14 shows two instances of a QUARL which are of importance for wave digital filters.

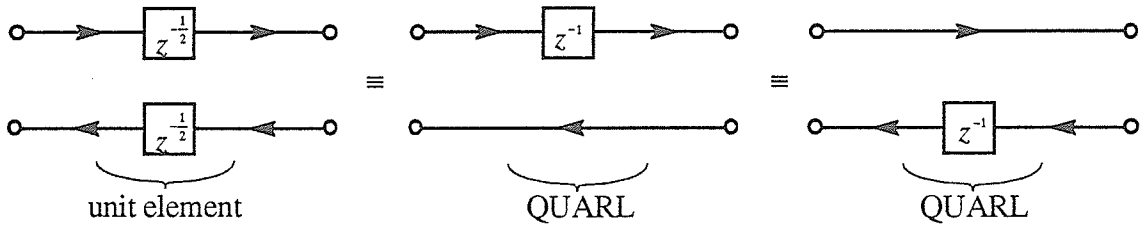

Figure 2.14 Unit element and two instances of a QUARL that are equivalent to within a constant group delay in the transmittance.

Two other important one-port terminations are the resistive load and a voltage source in series with a resistor. Using Eq. (2.2), we can derive the WD images as shown in Fig. 2.15.

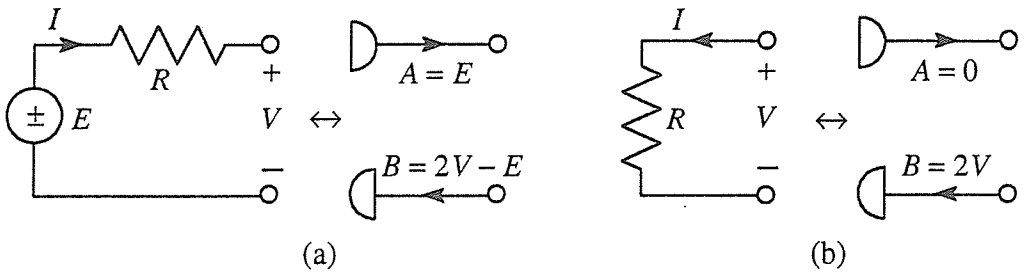

Figure 2.15 Resistive one-port terminations and their WD images.

2.5 Belevitch's Representation of Lossless Two-Port Networks

The usual approach to characterize a lossless two-port network with port references R_1 and R_2, as shown in Fig. 2.16a, is to use normalized scattering variables

$$A_i = \frac{V_i + R_i I_i}{2\sqrt{R_i}} \qquad B_i = \frac{V_i - R_i I_i}{2\sqrt{R_i}} \qquad i = 1,\ 2 \tag{2.15}$$

which are known as the incident and reflected power waves, respectively [5]. Power waves are scaled (normalized) voltage waves (see Eq. (2.2)), and are used in the following chapters for convenience. As seen in Section 2.2, one can convert a voltage-wave two port to power-wave two port by simply inserting an ideal transformer (see Fig. 2.3). The port references for power wave circuits are usually ignored, as they may all be set to one for convenience, and the resistive terminations are accounted for later with the insertion of appropriate inverse multipliers.

Belevitch [5] presented three useful groupings of the scattering variables and coefficients for real lossless two-ports:

$$\begin{bmatrix} B_1 \\ B_2 \end{bmatrix} = \mathbf{S}\begin{bmatrix} A_1 \\ A_2 \end{bmatrix}, \qquad \begin{bmatrix} B_1 \\ A_1 \end{bmatrix} = \mathbf{T}\begin{bmatrix} A_2 \\ B_2 \end{bmatrix}, \qquad \begin{bmatrix} B_1 \\ A_2 \end{bmatrix} = \mathbf{H}\begin{bmatrix} A_1 \\ B_2 \end{bmatrix} \tag{2.16}$$

where **S**, **T**, and **H** are 2×2 matrices referred to as the scattering, transfer and hybrid matrix, respectively. Fettweis modified Belevitch's theorem for complex lossless two-ports [7] and showed that a canonic representation of the scattering coefficients can be expressed using three polynomials and a unimodular constant, which take on the following forms:

$$\mathbf{S}=\frac{1}{g}\begin{bmatrix} h & \sigma f_* \\ f & -\sigma h_* \end{bmatrix}\ ,\quad \mathbf{T}=\frac{1}{f}\begin{bmatrix} \sigma g_* & h \\ \sigma h_* & g \end{bmatrix}\ ,\quad \mathbf{H}=\frac{1}{-\sigma h_*}\begin{bmatrix} -\sigma g_* & \sigma f_* \\ -f & g \end{bmatrix} \tag{2.17}$$

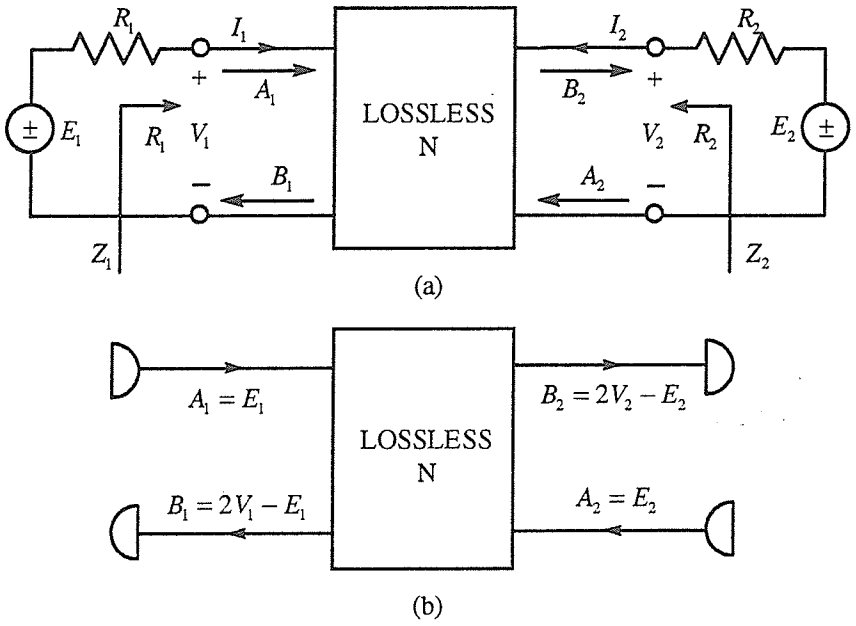

Figure 2.16 (a) A lossless two-port network N between resistive terminations, and (b) its wave digital equivalent.

The polynomials f, g, h satisfy the following conditions:

1) $f=f(\psi)$, $g=g(\psi)$, $h=h(\psi)$ are real or complex polynomials (i.e. real or complex coefficients) in some complex frequency variable ψ. The subscript asterisk denotes paraconjugation, i.e., $f_*(\psi)\equiv f^*(-\psi^*)$ where the superscript asterisk designates 'complex conjugate'. Due to the conformal nature of the mapping $\psi=(z-1)/(z+1)$, this representation also holds for the wave digital domain, and paraconjugation here means

$$f_*(z^{-1})\equiv z^{-m}f^*(z^*)\ ,\quad g_*(z^{-1})\equiv z^{-m}g^*(z^*)\ ,\quad h_*(z^{-1})\equiv z^{-m}h^*(z^*) \tag{2.18}$$

where m is the highest degree in $\mathbf{S}$ (Note that it is possible for g to be of lower degree than g_*).

2) $g(\psi)$ is a Hurwitz polynomial with all its zeros strictly in the left-hand plane, and $g(z^{-1})$ has all its zeros outside the unit circle in the z^{-1} plane.

3) The three polynomial f, g, and h satisfy losslessness

$$gg_* = hh_* + ff_* \tag{2.19}$$

which is the analytic continuation of the Feldkeller equation.

4) σ is complex but unimodular (i.e. $|\sigma| = 1$).

5) We can see that by rewriting Eq. (2.19) as

$$1 = \left|\frac{h}{g}\right|^2 + \left|\frac{f}{g}\right|^2 \quad \text{for} \quad \psi = j\phi \ \left(z^{-1} = e^{-j\omega T}\right) \quad \textit{where} \ \ \phi = \tan\left(\frac{\omega T}{2}\right) \tag{2.20}$$

which clearly shows the complementary nature of the scattering coefficients, where f/g is defined as the transmittance and h/g is the reflectance. Both transmittance and reflectance are passive (bounded) functions, i.e.,

$$\left|\frac{f}{g}\right| \le 1 \ , \quad \left|\frac{h}{g}\right| \le 1 \qquad \psi = j\phi \ \left(z^{-1} = e^{-j\omega T}\right) \tag{2.21}$$

6) The zeros of f are called transmission zeros. We have $\left(\frac{h}{g}\right)_* = \left(\frac{h}{g}\right)^*$ for transmission zeros on the $\psi = j\phi$ axis or in the z^{-1} domain for $z^{-1} = e^{-j\omega T}$ (unit circle). From Eq. (2.20), we have

$$1 = \left|\frac{h}{g}\right|^2 \Leftrightarrow \frac{h}{g} = e^{j\alpha} \tag{2.22}$$

For transmission zeros with $\mathrm{Re}\,\psi > 0$ ($\left|z^{-1}\right| < 1$, i.e. inside unit circle), the passivity property implies that

$$\left|\frac{h}{g}\right| < 1 \ , \qquad \left|\frac{h_*}{g_*}\right| > 1 \tag{2.23a,b}$$

where Eq. (2.23b) follows from Eq. (2.19) with $ff_* = 0$.

7) A function defined by

$$\delta\left(z^{-1}\right) := -z^{-1}\left[\ln\left(\frac{g}{h}\right)\right]' = -z^{-1}\left(\frac{g'}{g}\left(z^{-1}\right) - \frac{h'}{h}\left(z^{-1}\right)\right) \tag{2.24}$$

will be referred to as the delay. By substituting the expression for the reflection coefficient $\frac{h}{g}(e^{-j\omega}) = \rho(\omega)e^{j\phi(\omega)}$ into Eq. (2.24), it can be readily shown that $\delta(e^{-j\omega_0}) = j\frac{\rho'(\omega_0)}{\rho(\omega_0)} - \phi'(\omega_0)$. The reflection coefficient of a lossless two-port evaluated at a transmission zero, $e^{-j\omega_0}$, has the property $\rho(\omega_0) = 1$ and, because $\rho(\omega) \le 1 \ \forall \ \omega$, we have $\rho'(\omega_0) = 0$. It follows that $\delta(e^{-j\omega_0}) = -\phi'(\omega_0)$, i.e., $\delta(e^{-j\omega_0})$ is the return group delay and, as was shown in [16], $-\phi'(\omega_0) > 0$.

We can associate a transfer function to be realized with either scattering coefficient f/g (transmittance) or h/g (reflectance). The criteria governing the choice of realization are [8]:

1) the total number of 2-port adaptors (planar rotations) in the realization.
2) whether it is important to tune each transmission zero individually,
3) or to tune each reflection zero individually.

Generally, choose f/g if point (2) is of importance, and h/g for point (3).

2.6 Cascade Connection of two two-ports

A cascade connection of two lossless two-ports N_a and N_b is shown in Fig. 2.17. The transfer matrices of N_a and N_b are given by

$$\begin{bmatrix} B_1 \\ A_1 \end{bmatrix} = \frac{1}{f_a}\begin{bmatrix} \sigma_a g_{a*} & h_a \\ \sigma_a h_{a*} & g_a \end{bmatrix}\begin{bmatrix} A_{2a} \\ B_{2a} \end{bmatrix} = \mathbf{T}_a\begin{bmatrix} A_{2a} \\ B_{2a} \end{bmatrix}, \qquad \begin{bmatrix} B_{1b} \\ A_{1b} \end{bmatrix} = \frac{1}{f_b}\begin{bmatrix} \sigma_b g_{b*} & h_b \\ \sigma_b h_{b*} & g_b \end{bmatrix}\begin{bmatrix} A_2 \\ B_2 \end{bmatrix} = \mathbf{T}_b\begin{bmatrix} A_{2b} \\ B_{2b} \end{bmatrix} \tag{2.25}$$

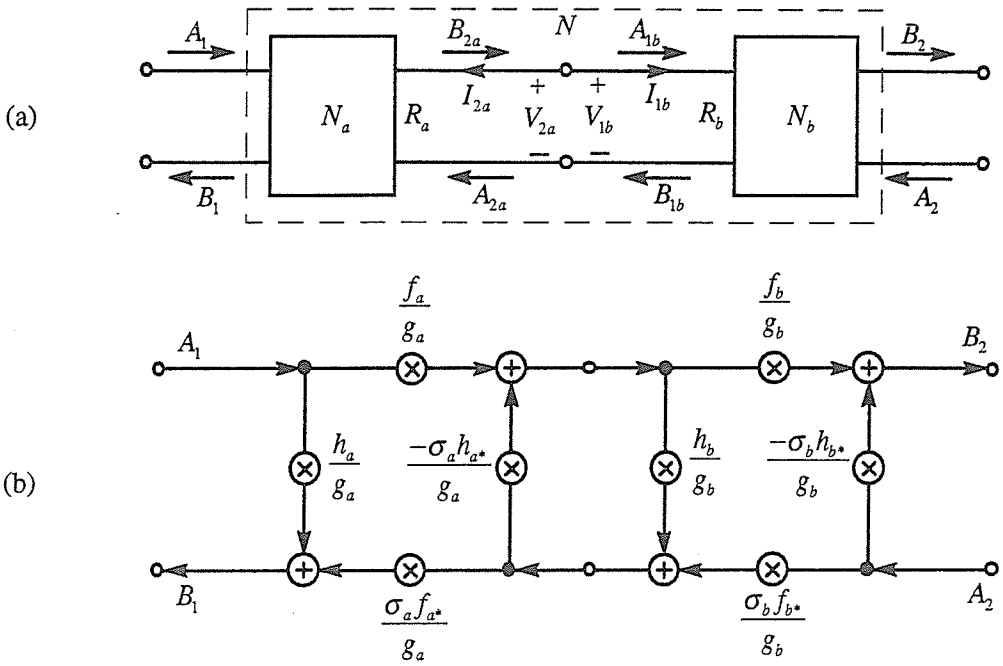

Figure 2.17 (a) Cascade connection of N_a and N_b, and (b) its signal flowgraph.

A direct interconnection between the two two-ports requires $V_{2a} = V_{1b}$, $I_{2a} = -I_{1b}$ and $R_a = R_b$. It follows from Eq. (2.2) that $A_{2a} = B_{1b}$ and $B_{2a} = A_{1b}$. Together with Eq. (2.25), the transfer matrix for the combined network N is given by

$$\mathbf{T} = \mathbf{T}_a \mathbf{T}_b = \frac{1}{f}\begin{bmatrix} \sigma g_* & h \\ \sigma h_* & g \end{bmatrix} \qquad \text{where} \tag{2.26}$$

$$\sigma = \sigma_a \sigma_b \ , \ f = f_a f_b \ , \ g = g_a g_b + \sigma_a h_{a^*} h_b \ , \ h = h_a g_b + \sigma_a g_{a^*} h_b \tag{2.27a-d}$$

We consider the situation where $\mathbf{T}_a = \mathbf{T}_\theta$ corresponds to the transfer matrix of an ideal-transformer (2-port adaptor) (see Table 2.1). Extracting this two-port on the left leaves a remainder network with $\mathbf{T}_b = \mathbf{T}_\theta^{-1}\mathbf{T}$ where the canonic polynomials are given by

$$\begin{aligned} f_b &= f \sin\theta \\ g_b &= g + h\cos\theta \\ h_b &= h + g\cos\theta \\ \sigma_b &= \sigma \end{aligned} \tag{2.28}$$

as shown in Fig. 2.18a. This extraction is often used to force h_b to have a desired factor, e.g. z^{-1}. In this case

$$\cos\theta = -\frac{h}{g}(z^{-1}=0) \tag{2.29}$$

which can always be satisfied because the reflection coefficient h/g is bounded by one everywhere inside the unit circle (see Eq. (2.23)). Also note that the extraction of a 2-port does not change the zeros of f.

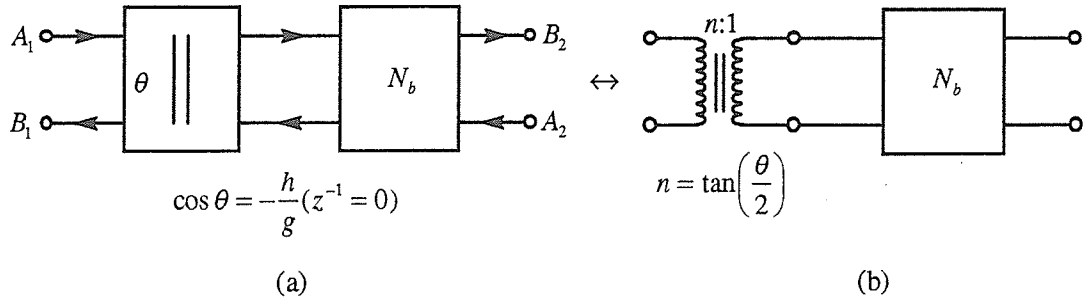

Figure 2.18 Extracting a 2-port adaptor, which forces a z^{-1} factor in h for the remaining network.

Extracting a 2-port in the wave digital domain is equivalent to extracting an ideal transformer (see Fig. 2.18b), which is a lossless element. Therefore, according to classical network theory, the remainder network N_b is also lossless.

2.7 Reflection-Free Property

A two-port network can be implemented using an interconnected network of smaller adaptors. An important consideration is to choose reflection-free ports for a direct interconnection of adaptors so that there are no delay-free loops (i.e. at least one delay must interpose somewhere along the loop) and, consequently, the structure is computable [11]. Computability allows us to write down an ordered sequence of computational steps for the filtering algorithm without creating infinite loops. Sedlmeyer and Fettweis [12] showed that for a direct interconnection (equal port reference) between two adaptors, either port can be made reflection-free (the reflected wave becomes independent of the incident wave at the reflection-free

port). The reflection-free property can be satisfied by having at least one factor of z^{-1} for the reflection coefficient (B_i/A_i) looking into the reflection-free port. The situation is illustrated in Fig. 2.19, with two interconnected sub-networks N_a and N_b that share one common port, and N_a is said to have a reflection-free port #2.

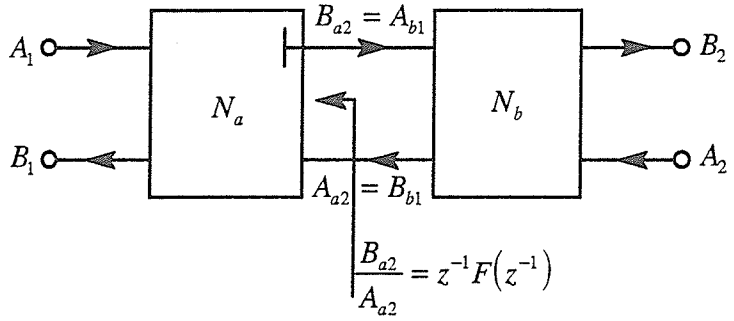

Figure 2.19 Direct interconnection of two adaptors with port #2 reflection-free; F is a rational function of z^{-1}.

CHAPTER III

SYNTHESIS OF PIPELINEABLE COMPLEX LOSSLESS (UNITARY) TWO-PORT WD CIRCUITS

In this chapter, we derive a pipelineable, complex, lossless (unitary), two-port network that will be referred to as the pipelinable unitary (PU) structure. The derivation of the circuit is based on iteratively interchanging the h and f polynomials [9] (see Eq. (2.17)). A way of obtaining the frequency response for the PU structure in the digital domain is also given. Three different forms of representing the polynomials can be used in the synthesis process, namely the coefficient, DFT-sample, and the zero form. We discuss the merits of each of these representations and their associated synthesis procedures. Finally, a general 1st-order complex section will be derived using the PU structure that is used in the cascade structure.

3.1 The process of interchanging the h and f polynomial

The main step in the PU-structure synthesis is the process of interchanging the h and f polynomials. In this section, we discuss what this step means in both the analog and WDF-domains.

Consider the two-port network N as shown in Fig. 3.1a, the scattering matrix can be factored into simple factors as follows

$$\mathbf{S}=\frac{1}{g}\begin{bmatrix} h & \sigma f_* \\ f & -\sigma h_* \end{bmatrix}=\begin{bmatrix} 0 & 1 \\ 1 & 0 \end{bmatrix}\frac{1}{g}\begin{bmatrix} f & -\sigma h_* \\ h & \sigma f_* \end{bmatrix}\triangleq\mathbf{S}_1\mathbf{S}_2 \tag{3.1}$$

The two-port network corresponding to the 1st factor $\mathbf{S}_1=\begin{bmatrix} 0 & 1 \\ 1 & 0 \end{bmatrix}$ is a trivial two-port that corresponds to a simple feed through in the digital-domain, and the 2nd factor describes a network N_2:

$$\mathbf{S}_2=\frac{1}{g_2}\begin{bmatrix} h_2 & \sigma_2 f_{2*} \\ f_2 & -\sigma_2 h_{2*} \end{bmatrix}=\frac{1}{g}\begin{bmatrix} f & -\sigma h_* \\ h & \sigma f_* \end{bmatrix} \tag{3.2}$$

where $f_2 = h$, $g_2 = g$, $h_2 = f$, $\sigma_2 = -\sigma$. Therefore, N_2 corresponds to a network with h and f interchanged.

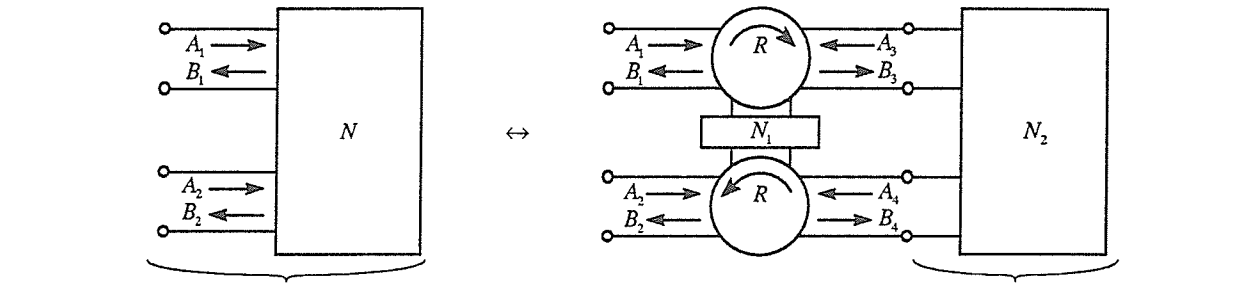

Figure 3.1 Decomposition of a two-port network which amounts to interchanging h and f.

A circuit that realizes a factorization of the scattering matrix $\mathbf{S} = \mathbf{S}_1\mathbf{S}_2$ is shown in Fig. 3.1b, which involves two identical circulators. A 3-port circulator is defined in Fig. 3.2a, and the corresponding WD circuit is shown in Fig. 3.2b.

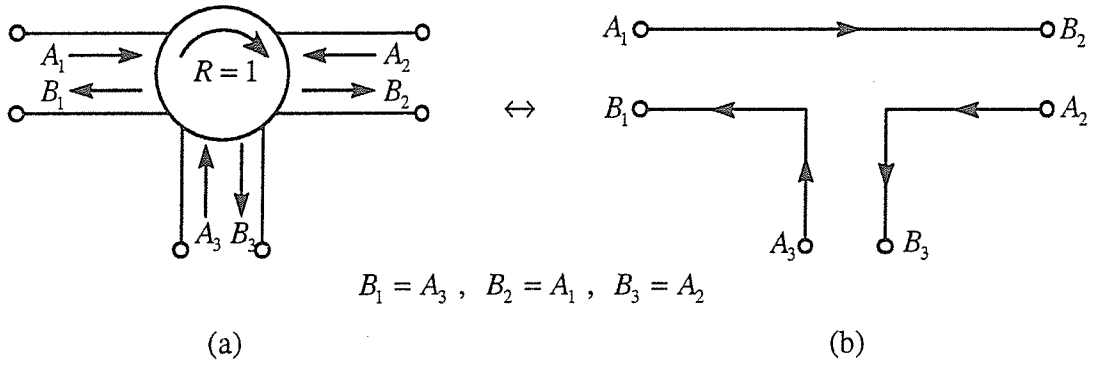

Figure 3.2 (a) A 3-port circulator, and (b) its WD circuit (just a trivial wiring problem).

Note that a WD simulation of a 3-port circulator is rather trivial. The resulting WD image of Fig. 3.1b is shown in Fig. 3.3.

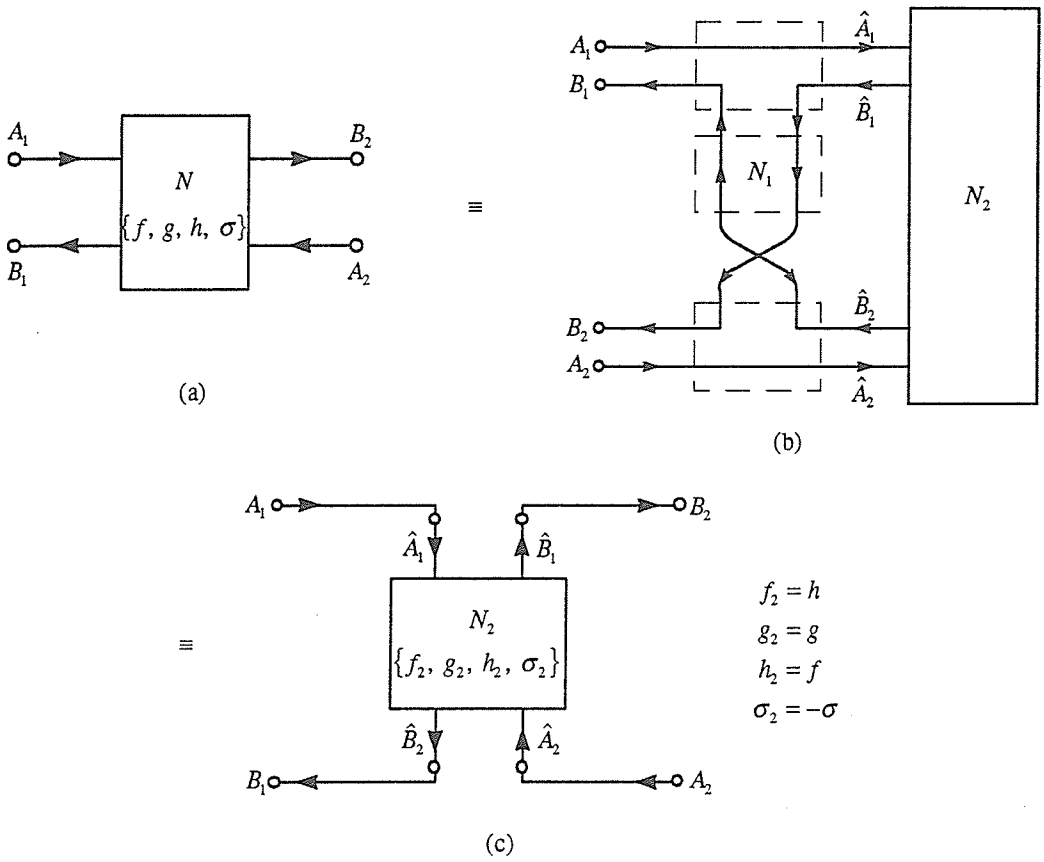

Figure 3.3 Interchanging h and f only amounts to a trivial routing problem in the WDF-domain.

3.2 PU synthesis algorithm

The synthesis algorithm for real two-port networks was first introduced by Rao and Kailath [10] and modified by Fettweis [9] using a network theory approach. In this section, we extend this to complex two-port networks using only one additional two-port element, and the unimodular multiplier section [4][5], as shown in section 2.3. The algorithm is quite simple, and step-by-step instructions are as follows.

Consider a two-port network N_1 described by the three polynomials $f_1(z^{-1})$, $g_1(z^{-1})$, and $h_1(z^{-1})$ of Nth degree shown in Fig. 3.3a. By first extracting a unimodular multiplier section with the proper parameter, we can ensure that for the remaining network, an extraction of an additional

real 2-port adaptor can force a factor z^{-1} in the h polynomial. The parameter of the extracted unimodular multiplier section is given by

$$\alpha_1 = \arg\left(\frac{h_1(0)}{g_1(0)}\right) - \pi \tag{3.3}$$

and the remaining network is shown in Fig. 3.4 together with its analog equivalent.

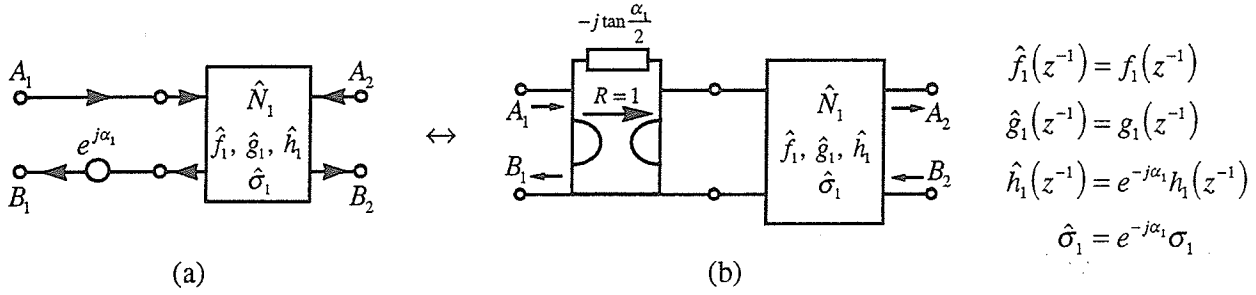

Figure 3.4 (a) Extraction of an unimodular multiplier section, and (b) its analog equivalent.

The next step of the algorithm is to extract a 2-port adaptor with the parameter

$$\cos\theta_1 = \left|\frac{\hat{h}_1(0)}{\hat{g}_1(0)}\right| = \left|\frac{h_1(0)}{g_1(0)}\right| \tag{3.4}$$

to ensure that for the remaining two-port $N_2\{f_2, g_2, h_2, \sigma_2\}$, we have $h_2(0) = 0$. See Eq. (2.29) for the choice of the extraction parameter. This is shown in Fig. 3.5.

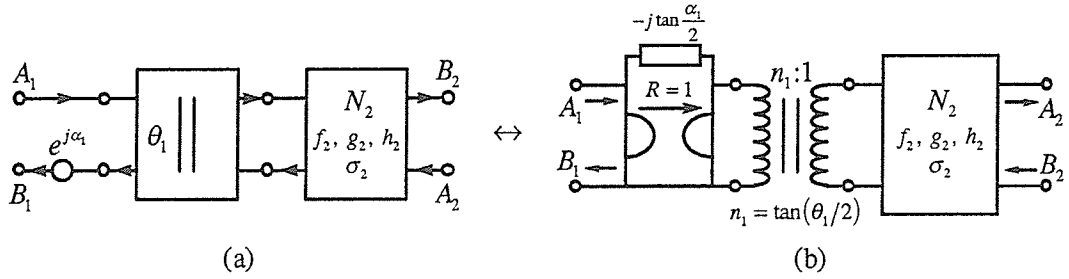

Figure 3.5 (a) Extraction of a 2-port adaptor, thus forcing a factor of z^{-1} in the h polynomial, and (b) its analog equivalent.

The unimodular multiplier section and the 2-port adaptor always go together to force a factor of z^{-1} in the h polynomial; therefore, we can group them together and rewrite

$$f_2 = f_1 \sin\theta_1 \ , \ g_2 = g_1 + e^{-j\alpha_1} h_1 \cos\theta_1 \ , \ h_2 = e^{-j\alpha_1} h_1 + g_1 \cos\theta_1 \ , \ \sigma_2 = e^{-j\alpha_1}\sigma_1 \qquad (3.5)$$

Thus together with Eq. (3.4) we obtain $h_2(0) = 0$. Next, we interchange h_2 and f_2 so that the remaining network $\hat{N}_2\{\hat{f}_2, \hat{g}_2, \hat{h}_2, \hat{\sigma}_2\}$ is described by $\hat{f}_2 = h_2$, $\hat{g}_2 = g_2$, $\hat{h}_2 = f_2$, $\hat{\sigma}_2 = -\sigma_2$ as shown in Fig. 3.6. Note that this is just simple routing problem in the WD-domain, while implementation of circulators in the analog domain is difficult.

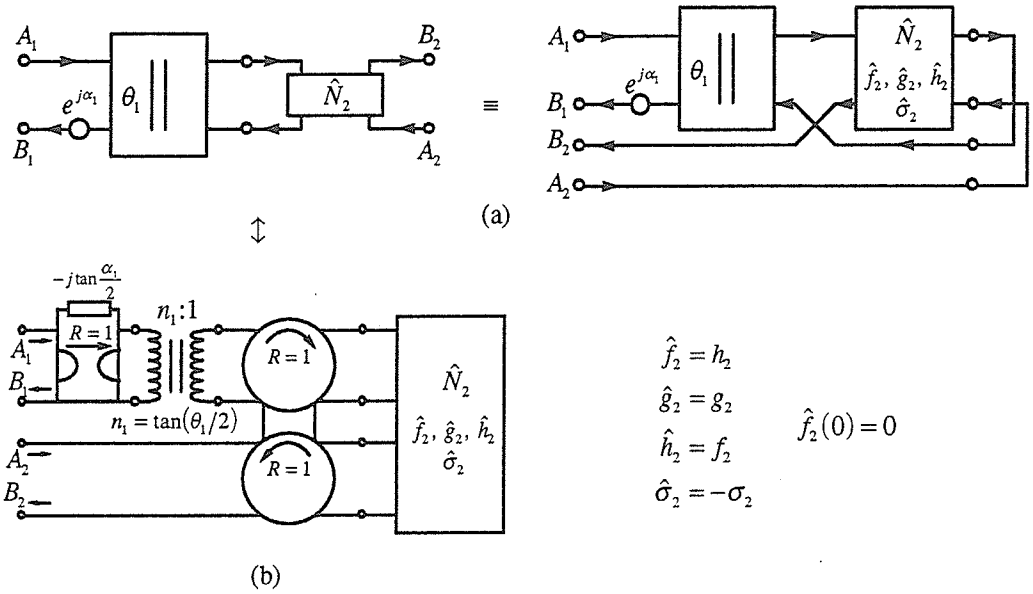

Figure 3.6 (a) Interchange h and f amounts to trivial routing problem in WD-domain; (b) analog equivalent that involves circulators.

Note that since the extracted two-ports are lossless, it follows from a classical network theory result that the remainder two-port also is lossless (see section 2.6). At this point, $\hat{f}_2(0) = h_2(0) = 0$. After the interchange, we repeat the first two basic steps, namely the extraction of a unimodular multiplier section ($\alpha_2 = \arg\left(\hat{h}_2(0)/\hat{g}_2(0)\right) - \pi$) together with a 2-port adaptor ($\cos\theta_2 = \left|\hat{h}_2(0)/\hat{g}_2(0)\right|$) as shown in Fig. 3.7 to force $\hat{h}_2(0) = 0$. The remaining network $N_3\{f_3, g_3, h_3, \sigma_3\}$ is described by

$$f_3 = \hat{f}_2 \sin\theta_2 \ , \ g_3 = \hat{g}_2 + e^{-j\alpha_2}\hat{h}_2 \cos\theta_2 \ , \ h_3 = e^{-j\alpha_2}\hat{h}_2 + \hat{g}_2 \cos\theta_2 \ , \ \sigma_3 = e^{-j\alpha_2}\hat{\sigma}_2 \qquad (3.6)$$

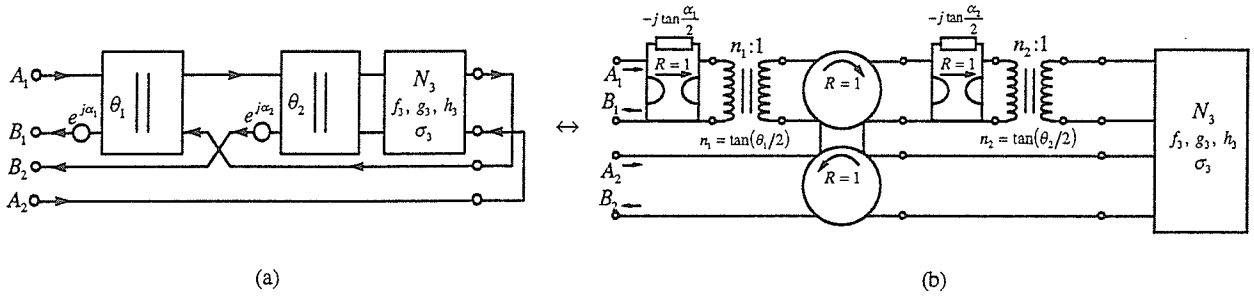

Figure 3.7 (a) Extraction of another unimodular multiplier and a 2-port; (b) its analog equivalent.

Since $f_3(0)=0$ and $h_3(0)=0$, and since $g_3(z^{-1})$ must have all its zeros outside the unit circle, it follows from the Feldkeller equation $gg_* = hh_* + ff_*$ that $g_{3*}(z^{-1})$ must also have a factor of z^{-1}. The factor of z^{-1} which is now common to f, g_*, and h can be extracted using a QUARL section [9] (see Fig. 3.8). In this way the degrees of the original h, g and f are reduced by one, i.e., the degree of N_3 is equal to $N-1$. The order reduction of $g_3(z^{-1})$ is accomplished by forcing the leading coefficient of $g_3(z^{-1})$ to zero. Another interchange of the h and f polynomials results in the circuit shown in Fig. 3.9. The seven steps described above lead to an order-reduced f_3, g_3, and h_3 that describe a lossless two-port, and will be referred to as the basic extraction step for the PU structure. Note that in the analog domain, the QUARL section and the second interchange can be combined into the circuit as shown in Fig. 3.10 [9].

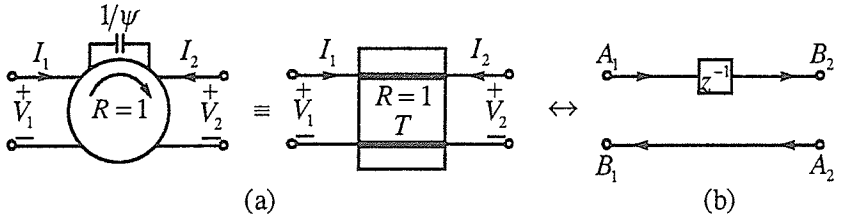

Figure 3.8 (a) A QURAL section , and (b) its digital equivalent.

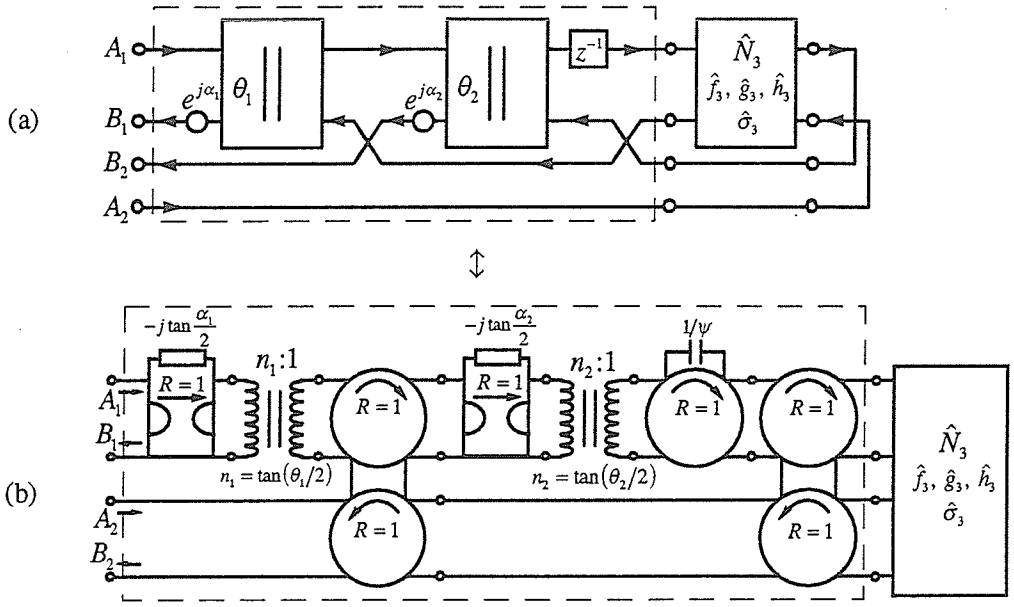

Figure 3.9 (a) The basic extraction step, (b) its analog equivalent.

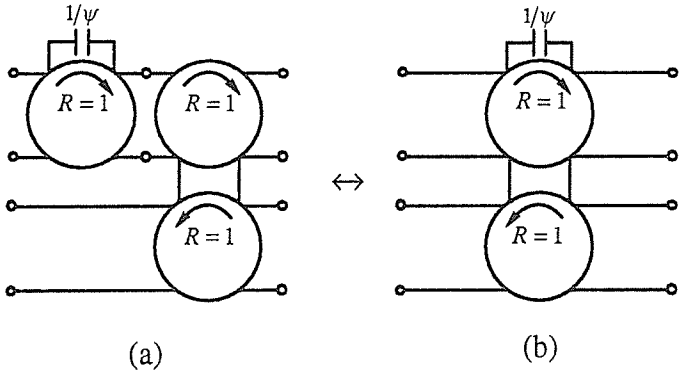

Figure 3.10 Combining the QUARL section and the second interchange.

The process of performing the PU-step is repeated iteratively until a zeroth-order network remains ($N=0$). Next an extraction of an unimodular multiplier and a 2-port will force $h(0)=0$, which is just a feed through, in the remaining network, and f/g is unimodular. The zeroth-order network can also be realized using the basic PU step but with the last 2-port being a decoupling 2-port, i.e., $\cos\theta_{2N+2}=1$ ($B_1=-A_1$ and $B_2=A_2$ for the last 2-port). This is shown in Fig. 3.11a.

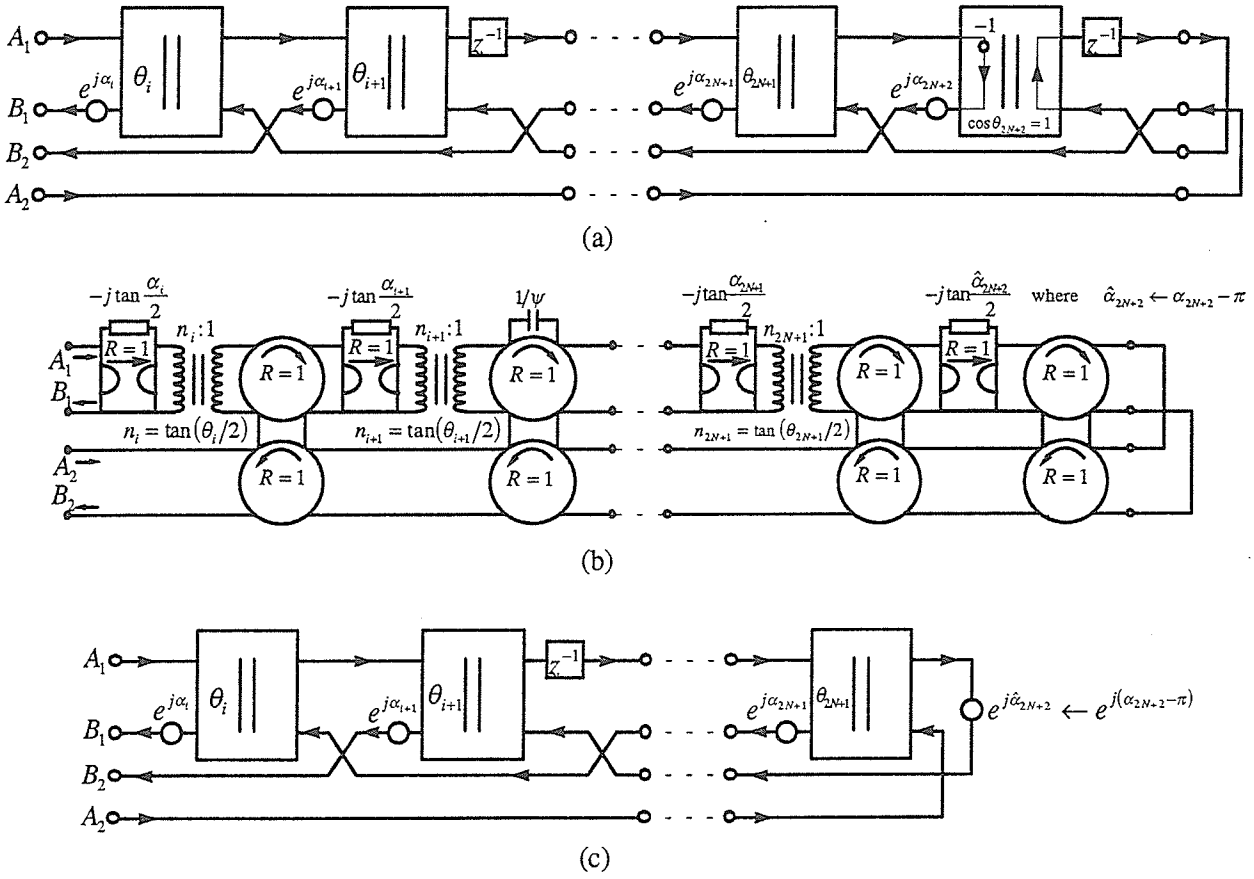

Figure 3.11 (a) The basic extraction blocks, and (b) their analog equivalents (c) simplified version of the last termination.

Note that the algorithm should automatically reach the last decoupling 2-port with the expected value of $\cos\theta_{2N+2} = 1$ because of the structure's design. A value different from one means either that there is accumulation of error during the extraction, and higher precision should be used during the calculations, or the input polynomials do not satisfy the losslessness condition $gg_* = hh_* + ff_*$. The necessary condition $\cos\theta_{2N+2} = 1$ offers a useful verification of the synthesis solution. The last 2-port with $\cos\theta_{2N+2} = 1$ corresponds to a multiplier with a value of -1 (see Fig. 3.11a) that can be combined with the last unimodular multiplier $e^{j\alpha_{2N+2}}$ (i.e. π is subtracted from the angle of the last unimodular multiplier) and the circuit is simplified, as shown in Fig. 3.11c. The second interchange of h and f is not necessary. However, it can be used as a degree of freedom to allow the designer to pick a more suitable value of $\cos\theta$ for quantization purposes (i.e., either choose $h(0)/g(0)$ or $f(0)/g(0)$).

The general PU structure for the digital domain in Fig. 3.11b can be redrawn to avoid the crossing of connections and is shown in Fig. 3.12. This version of the general PU structure makes it easier to visualize the signal flow, and it is especially useful for obtaining the frequency response which is described in the next section.

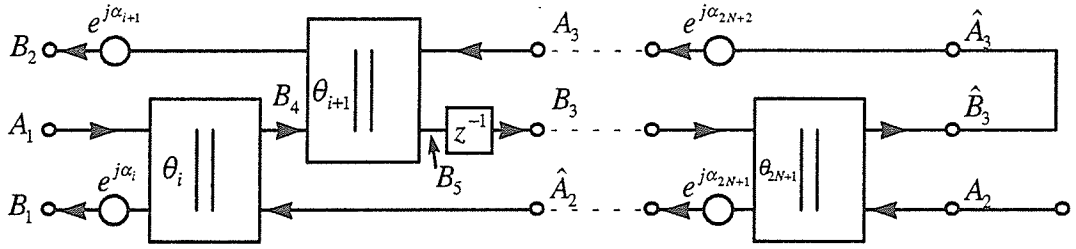

Figure 3.12 Another version of the general PU structure redrawn to avoid crossing of connections.

The PU structure is evaluated in a particular sequence imposed by the location of the delays within the circuit. With reference to Fig. 3.12 and assuming that the two subnetworks are connected, the computational sequence which must begin at port #2 is as follows:

1. With B_3 and A_2 as inputs, evaluate the 2-port with θ_{2N+1} as the rotation angle and obtain the two outputs $\hat{A}_2$ and A_3 by performing two additional rotations by $e^{j\alpha_{2N+2}}$ and $e^{j\alpha_{2N+1}}$.
2. With A_1 and $\hat{A}_2$ as inputs, evaluate the 2-port with θ_i as the rotation angle and obtain the two outputs B_1 (by performing an addition rotation by $e^{j\alpha_i}$) and B_4.
3. With B_4 and A_3 as inputs, evaluate the 2-port with θ_{i+1} as the rotation angle and obtain the two outputs B_2 (by performing an addition rotation by $e^{j\alpha_{i+1}}$) and B_5.
4. Replace B_3 with B_5 for the next sampling instance.

Now we return to step 2 and repeat with appropriate changes to the index i.

A summary of the PU synthesis algorithm is shown in Table 3.1.

1. Given three input polynomials f, g, h, and N, the order of the filter.
2. For the ith extraction step in which i goes from 1 to $2N+2$,
3. let $\cos\theta_i = \left|\frac{h(0)}{g(0)}\right| \Rightarrow \sin\theta_i = \sqrt{1-\cos^2\theta_i}$, $\alpha_i = \arg\left(\frac{h(0)}{g(0)}\right) - \pi$
4. Update the three polynomials:

$$f \leftarrow f\sin\theta_i$$
$$\hat{g} \leftarrow g + e^{-j\alpha_i} h\cos\theta_i$$
$$h \leftarrow e^{-j\alpha_i} h + g\cos\theta_i$$
$$g \leftarrow \hat{g}$$

5. Interchange h and f.
6. If i is even: divide h and f by z^{-1} to reduce the order by one. The g polynomial will be degree reduced automatically.
7. Go back to step 3) with the next i until $i > 2N+2$.
8. $\cos\theta_{2N+2}$ should be 1.
9. Update the last unimodular multiplier:

$$\alpha_{2N+2} \leftarrow \alpha_{2N+2} - \pi$$

Table 3.1 Summary of PU Synthesis Algorithm.

3.3 Computation of Frequency Response for the PU Structure with quantized multipliers

In this section, we present a direct method (as oppose to the indirect method of taking the DFT of the impulse response) to obtain the frequency response in the digital-domain, so that the more involved time-domain simulations can be avoided.

The frequency response can be obtained from the product of 3 by 3 transfer matrices $\mathbf{T}_i$, each of which represents a basic PU extraction block, and the 3 by 3 matrix for the last termination. Fig. 3.13 shows the 3 by 3 matrices representing the PU block.

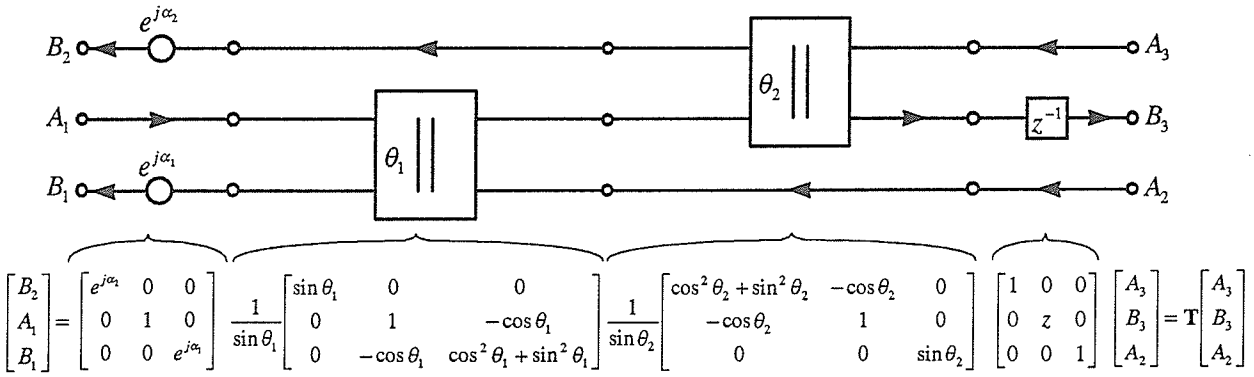

Figure 3.13 3x3 matrices for each subsection of the PU extraction block.

In the case of lossless 2-ports (i.e. $\cos^2\theta_i + \sin^2\theta_i = 1$), the 3 by 3 transfer matrix $\mathbf{T}_i$ for the PU block can be simplified to

$$\mathbf{T}_i = \begin{bmatrix} \beta_{i+1}+j\chi_{i+1} & 0 & 0 \\ 0 & 1 & 0 \\ 0 & 0 & \beta_i+j\chi_i \end{bmatrix} \frac{1}{b_i} \begin{bmatrix} b_i & 0 & 0 \\ 0 & 1 & -a_i \\ 0 & -a_i & 1 \end{bmatrix} \frac{1}{b_{i+1}} \begin{bmatrix} 1 & -a_{i+1} & 0 \\ -a_{i+1} & 1 & 0 \\ 0 & 0 & b_{i+1} \end{bmatrix} \begin{bmatrix} 1 & 0 & 0 \\ 0 & z & 0 \\ 0 & 0 & 1 \end{bmatrix}$$

$$= \frac{1}{b_i b_{i+1}} \begin{bmatrix} (\beta_{i+1}+j\chi_{i+1})b_i & -(\beta_{i+1}+j\chi_{i+1})b_i a_{i+1} z & 0 \\ -a_{i+1} & z & -a_i b_{i+1} \\ (\beta_i+j\chi_i)a_i a_{i+1} & -(\beta_i+j\chi_i)a_i z & (\beta_i+j\chi_i)b_{i+1} \end{bmatrix} \tag{3.7}$$

where $a_i = \cos\theta_i$, $b_i = \sin\theta_i$, $e^{j\alpha_i} = \beta_i + j\chi_i$. However, when the eight multipliers $\{a_i, b_i, \beta_i, \chi_i, a_{i+1}, b_{i+1}, \beta_{i+1}, \chi_{i+1}\}$ are quantized, the transfer matrix of the PU block can no longer be put in the lossless form. Instead, the transfer matrix is given by

$$\mathbf{T}_i = \begin{bmatrix} \beta_{i+1}+j\chi_{i+1} & 0 & 0 \\ 0 & 1 & 0 \\ 0 & 0 & \beta_i+j\chi_i \end{bmatrix} \frac{1}{b_i} \begin{bmatrix} b_i & 0 & 0 \\ 0 & 1 & -a_i \\ 0 & -a_i & a_i^2+b_i^2 \end{bmatrix} \frac{1}{b_{i+1}} \begin{bmatrix} a_{i+1}^2+b_{i+1}^2 & -a_{i+1} & 0 \\ -a_{i+1} & 1 & 0 \\ 0 & 0 & b_{i+1} \end{bmatrix} \begin{bmatrix} 1 & 0 & 0 \\ 0 & z & 0 \\ 0 & 0 & 1 \end{bmatrix}$$

$$= \frac{1}{b_i b_{i+1}} \begin{bmatrix} (\beta_{i+1}+j\chi_{i+1})b_i(a_{i+1}^2+b_{i+1}^2) & -(\beta_{i+1}+j\chi_{i+1})b_i a_{i+1} z & 0 \\ -a_2 & z & -a_i b_{i+1} \\ (\beta_i+j\chi_i)a_i a_{i+1} & -(\beta_i+j\chi_i)a_i z & (\beta_i+j\chi_i)(a_i^2+b_i^2)b_{i+1} \end{bmatrix} \tag{3.8}$$

In order to obtain a frequency response of a quantized design, we form the product of all transfer matrices $\mathbf{T} = \prod_{i=1(2)2N} \mathbf{T}_i$ for each PU block (i=1(2)2N), together with the transfer matrix for the last termination section as shown in Fig. 3.14.

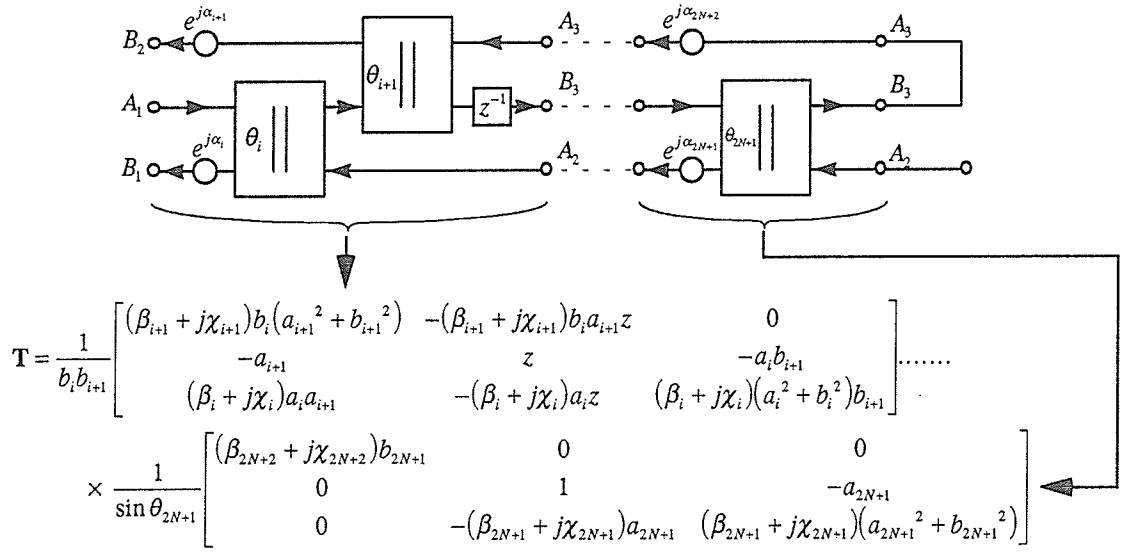

Figure 3.14 The overall 3 by 3 matrix for the PU structure.

Due to the fact that $A_3 = B_3$ at the last termination section, we can reduce the 3 by 3 matrix to the 2 by 2 scattering matrix, which is given by

$$\begin{bmatrix} B_1 \\ B_2 \end{bmatrix} = \frac{1}{\mathbf{T}_{22}+\mathbf{T}_{21}} \begin{bmatrix} \mathbf{T}_{32}+\mathbf{T}_{31} & \mathbf{T}_{33}(\mathbf{T}_{22}+\mathbf{T}_{31})-\mathbf{T}_{23}(\mathbf{T}_{32}+\mathbf{T}_{31}) \\ \mathbf{T}_{12}+\mathbf{T}_{11} & \mathbf{T}_{13}(\mathbf{T}_{22}+\mathbf{T}_{21})-\mathbf{T}_{23}(\mathbf{T}_{12}+\mathbf{T}_{11}) \end{bmatrix} \begin{bmatrix} A_1 \\ A_2 \end{bmatrix} = \frac{1}{g} \begin{bmatrix} h & \sigma f_* \\ f & -\sigma h_* \end{bmatrix} \begin{bmatrix} A_1 \\ A_2 \end{bmatrix} \tag{3.9}$$

Therefore

$$g(z^{-1}) = \mathbf{T}_{22}+\mathbf{T}_{21}\ ,\ f(z^{-1}) = \mathbf{T}_{12}+\mathbf{T}_{11}\ ,\ h(z^{-1}) = \mathbf{T}_{32}+\mathbf{T}_{31} \tag{3.10}$$

The frequency response for the transmittance is given by $\frac{f}{g}(z^{-1})$ and the reflectance is $\frac{h}{g}(z^{-1})$. Note that the factors outside the 3 by 3 transfer matrices can be ignored when evaluating the transfer functions because they appear in both the numerators and denominators.

To verify the PU synthesis and analysis algorithm, pick an arbitrary set of $\{\alpha_i, \theta_i: 1(1)2N+2\}$ and obtain frequency response on $N+1$ frequency points along the unit circle using Eq. (3.10). These frequency points can now be used as the input sample representation for the synthesis algorithm. Resynthesize the data using the sample representation should result in the $\{\alpha_i, \theta_i: 1(1)2N+2\}$ we picked at the outset. If values for θ_i are critical (i.e. close to 0 or $\pi/2$), the roundoff error is significant.

3.4 The associated synthesis procedures for 3 different polynomial representations

The *f*, *g*, and *h* polynomials for the synthesis process can be represented by three different forms, namely the coefficient, DFT-sample, and the zero form. The coefficient-form representation for a polynomial *p* is given by

$$p(z^{-1}) = \sum_{n=0}^{N} c_n (z^{-1})^n \tag{3.11}$$

where c_n are the coefficients of the polynomial and N is the degree of the polynomial. The zero form representation is given by

$$p(z^{-1}) = c\prod_{n=1}^{N}(z^{-1} - z_i) \tag{3.12}$$

where c is the constant factor, N is the degree, and z_i are the zeros of the polynomial. Both representations are straight forward in the synthesis process except that the zero form requires a zero-finding routine for updating the g and h polynomials. The DFT-sample representation defines samples for a polynomial $p(z^{-1})$ evaluated along the unit circle, which are given by

$$p_k = p(w^k) \ , \quad w = e^{-j\frac{2\pi}{N}} \ , \ k = 0(1)N \tag{3.13}$$

where N is the degree of the polynomial, and

$$p(0) = \sum_k p_k \tag{3.14}$$

The associated synthesis process requires minor modification for the DFT-sample representation as shown in Table 3.2.

The DFT-sample representation synthesis algorithm effects order reduction implicitly (see step 6 in Table 3.2) without having to do an actual degree reduction. Although, after each basic extraction step it is possible to obtain a sample set of lower degree, we choose to retain the original size in order to make the algorithm easier to implement, i.e., we allow the redundancy to grow.

1. Given three input polynomials f, g, h, and N, the order of the filter.

1b. Compute samples on the unit circle

$$f_k = f(w^k),\ g_k = g(w^k),\ h_k = h(w^k) \qquad k = 0(1)N$$

where $w^k = e^{-j\frac{2\pi}{N}}$.

2. For the ith extraction step in which i goes from 1 to $2N+2$,

3. Let $\cos\theta_i = \left|\frac{h(0)}{g(0)}\right| \Rightarrow \sin\theta_i = \sqrt{1-\cos^2\theta_i}$, $\alpha_i = \arg\left(\frac{h(0)}{g(0)}\right) - \pi$

where $h(0) = \sum_k h_k$ and $g(0) = \sum_k g_k$.

4. Update all samples ($k = 0(1)N$) for the three polynomials:

$$f_k \leftarrow f_k \sin\theta_i$$
$$\hat{g}_k \leftarrow g_k + e^{-j\alpha_i} h_k \cos\theta_i$$
$$h_k \leftarrow e^{-j\alpha_i} h_k + g_k \cos\theta_i$$
$$g_k \leftarrow \hat{g}_k$$

5. Interchange all h_k and f_k.

6. If i is even, reduce the order of h and f by updating the samples:

$$h_k \leftarrow \frac{h_k}{w^k} \ , \quad f_k \leftarrow \frac{f_k}{w^k}$$

7. Go back to step 3 with the next i until $i > 2N+2$.

8. $\cos\theta_{2N+2}$ should be 1.

9. Update the last unimodular multiplier:

$$\alpha_{2N+2} \leftarrow \alpha_{2N+2} - \pi$$

Table 3.2 Summary of the Synthesis Algorithm via DFT Samples.

3.5 Design Example for the PU Structure

In this section, we use an 8th order band-pass filter example to illustrate the difference in synthesis results using the three forms of representation for the polynomials. The input data is from Jarmasz's Ph.D thesis [3], and is converted to the z^{-1}-domain with 12 digits of precision. This set of data caused premature termination in the PU synthesis algorithm because the Feldkeller equation was not satisfied accurately enough. Therefore we regenerated the input data so that the Feldkeller equation was satisfied to 15 decimal places, and the results are given in Table 3.3. The input data is in zero form and will be converted to the required polynomial representation by the PU synthesis program discussed in Chapter 5. All the calculations for the synthesis program are based on a precision of 18 digits.

f zeros	magnitude	angle / π
constant	0.00090521	0.0
1	1.0	0.430034232
2	1.0	-0.430034232
3	0.0	0.0
4	0.0	0.0
5	1.0	0.320538560
6	1.0	-0.320538560
7	0.0	0.0
8	0.0	0.0

h zeros	magnitude	angle / π
constant	0.938442111704	0.0
1	1.0	0.351732711368
2	1.0	-0.351732711368
3	1.0	0.365109796566
4	1.0	-0.365109796566
5	1.0	0.385182448776
6	1.0	-0.385182448776
7	1.0	0.398308216049
8	1.0	-0.398308216049

g zeros	magnitude	angle / π
constant	0.880673595637835194	0.0
1	1.008341527656365750	-0.399341528997245882
2	1.008341527656365750	0.399341528997245882
3	1.008545764020980650	-0.350675396462379855
4	1.008545764020980650	0.350675396462379855
5	1.023795851013025390	-0.364509517733878304
6	1.023795851013025390	0.364509517733878304
7	1.023471807530125960	-0.385806739150357242
8	1.023471807530125960	0.385806739150357242

Table 3.3 An 8th ordered design example with up to 18 decimal places of precision.

The PU synthesis results based on the three forms of polynomial representation is shown in Table 3.4. Note that this example is for a real two-port, therefore we expect $\alpha_i/\pi = 0, \pm 1 \; \forall \; i$.

i	$\cos\theta_i$		
	Coefficient Form	DFT-sample Form	Zero Form
1	0.938442110231743403	0.938442110231743403	0.938442110231743403
2	0.000000000000000000	0.000000000000000000	0.000000000000000000
3	0.382034996637063182	0.382034996637063168	0.382034996637064448
4	0.000000000000000000	0.000000000000000000	0.000000000000000000
5	0.994879530326316620	0.994879530326316598	0.994879530326326402
6	0.000000000000000000	0.000000000000000000	0.000000000000000000
7	0.383096500999031838	0.383096500999031771	0.383096501007988522
8	0.000000000000000000	0.000000000000000000	0.000000000000000000
9	0.995858180702095568	0.995858180702094174	0.995858180756248036
10	0.334065090667967128	0.334065090667910315	0.334065092864509806
11	0.360640861943750237	0.360640861943088380	0.360640866904119160
12	0.136479907863578986	0.136479907863264483	0.136479911038747653
13	0.932253262419454669	0.932253262417567694	0.932253265729075537
14	0.955467770295318026	0.955467770279996041	0.955467805784553804
15	0.140971140077849394	0.140971140142782783	0.140971216910977927
16	0.402851061536305702	0.402851061087418612	0.402851317224768357
17	0.011855555896985612	0.011855555853028907	0.011855835657636921
18	1.000000137921265430	1.000000136507671310	1.000000288742289130

i	α_i/π		
	Coefficient Form	DFT-sample Form	Zero Form
1	-1.000000000000000000	-1.000000000000000000	-1.000000000000000000
2	-1.000000000000000000	-1.000000000000000000	-1.000000000000000000
3	-1.000000000000000000	-1.000000000000000000	-1.000000000000000000
4	-1.000000000000000000	-1.000000000000000000	-1.000000000000000000
5	-1.000000000000000000	-1.000000000000000000	-1.000000000000000000
6	-1.000000000000000000	-1.000000000000000000	-1.000000000000000000
7	-1.000000000000000000	-1.000000000000000000	-1.000000000000000000
8	-1.000000000000000000	-1.000000000000000000	-1.000000000000000000
9	-1.000000000000000000	-1.000000000000000000	-1.000000000000000000
10	-1.000000000000000000	-1.000000000000000000	-1.000000000000000000
11	-1.000000000000000000	-1.000000000000000000	-1.000000000000000000
12	-1.000000000000000000	-1.000000000000000000	-1.000000000000000000
13	-1.000000000000000000	-1.000000000000000000	-1.000000000000000000
14	-1.000000000000000000	-1.000000000000000000	-1.000000000000000000
15	0.000000000000000000	0.000000000000000000	0.000000000000000000
16	-1.000000000000000000	-1.000000000000000000	-1.000000000000000000
17	0.000000000000000000	0.000000000000000000	0.000000000000000000
18	-1.000000000000000000	-1.000000000003691340	-1.000000000000000000

Table 3.4 Synthesis results for the 8th-order design example (18 decimal places of precision).

We can see that the last $\cos\theta$ for all three representations are very close to one. The last $\cos\theta$ is set to one to make the overall structure lossless. The three frequency plots for the different polynomial representation match the nominal result (not shown separately because all the curves are overlapping and the nominal response is shown in Fig. 3.15). The synthesis results based on all three representations are acceptable.

Next, we quantize the constant terms (it is known that the overall response of a two-port is sensitive to these constants) of h and g to 9 decimal places to determine how inaccuracy in the losslessness condition in the input data affects the synthesis results. The input data is shown in Table 3.5, and Table 3.6 shows the percentage error of $\cos\theta_i$ for the synthesis results. As can be seen, the error grows very rapidly and the last $\cos\theta$ for the coefficient form and DFT-sample form are not close to one, while the zero-form yields a much better result than the other two approaches. If the last $\cos\theta$ is set to one, the frequency response plot is as shown in Fig. 3.15. The frequency response for the coefficient form and DFT-sample form do not match the nominal response. On the other hand, the zero-form gives acceptable results.

f zeros	magnitude	angle / π
constant	0.00090521	0.0
1	1.0	0.430034232
2	1.0	-0.430034232
3	0.0	0.0
4	0.0	0.0
5	1.0	0.320538560
6	1.0	-0.320538560
7	0.0	0.0
8	0.0	0.0

h zeros	magnitude	angle / π
constant	0.938442112	0.0
1	1.0	0.351732711368
2	1.0	-0.351732711368
3	1.0	0.365109796566
4	1.0	-0.365109796566
5	1.0	0.385182448776
6	1.0	-0.385182448776
7	1.0	0.398308216049
8	1.0	-0.398308216049

g zeros	magnitude	angle / π
constant	0.880673596	0.0
1	1.008341527656365750	-0.399341528997245882
2	1.008341527656365750	0.399341528997245882
3	1.008545764020980650	-0.350675396462379855
4	1.008545764020980650	0.350675396462379855
5	1.023795851013025390	-0.364509517733878304
6	1.023795851013025390	0.364509517733878304
7	1.023471807530125960	-0.385806739150357242
8	1.023471807530125960	0.385806739150357242

Table 3.5 8th-order design example with constant term quantized to 9 decimal places.

i	percentage error for $\cos\theta_i$		
	Coefficient Form	DFT-sample Form	Zero Form
1	9.6E-09	9.6E-09	9.6E-09
2	0	0	0
3	1.516E-07	1.516E-07	2.1E-06
4	0	0	0
5	2.3E-07	2.3E-07	6.1E-06
6	0	0	0
7	0.000113	0.000113	0.00118
8	0	0	0
9	0.000135	0.000135	0.00040
10	0.0162	0.0162	0.049
11	0.113	0.113	0.101
12	0.148	0.148	0.172
13	0.128	0.128	0.026
14	1.01	1.01	0.28
15	25	26	3.4
16	56	56	5.0
17	57	57	98
18	51	51	1.3

Table 3.6 Synthesis results (percent error compared to Table 3.2) for the 8th-order design example (constant terms quantized to 9 decimal places).

From the above two examples and many more that have been examined in the course of this research, we observe that the DFT-form and coefficient form always give similar results, and the PU synthesis is extremely sensitive to initial input data. A slight difference in the input data yields completely different results. The proper steps for the PU synthesis are as follows:

1) Assume the given f, g, and h polynomials satisfy the losslessness condition.
2) Attempt PU synthesis using the simplest algorithm, namely the DFT-sample representation.
3) If the last $\cos\theta$ is close to one, the synthesis should give the right solution for the problem, and the frequency response can be used for a consistency check. Goto (6).
4) If the last $\cos\theta$ is not close to one, use the zero-form synthesis algorithm instead. If the zero-form gives a one for the last $\cos\theta$, perform frequency response for a consistency check. Goto (6).

5) If both the DFT-sample and the zero-form algorithm fail, regenerate the input polynomial set by using a zero-finding routine to recalculate one of the polynomials in the Feldkeller equation. Go back to step (1).

6) The solution for the PU synthesis is completed.

Generally, the zero form representation is less efficient, hardest to implement, requires longer synthesis time due to more computations in the zero-finding routine. The coefficient and the DFT-sample representation on the other hand are more efficient and require much shorter synthesis time. However, the zero form representation is fairly insensitive to input data inaccuracy, while the other two representations give unacceptable results for the same input data.

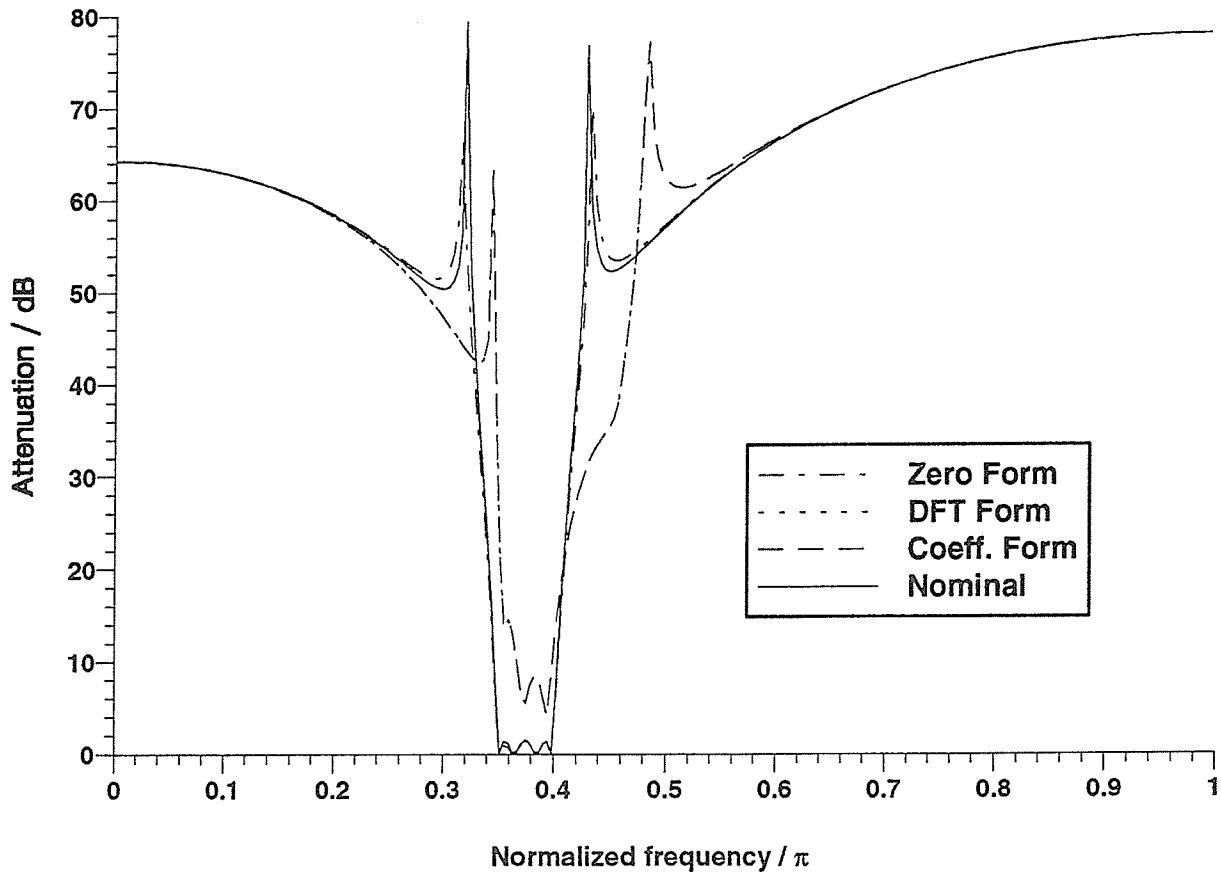

Figure 3.15 Frequency response plots for the 8th-ordered bandpass example.

3.6 Derivation of a general 1st-order complex section with reflection-free load port

In this section, we apply the PU structure synthesis and hope to obtain a 1st-order complex section that will result in a two-port that has a reflection-free load port (port #2), and can be used in the next chapter as a basic building block for the cascade synthesis algorithm.

Starting from basic considerations, the polynomial set that characterizes a general 1st-order complex section with a reflection-free load port (port #2) can take on the following form:

$$f = \gamma e^{jb}\left(z^{-1} - ke^{-j\omega_0}\right) \;,\; g = 1 + Ae^{jc}z^{-1} \;,\; h = Be^{j\alpha} \tag{3.15}$$

where $ke^{-j\omega_0}$ is the location of the transmission zero and all the constants $\{\alpha,\gamma,k,b,c,A,B\}$ are real. In order to induce a reflection-free property on the load port, which is necessary for computability [1], h_* must have a z^{-1} factor which implies that h is a complex constant. Moreover, one coefficient among the f, g and h polynomials can always be fixed [7]. Substituting the above constraints in the losslessness condition $gg_* = hh_* + ff_*$ yields

$$Ae^{jc} = -\gamma^2 ke^{j\omega_0} \quad \text{and} \quad B = \sqrt{\left(1-\gamma^2\right)\left(1-k^2\gamma^2\right)} \tag{3.16}$$

The unimodular constant e^{jb} can always be chosen for convenience by cascading the 1st-order section with a pair of conjugate unimodular multipliers [4]. We chose $e^{jb} = -e^{j\omega_0}$ to eliminate one of the unimodular multipliers generated by the PU cycle and thereby simplify the final realization. It is apparent that there are four degrees of freedom from Eq. (3.15) and Eq. (3.16), and the canonic polynomials are given by

$$f = -\gamma e^{j\omega_0}\left(z^{-1} - ke^{-j\omega_0}\right) \;,\; g = 1 - k\gamma^2 e^{j\omega_0}z^{-1} \;,\; h = \sqrt{\left(1-\gamma^2\right)\left(1-k^2\gamma^2\right)}e^{j\alpha} \tag{3.17}$$

We synthesize a PU structure for the above polynomial set that characterizes a general 1st order complex section using the PU algorithm, with the results shown in Fig. 3.16.

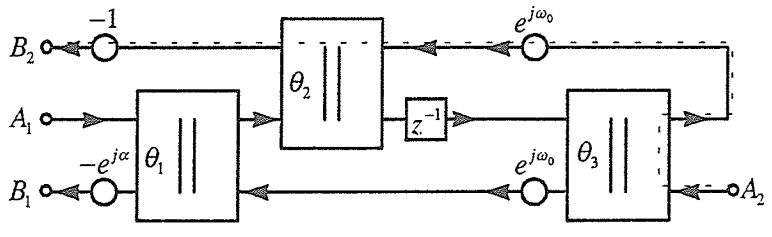

$$\cos\theta_1 = \sqrt{\left(1-\gamma^2\right)\left(1-k^2\gamma^2\right)}$$

$$\cos\theta_2 = \frac{k\gamma}{\sin\theta_1}$$

$$\cos\theta_3 = \frac{k\gamma\sqrt{1-\gamma^2}}{\sin\theta_1}$$

Figure 3.16 Synthesis of a 1st-order complex section with reflection-free port #2 using the PU structure.

However, there is a problem with the circuit in Fig. 3.16. It can be seen clearly that a direct path can be drawn from A_2 to B_2 without any delay in between (see path with the dotted line), which means that the structure is not structurally reflection-free at port #2 and therefore not computable. For computability, every directed loop must have at least one delay [1]. In order to obtain a general 1st order complex section structurally reflection-free at port #2 using the PU algorithm, we interchange ports #1 and #2 and then apply the PU synthesis. The initial polynomial set is given by

$$\begin{aligned}\hat{f} &= \sigma f_* = -\gamma e^{-j\omega_0}\left(1-ke^{j\omega_0}z^{-1}\right)\\ \hat{g} &= g = 1-k\gamma^2 e^{j\omega_0}z^{-1}\\ \hat{h} &= -\sigma h_* = -e^{-j\alpha}\sqrt{\left(1-\gamma^2\right)\left(1-k^2\gamma^2\right)}z^{-1}\end{aligned} \tag{3.18}$$

where σ is initially chosen to be one but is changed to some unimodular value in the final realization in order to simplify that realization, i.e., a circuit with the fewest number of unimodular multipliers fixes its own σ. The circuit resulting from the PU algorithm is shown in Fig. 3.17.

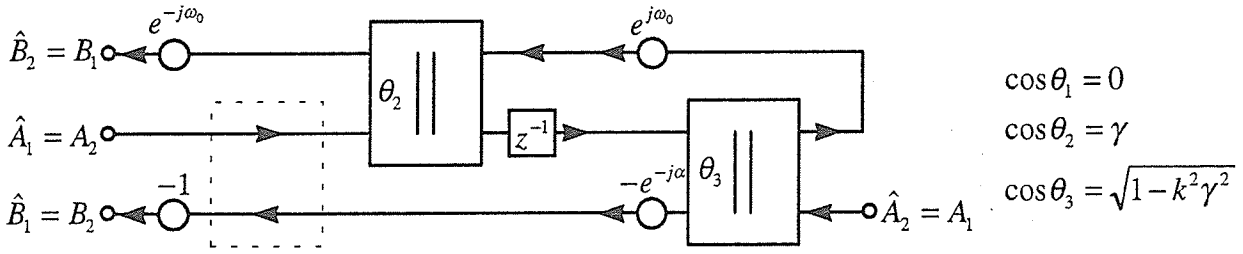

Figure 3.17 Synthesis of the general 1st order complex section with port #1 and #2 interchanged.

By redrawing Fig. 3.17 and applying the normalized 2-port adaptor equivalences from Fig. 2.5-6, we obtain the structure as shown in Fig. 3.18. This structure will be used in the next chapter as a basic extraction block for the cascade synthesis. Note that a delay is imposed between the path from A_2 to B_2 (dotted line), thus making this circuit structurally reflection-free at port #2 and therefore algorithmically computable. The circuit is optimum in the number of unimodular multipliers (there are four degrees of freedom which is the original number) which is accomplished by setting $e^{j\beta} = -e^{j\omega_0}$ and $\sigma = -e^{j(\alpha+\omega_0)}$.

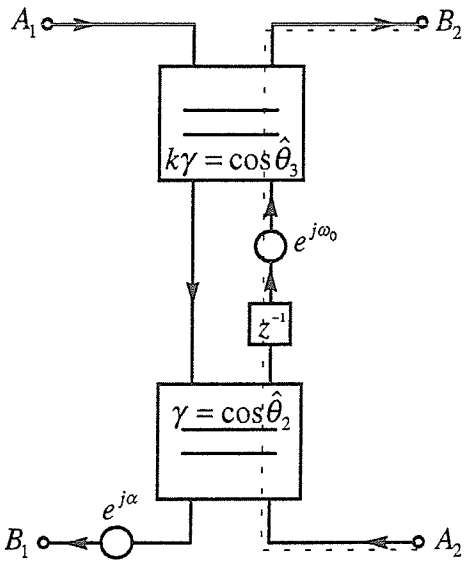

Degrees of Freedom: $\{k,\ \omega_0,\ \alpha,\ \gamma\}$

Canonic Polynomials: $f = -\gamma e^{j\omega_0}(z^{-1} - ke^{-j\omega_0})$

$g = 1 - k\gamma^2 e^{j\omega_0} z^{-1} \qquad h = e^{j\alpha}\sqrt{1-\gamma^2}\sqrt{1-k^2\gamma^2}$

$\sigma = -e^{j(\alpha+\omega_0)}$

Figure 3.18 A CWD circuit for the 1st-order elementary complex section with a transmission zero at $z^{-1} = ke^{-j\omega_0}$.

3.7 Characterization of a General 1st-order Complex Section

As was shown in section 3.6, the canonic polynomial set that characterizes a general 1st-order complex section with a reflection-free load port is given by

$$f = -\gamma e^{j\omega_0}\left(z^{-1} - ke^{-j\omega_0}\right)\ ,\ g = 1 - k\gamma^2 e^{j\omega_0} z^{-1}\ ,\ h = \sqrt{\left(1-\gamma^2\right)\left(1-k^2\gamma^2\right)}e^{j\alpha}\ ,\ \sigma = -e^{j(\alpha+\omega_0)} \quad (3.19)$$

with four degrees of freedom. The reflectance evaluated at the transmission zero yields

$$\frac{h}{g}\left(ke^{-j\omega_0}\right) = \sqrt{\frac{1-\gamma^2}{1-k^2\gamma^2}}e^{j\alpha} \equiv \beta e^{j\alpha} \quad \Rightarrow \quad \gamma = \sqrt{\frac{1-\beta^2}{1-k^2\beta^2}} \qquad (3.20)$$

For a passive (i.e., stable and bounded) reflectance, we have $k \gtrless 1 \Leftrightarrow \beta \gtrless 1$ (see Eq. (2.22)), which implies that $0 < \gamma < 1$. Hence, if the reflectance is known, we can solve for γ and α using Eq. (3.20). For the case $k = 1$, the reflectance in Eq. (3.20) is necessarily unimodular, and we must use Eq. (2.24) and the fact that the return group delays of the overall and the extracted two-port are equal at transmission zeros, i.e.,

$$\frac{g'}{g}\left(e^{-j\omega_0}\right)-\frac{h'}{h}\left(e^{-j\omega_0}\right)=\frac{-\gamma^2}{1-\gamma^2}e^{j\omega_0}\equiv-\delta e^{j\omega_0}\;\Rightarrow\;\gamma=\sqrt{\frac{\delta}{\delta+1}} \tag{3.21}$$

From point (7) in section 2.5, because $\delta>0$, this implies that $0<\gamma<1$.

In summary, the four real numbers $\{k,\ \omega_0,\ \alpha,\ \gamma\}$ fully specify a 1st-order complex section to within unimodular scaling. Parameters α and γ are obtained from the value of the reflectance in Eq. (3.20), and for $k=1$, γ is obtained from the return group delay in Eq. (3.21). These results are summarized in Fig. 3.19a.

Some noteworthy features of the realization in Fig. 3.19a are as follows:

1) The circuit has four degrees of freedom $\{k,\ \omega_0,\ \alpha,\ \gamma\}$, but in practice eight real multipliers are required: $\left\{\gamma,\ \sqrt{1-\gamma^2},\ k\gamma,\ \sqrt{1-k^2\gamma^2},\ \cos\alpha,\ \sin\alpha,\ \cos\omega_0,\ \sin\omega_0\right\}$.

2) The scattering matrix $\mathbf{S}_\gamma$ of a normalized 2-port adaptor can be identified with a Givens planar rotation, i.e.,

$$\mathbf{S}_\gamma=\begin{bmatrix}-\gamma & \sqrt{1-\gamma^2}\\ \sqrt{1-\gamma^2} & \gamma\end{bmatrix}\rightarrow\mathbf{S}_\theta=\begin{bmatrix}-1 & 0\\ 0 & 1\end{bmatrix}\begin{bmatrix}\cos\theta & -\sin\theta\\ \sin\theta & \cos\theta\end{bmatrix}\quad\text{where}\quad\begin{matrix}\cos\theta=\gamma\\ \sin\theta=\sqrt{1-\gamma^2}\end{matrix} \tag{3.22}$$

By separating the signals in Fig. 3.19a into their real and imaginary parts, a circuit with six planar rotations can be derived, as shown in Fig. 3.19b. Although $\mathbf{S}_\gamma$ is lossless, it cannot be maintained so when the two multipliers, say γ and $l\sqrt{1-\gamma^2}$, have been quantized to a finite number of bits. An analog circuit corresponding to a quantized $\mathbf{S}_\gamma$ is shown in Fig. 3.20. Clearly, $\mathbf{S}_\gamma$ is passive ($R>0$) if and only if $l^2<1$ – a condition that is enforced in practice to allow the various nonlinear stability arguments to apply.

3) For the important case of a unit-circle transmission zero ($k=1$), the circuit in Fig. 3.19a simplifies to an equivalent circuit shown in Fig. 3.21. The series adaptor requires only one multiplication and four additions [1] and the pair of inverse multipliers can be ignored in the final realization. Also, the circuit in Fig. 3.21 is a WD equivalent of an analog section used in the Brune cycle [5] but with a reflection-free port on the right.

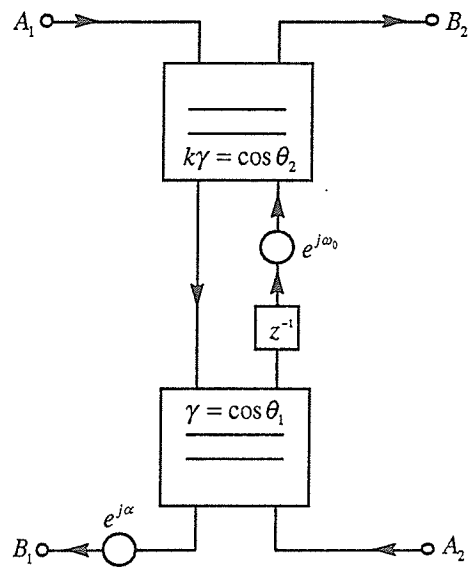

Degrees of Freedom :	$\{k,\ \omega_0,\ \alpha,\ \gamma\}$
Canonic Polynomials :	$f = -\gamma e^{j\omega_0}(z^{-1} - ke^{-j\omega_0})$
	$g = 1 - k\gamma^2 e^{j\omega_0} z^{-1}$ $\quad h = e^{j\alpha}\sqrt{1-\gamma^2}\sqrt{1-k^2\gamma^2}$ $\quad \sigma = -e^{j(\alpha+\omega_0)}$
Reflectance :	$\frac{h}{g}(ke^{-j\omega_0}) = \frac{e^{j\alpha}\sqrt{1-\gamma^2}}{\sqrt{1-k^2\gamma^2}} = \beta e^{j\alpha}$
Stability Relation :	$\beta \gtreqless 1 \Leftrightarrow k \gtreqless 1 \Rightarrow \gamma^2 < 1$
Return Group Delay :	$e^{-j\omega_0}\left(\frac{h'}{h}(e^{-j\omega_0}) - \frac{g'}{g}(e^{-j\omega_0})\right) = \frac{\gamma^2}{1-\gamma^2} = \delta > 0$
Parameter Value :	$(k \neq 1)\quad \gamma = \sqrt{\frac{1-\beta^2}{1-k^2\beta^2}} = \cos\theta_1$
Case:	$(k = \beta = 1)\quad \gamma = \sqrt{\frac{\delta}{\delta+1}}$

(a)

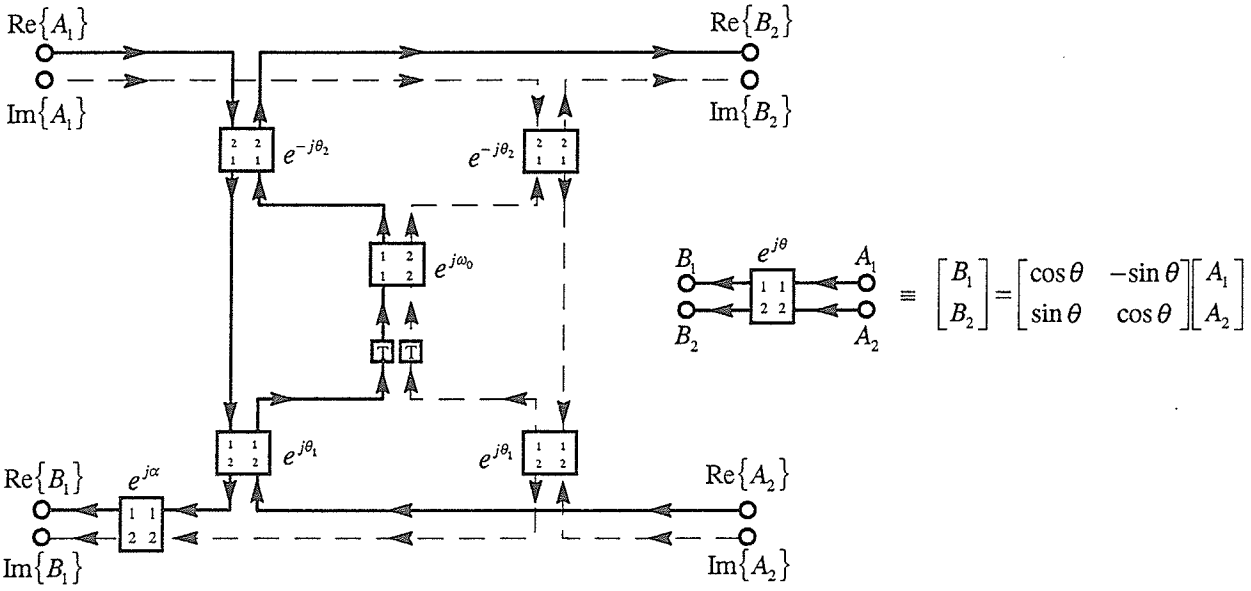

(b)

Figure 3.19 (a) A CWD circuit for the 1st-order elementary complex section with a transmission zero at $z^{-1} = ke^{-j\omega_0}$; (b) an equivalent circuit comprised of rotator operators.

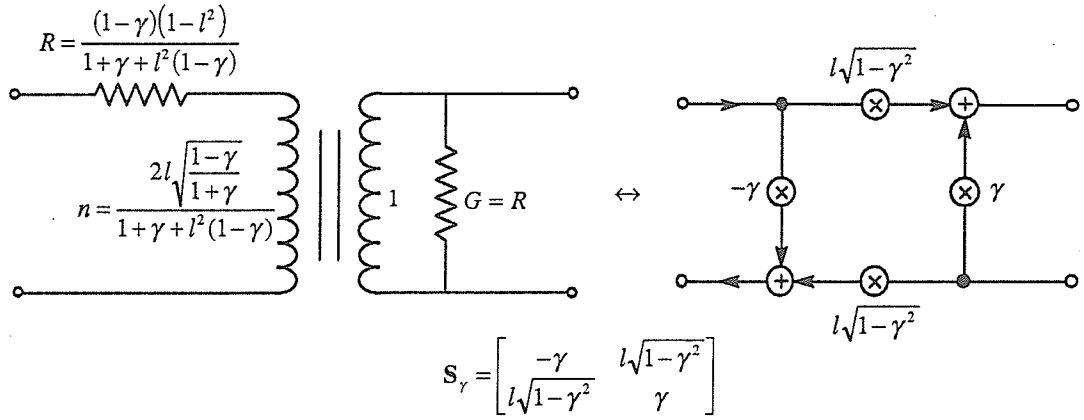

Figure 3.20 Passive ($l^2 < 1$) quantization of the normalized 2-port adaptor.

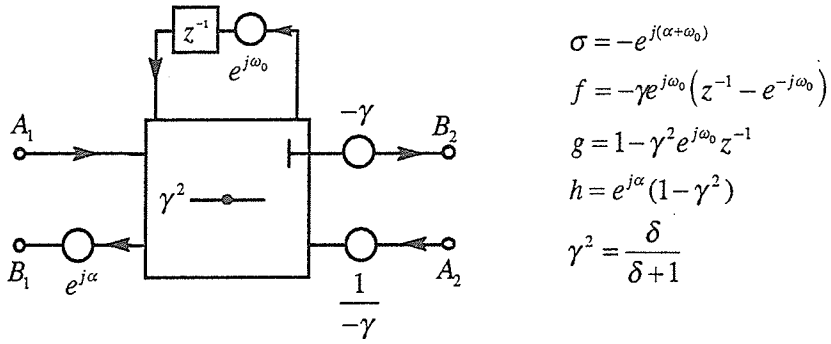

Figure 3.21 An equivalent implementation of Fig. 3.19a (case $k=1$) that uses a 3-port reflection-free series adaptor.

When the eight multipliers in (1) are quantized, the resulting transfer matrix of the circuit in Fig. 3.19a can no longer be put in the lossless form as in Eq. 2.17b. Instead, the transfer matrix is given by

$$\mathbf{T}=\begin{bmatrix}\alpha_1+j\beta_1 & 0\\ 0 & 1\end{bmatrix}\frac{\begin{bmatrix}(a_1^2+b_1^2)(a_2^2+b_2^2)(\omega_1+j\omega_2)z^{-1}-a_1a_2 & -b_1b_2\\ b_1b_2(\omega_1+j\omega_2)z^{-1} & a_1a_2(\omega_1+j\omega_2)z^{-1}-1\end{bmatrix}}{a_1(a_2^2+b_2^2)(\omega_1+j\omega_2)z^{-1}-a_2} \tag{3.23}$$

where $e^{j\alpha}=\alpha_1+j\beta_1$, $e^{j\omega_0}=\omega_1+j\omega_2$, $e^{j\theta_1}=a_1+jb_1$, $e^{j\theta_2}=a_2+jb_2$. The two multipliers associated with each rotation are quantized in a passive way (see (2) above) resulting in four

sources of passivity. For the case $k=1$ ($\theta_1=\theta_2$) realized as in (see (3) above), the transfer matrix is given by

$$\mathbf{T}=\begin{bmatrix}\alpha_1+j\beta_1 & 0\\ 0 & 1\end{bmatrix}\frac{\begin{bmatrix}(\omega_1+j\omega_2)z^{-1}-\gamma^2 & \gamma^2-1\\ (1-\gamma^2)(\omega_1+j\omega_2)z^{-1} & \gamma^2(\omega_1+j\omega_2)z^{-1}-1\end{bmatrix}}{\gamma(\omega_1+j\omega_2)z^{-1}-\gamma} \tag{3.24}$$

with $\gamma=\cos\theta_1$ and there are only two sources of passivity. Note that the location of the transmission zero is directly controlled by the multiplier $\omega_1+j\omega_2$.

CHAPTER IV

SYNTHESIS OF PIPELINEABLE CASCADE COMPLEX WAVE DIGITAL FILTERS

In this chapter, another decomposition algorithm is presented for the synthesis of pipelineable, modular, cascade, complex wave (unitary) digital filters (CWDFs). The main features of the algorithm are the following:

1. The extraction step obviates coefficient-form polynomial arithmetic and zero-finding operations by using an alternative (sample) representation of the canonic polynomials that describe the lossless two-port - an idea that was first introduced for real two-ports in [13];
2. First-order sections that effect pipelineability are treated like any other section (they realize a transmission zero at $z^{-1} = 0$), thus eliminating the need for special treatment;
3. A fully general 1st-order complex section that can realize a "transmission zero" anywhere in the z-plane from Section 3.7 is the only section required for the cascade decomposition.
4. Each transmission zero in the cascade realization can be fine tuned individually because each cascade section realizes a distinct transmission zero.

The algorithm can also be used to synthesize real two-port networks; equivalences are given between a cascade of two complex sections with $ke^{\pm j\omega_0}$ transmission zeros and a 2nd-order real section. Also, a method is presented for investigating coefficient quantization effects directly in the z-domain.

4.1 Decomposition of Complex Lossless Two-Ports

As shown in section 2.6, cascade decomposition amounts to factoring the transfer matrix $\mathbf{T}$

$$\mathbf{T} = \mathbf{T}_i \mathbf{T}_b \tag{4.1}$$

with each factor having the same form and properties as in Eq. (2.17b). Rewriting Eq. (2.27), we have the remainder polynomials given by

$$\sigma_b = \frac{\sigma}{\sigma_i} \quad , \quad f_b = \frac{f}{f_i} \quad , \quad h_b = \frac{g_i h - h_i g}{\sigma_i f_i f_{i*}} \quad , \quad g_b = \frac{g_{i*} g - h_{i*} h}{f_i f_{i*}} \tag{4.2a,b,c}$$

which, by construction, characterize a lower-order lossless (i.e. $g_b g_{b*} = h_b h_{b*} + f_b f_{b*}$) network.

A factorization resulting in a realizable network always exists, as was proved by Fettweis [14] for the $\psi = (z-1)/(z+1)$-domain. However, the mechanics of carrying it out are usually quite involved. Operations such as zero finding, solving a set of simultaneous equations, or having to deal with numerically sensitive coefficient-form polynomials are usually required. However, as was the case for real two-ports, in the process of extracting a complex two-port it is also unnecessary to find h_b and g_b in their order-reduced polynomial form to continue on with the factorization. The process of extraction followed by the determination of the remainder network can be greatly simplified if the h and g as well as h_b and g_b polynomials are given a noncanonic (redundant) representation, called the sample representation [13]. These are defined as follows: we assume that f has $m+1$ factors (transmission zeros), i.e.,

$$f = \prod_{j=1}^{m+1} f_j \quad \text{where} \quad f_j = z^{-1} - z_j^{-1} \quad , \quad z_j \neq 0 \quad , \quad z_{m+1}^{-1} = 0 \tag{4.3}$$

The last factor $f_{m+1} = z^{-1}$ is introduced in order to be able to extract the last zeroth-order section without special treatment. Such a section is shown in Fig. 4.1.

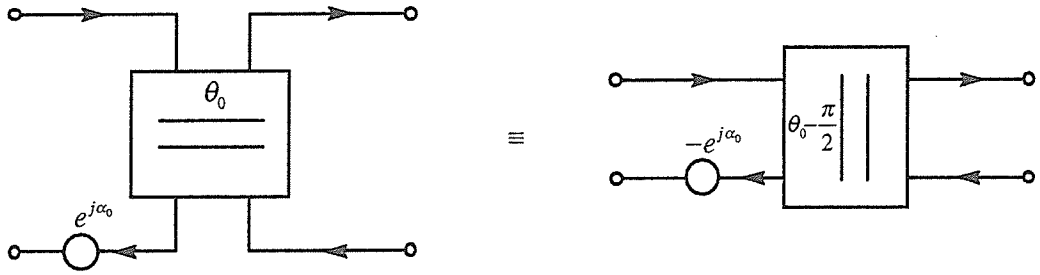

Figure 4.1 Two equivalent elementary sections that realize a zeroth-order section.

For each transmission zero z_j^{-1}, we compute $N = m+1$ samples of h and g located on a circle of radius r centered at z_j^{-1}, i.e.,

$$\left\{h_{jn}:\ h_{jn} \equiv h\left(z_j^{-1} + rW^n\right),\ n = 0(1)m\right\} \quad , \quad \left\{g_{jn}:\ g_{jn} \equiv g\left(z_j^{-1} + rW^n\right),\ n = 0(1)m\right\} \tag{4.4a,b}$$

where $W = e^{j\frac{2\pi}{N}}$. Typically $r = 1$ can be chosen. However, in some rare situations $f_i f_{i*}$ in Eq. (4.2) may become zero at some stage during the extraction. In this case, we have to choose a different r (say $r = 1/2$) and try again. One strategy that eliminates this problem is to always choose r to be less than the Euclidean distance between two nearest transmission zeros. Sample locations for an arbitrary 3rd-order example are shown in Fig. 4.2.

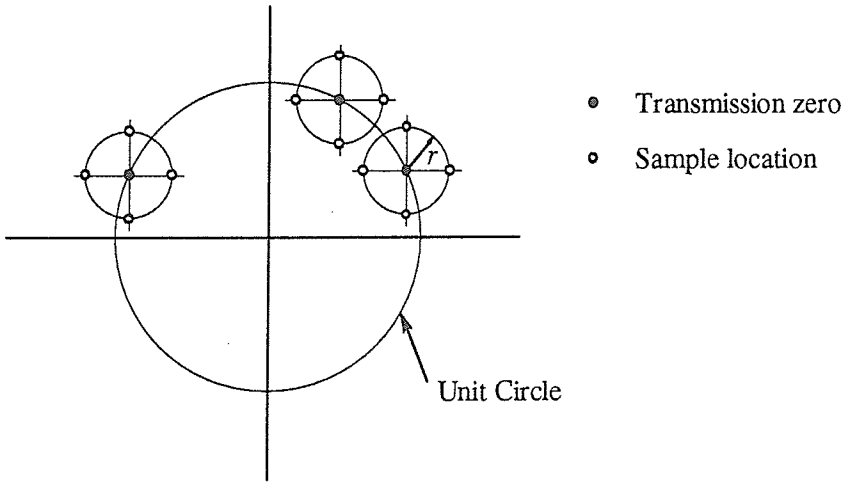

Figure 4.2 Sample locations in the z^{-1} plane for an arbitrary 3rd-order example.

Assume that we have reached the ith extraction step. It will be shown in the next section that the sample sets $\{h_{in}\}$ and $\{g_{in}\}$ together with the transmission zero z_i^{-1}, can be easily transformed to the polynomial set $\{f_i, h_i, g_i, \sigma_i\}$ which characterizes a general 1st-order complex section. Sample sets for the remaining transmission zeros, i.e., $f_b = \sum_{j=i+1}^{m+1} f_j$, are recomputed using Eq. (4.2), i.e.,

$$h_{bjn} = \left[\frac{h_{jn}g_i - g_{jn}h_i}{\sigma_i f_i f_{i*}}\right]_{z^{-1}=z_{jn}^{-1}}, \quad g_{bjn} = \left[\frac{g_{jn}g_{i*} - h_{jn}h_{i*}}{f_i f_{i*}}\right]_{z^{-1}=z_{jn}^{-1}}, \quad j = 1(1)N, \quad n = 0(1)m \tag{4.5}$$

Note that the sample representation of the remainder network is obtained quite easily without polynomial arithmetic (only complex multiplications and divisions are required), which is a consequence of the inherent redundancy in the sample representation.

The form of the recomputation formulae together with the proper choice of $\{f_i,\ h_i,\ g_i,\ \sigma_i\}$ ensure that the sample sets $\{h_{bjn}\}$, $\{g_{bjn}\}$ and the remaining transmission zeros z_j^{-1} describe a lower-order network. Explicit order reduction is unnecessary and further algorithmic simplicity is maintained by allowing the redundancy of the sample sets to grow by keeping their size unchanged. Also, although only sets $j=i+1$ to $j=N$ need to be recomputed at stage i, we choose to recompute all the original sets $(j=1,\ldots,N)$ in order to be able to check the consistency in evaluating the terminating zeroth-order section. The extraction step is depicted in Fig. 4.3.

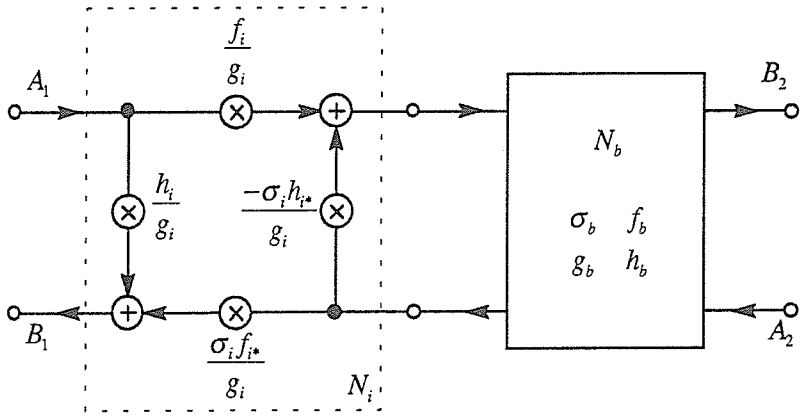

Figure 4.3 Flow graph for cascade (chain) connection of lossless two-ports.

It can be observed that evaluating the overall cascade at the transmission zero z_i^{-1} forces $f_i/g_i=0$, which decouples the remainder network N_b from the overall network. This means that the overall reflectance is equal to the reflectance of section N_i evaluated at z_i^{-1}. Another way of showing this is by rewriting Eq. (4.2b,c) as

$$h_b=\frac{gg_i}{\sigma_i f_i f_{i*}}\left(\frac{h}{g}-\frac{h_i}{g_i}\right),\quad g_b=\frac{gg_{i*}}{f_i f_{i*}}\left(1-\frac{h}{g}\frac{h_{i*}}{g_{i*}}\right) \tag{4.6a,b}$$

and noting that to effect order reduction, the factor $f_i f_{i*}$ must divide the numerators in Eq. (4.2b,c). It follows from Eq. (4.6a) that for $f_i\left(z_i^{-1}\right)=0$, we must have

$$\frac{h}{g}\left(z_i^{-1}\right)=\frac{h_i}{g_i}\left(z_i^{-1}\right)=\frac{g_{i*}}{h_{i*}}\left(z_i^{-1}\right)=\frac{g_*}{h_*}\left(z_i^{-1}\right) \tag{4.7}$$

where the last two equalities follow from the assumed losslessness of the overall and the extracted two-ports. The second equality in Eq. (4.7) ensures that the numerator in Eq. (4.6b) also has the required factor. (Note that we are assuming the usual case that g and f as well as g and f_* are mutually prime.) Applying the definition of paraconjugation $(h_*(z^{-1}) \equiv h^*(z^*)z^{-m}$ where m is the highest degree in the polynomial set) to Eq. (4.7), taking the complex conjugate and reciprocating yields $\frac{h}{g}(z_i^*) = \frac{h_i}{g_i}(z_i^*) = \frac{g_{i*}}{h_{i*}}(z_i^*)$, which implies that the factor f_{i*}, which has a zero at z_i^*, also divides both numerators in Eq. (4.2b,c) without imposing additional constraints.

For the case $z_i^{-1} = e^{-j\omega_i}$, the factor $f_i f_{i*}$ has a 2nd-order zero at $z_i^{-1} = e^{-j\omega_i}$, which means that the 1st-order derivatives with respect to z^{-1} of the numerators and denominators in Eq. (4.2) evaluated at $z_i^{-1} = e^{-j\omega_i}$ must also vanish. This imposes another condition:

$$\frac{g'}{g} - \frac{h'}{h} = \frac{g_i'}{g_i} - \frac{h_i'}{h_i} \quad \text{at} \quad z^{-1} = e^{-j\omega_i} \tag{4.8}$$

which equates the return group delays (see point (7) of section 2.5) of the overall and the extracted two-ports. These two conditions are sufficient in characterizing a 1st-order complex section, as was shown in section 3.7, from which we obtain the required $\{f_i,\ h_i,\ g_i,\ \sigma_i\}$.

To obtain the reflectance and return group delay values from the sample representation, note that it is always possible to express g as

$$g(z^{-1}) = \sum_{i=0}^{N-1} G_i (z^{-1} - z_j^{-1})^i \tag{4.9}$$

where $\{G_i\colon\ i = 0(1)m\}$ are coefficients of the Taylor series expansion about $z^{-1} = z_j^{-1}$. Evaluating Eq. (4.9) at $z_j^{-1} + rW^n$ yields

$$g_{jn} = \sum_{i=0}^{N-1} G_i r^i W^{ni} \tag{4.10}$$

It can be seen that the sets $\{G_i\}$ and $\{g_{jn}\}$ form a DFT pair generalized to radius r. It follows that

$$g\left(z_j^{-1}\right) = G_0 = \frac{1}{N}\sum_{n=0}^{N-1} g_{jn} \quad \text{and} \quad g'\left(z_j^{-1}\right) = G_1 = \frac{1}{rN}\sum_{n=0}^{N-1} g_{jn} W^{-n} \tag{4.11a,b}$$

The same expressions hold for the h polynomial with G_i replaced with H_i.

The remaining proof is to show that h_b/g_b is a stable and bounded reflection coefficient. We can do this by expressing the reflection coefficients as

$$\frac{h}{g}\left(e^{j\omega}\right) = \rho(\omega)e^{j\phi(\omega)} \quad \text{and} \quad \frac{h_i}{g_i}\left(e^{j\omega}\right) = \rho_i(\omega)e^{j\phi_i(\omega)} \tag{4.12a,b}$$

It readily follows from Eq. (4.6a,b) and Eq. (4.12) that for $z = e^{j\omega}$

$$\left|\frac{h_b}{g_b}\right|^2 = \frac{\rho^2 + \rho_i^2 - 2\rho\rho_i\cos(\phi - \phi_i)}{1 + \rho^2\rho_i^2 - 2\rho\rho_i\cos(\phi - \phi_i)} \tag{4.13}$$

Since the magnitudes of normalized reflection coefficients are bounded by one [5], we have $\left(1-\rho^2\right)+\rho^2 \geq \left(1-\rho^2\right)\rho_i^2 + \rho^2 \;\Rightarrow\; 1+\rho^2\rho_i^2 \geq \rho^2 + \rho_i^2$, which together with Eq. (4.13) implies that $\left|h_b/g_b\right| \leq 1$. By construction, we have $g = g_i g_b + \sigma_i h_{i*} h_b$. Therefore on the unit circle, we have $\left|g_i\right| \geq \left|h_i\right| = \left|h_{i*}\right|$, $\left|\sigma_i\right| = 1$, $\left|g_b\right| \geq \left|h_b\right|$ and thus $\left|g_i g_b\right| \geq \left|\sigma_i h_{i*} h_b\right|$. Furthermore by assumption $g \neq 0$ on the unit circle, it follows by the extended Rouché's Theorem [15] that g and $g_i g_b$ have the same number of zeros inside the unit circle in the z^{-1}-plane (namely zero). Therefore g_b has no zeros inside the unit circle, nor on the unit circle since h_b/g_b is bounded there, i.e. g_b has all its zeros outside the unit circle in the z^{-1}-plane and is thus stable.

After m+1 extraction steps when all the transmission zeros have been exhausted, the remaining sample sets $\{h_{jn}\}$ and $\{g_{jn}\}$ characterize a zeroth-order two-port with zero reflection, i.e., the expected values are $h_{jn} = 0$ and $\left|g_{jn}\right| = 1 \quad j = 1(1)N$ and $n = 0(1)m$. In practice, the remaining sample sets will only approximate the expected values to the degree that the input polynomials satisfy the losslessness condition $gg_* = hh_* + ff_*$. It is up to the designer to judge whether the final results are acceptable. In any case, the remainder sets offer a useful consistency check.

4.2 The Cascade Synthesis Algorithm

In summary, the cascade decomposition algorithm is without special cases and is comprised of two steps:

1) From the given h and g polynomials (which can be in either coefficient or zero-form) and the set of transmission zeros $\left\{z_j^{-1} = k_j e^{-j\omega_j},\ j = 1(1)N;\ z_N^{-1} = 0\right\}$, where $N = m+1$, and m being the original order of the filter, compute the sample sets $\{h_{jn}\}$ and $\{g_{jn}\}$ using

$$\left\{h_{jn}:\ h_{jn} \equiv h\left(z_j^{-1} + rW^n\right),\ n = 0(1)m\right\} \quad , \quad \left\{g_{jn}:\ g_{jn} \equiv g\left(z_j^{-1} + rW^n\right),\ n = 0(1)m\right\} \tag{4.14}$$

2) For $i = 1(1)N$, compute $h\left(z_i^{-1}\right)$ and $g\left(z_i^{-1}\right)$ using

$$g\left(z_j^{-1}\right) = G_0 = \frac{1}{N}\sum_{n=0}^{N-1} g_{jn} \qquad \text{and} \qquad h\left(z_j^{-1}\right) = H_0 = \frac{1}{N}\sum_{n=0}^{N-1} h_{jn} \tag{4.15a,b}$$

and if $k_i = 1$, compute $h'\left(z_i^{-1}\right)$ and $g'\left(z_i^{-1}\right)$ also using

$$g'\left(z_j^{-1}\right) = G_1 = \frac{1}{rN}\sum_{n=0}^{N-1} g_{jn} W^{-n} \qquad \text{and} \qquad h'\left(z_j^{-1}\right) = H_1 = \frac{1}{rN}\sum_{n=0}^{N-1} h_{jn} W^{-n} \tag{4.16a,b}$$

From these values, α_i and γ_i are computed using

$$\frac{h}{g}\left(k_i e^{-j\omega_i}\right) = \sqrt{\frac{1-\gamma_i^2}{1-k_i^2\gamma_i^2}}\, e^{j\alpha_i} \equiv \beta_i e^{j\alpha_i} \quad \Rightarrow \quad \gamma_i = \sqrt{\frac{1-\beta_i^2}{1-k_i^2\beta_i^2}} \tag{4.17}$$

and for the case $k = 1$, obtain γ_i by

$$\frac{g'}{g}\left(e^{-j\omega_i}\right) - \frac{h'}{h}\left(e^{-j\omega_i}\right) = \frac{-\gamma_i^2}{1-\gamma_i^2} e^{j\omega_i} \equiv -\delta_i e^{j\omega_i} \quad \Rightarrow \quad \gamma_i = \sqrt{\frac{\delta_i}{\delta_i + 1}} \tag{4.18}$$

From the set $\{k_i,\ \omega_i,\ \alpha_i,\ \gamma_i\}$, we obtain $\{f_i,\ h_i,\ g_i,\ \sigma_i\}$ via

$$\begin{aligned} f_i &= -\gamma_i e^{j\omega_i}\left(z^{-1} - k_i e^{-j\omega_i}\right) \quad , \quad g_i = 1 - k_i\gamma_i^2 e^{j\omega_i} z^{-1} \\ h_i &= \sqrt{\left(1-\gamma_i^2\right)\left(1-k_i^2\gamma_i^2\right)}\, e^{j\alpha_i} \quad , \quad \sigma_i = -e^{j(\alpha_i+\omega_i)} \end{aligned} \tag{4.19}$$

and the recomputed sets $\{h_{bjn}\}$ and $\{g_{bjn}\}$ using

$$h_{bjn} = \left[\frac{h_{jn}g_i - g_{jn}h_i}{\sigma_i f_i f_{i*}}\right]_{z^{-1}=z_{jn}^{-1}}, \quad g_{bjn} = \left[\frac{g_{jn}g_{i*} - h_{jn}h_{i*}}{f_i f_{i*}}\right]_{z^{-1}=z_{jn}^{-1}}, \quad j = 1(1)N \ , \quad n = 0(1)m \tag{4.20}$$

After N iterations, the set $\{k_i,\ \omega_i,\ \alpha_i,\ \gamma_i:\ i = 1(1)N\}$ forms the solution to the decomposition problem, and the structure for the cascade synthesis is shown in Fig. 4.4. The remainder sample sets should be $\{h_{jn} = 0\}$ and $\{|g_{jn}| = 1\}$ and can be used as a check for consistency.

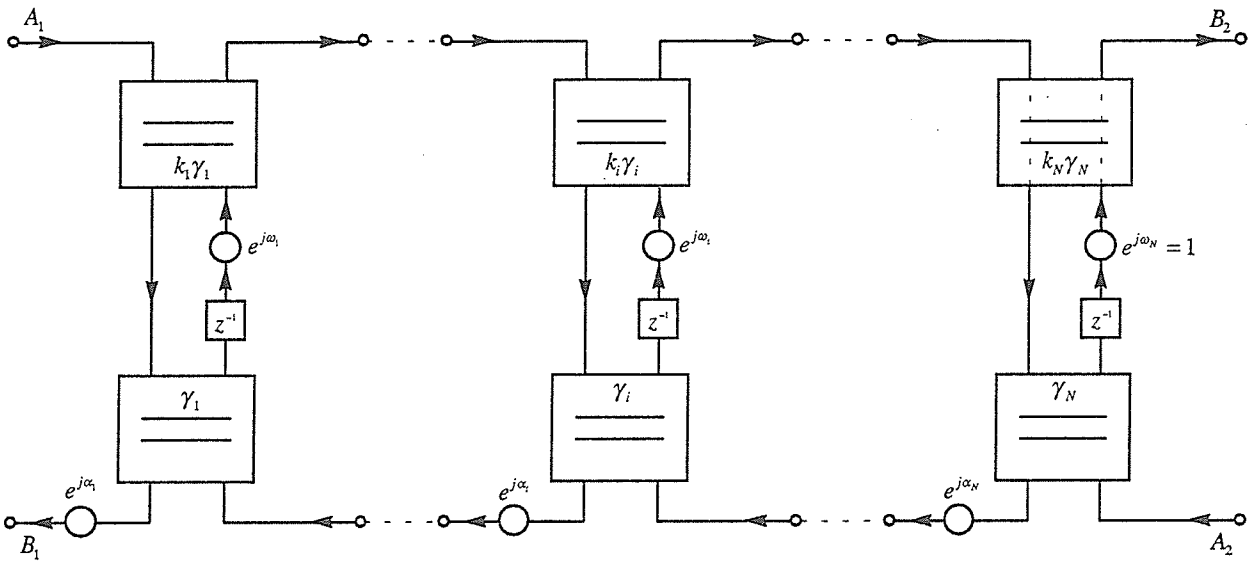

Figure 4.4 The cascade synthesis structure with the cascade of N 1st-order complex sections.

In order to obtain a frequency response of a quantized design, we form the product $\hat{\mathbf{T}} = \prod_{i=1}^{N} \mathbf{T}_i$ where for the case $k \neq 1$:

$$\mathbf{T}_i = \begin{bmatrix} \alpha_{1i} + j\beta_{1i} & 0 \\ 0 & 1 \end{bmatrix} \frac{\begin{bmatrix} (a_{1i}^2 + b_{1i}^2)(a_{2i}^2 + b_{2i}^2)(\omega_{1i} + j\omega_{2i})z^{-1} - a_{1i}a_{2i} & -b_{1i}b_{2i} \\ b_{1i}b_{2i}(\omega_{1i} + j\omega_{2i})z^{-1} & a_{1i}a_{2i}(\omega_{1i} + j\omega_{2i})z^{-1} - 1 \end{bmatrix}}{a_{1i}(a_{2i}^2 + b_{2i}^2)(\omega_{1i} + j\omega_{2i})z^{-1} - a_{2i}} \tag{4.21}$$

with $e^{j\alpha_i} = \alpha_{1i} + j\beta_{1i}$, $e^{j\omega_i} = \omega_{1i} + j\omega_{2i}$, $e^{j\theta_{1i}} = a_{1i} + jb_{1i}$, $e^{j\theta_{i2}} = a_{2i} + jb_{2i}$, and if $k = 1$:

$$\mathbf{T}_i = \begin{bmatrix} \alpha_{1i} + j\beta_{1i} & 0 \\ 0 & 1 \end{bmatrix} \frac{\begin{bmatrix} (\omega_{1i} + j\omega_{2i})z^{-1} - \gamma_i^2 & \gamma_i^2 - 1 \\ (1-\gamma_i^2)(\omega_{1i} + j\omega_{2i})z^{-1} & \gamma_i^2(\omega_{1i} + j\omega_{2i})z^{-1} - 1 \end{bmatrix}}{\gamma_i(\omega_{1i} + j\omega_{2i})z^{-1} - \gamma_i} \tag{4.22}$$

with $\gamma_i = \cos\theta_{1i}$. The coefficients $1/\hat{T}_{22}$ and $\hat{T}_{12}/\hat{T}_{22}$ represent the transmittance and reflectance, respectively. In this way, the more involved time-domain simulations to obtain a frequency response can be avoided.

4.3 Synthesis of Pipelineable Cascades

The critical path for the cascade of 1st-order complex sections with reflection-free ports traverses every section, i.e., the longest computational delay-free path that must be computed before the next input sample can be accepted involves every section (see [18] for a discussion of critical paths and pipelineability). This is unacceptable for a VLSI implementation or a high-sampling-rate multi-DSP realization where the maximum throughput rate must not depend on the filter order. However, it is well known ([1], p. 295-297) that a cascade can be made pipelineable by interposing a "unit element" section or, what is essentially equivalent, a QUARL (see section 2.4), between every two nearest-neighbor sections as shown in Fig. 4.5.

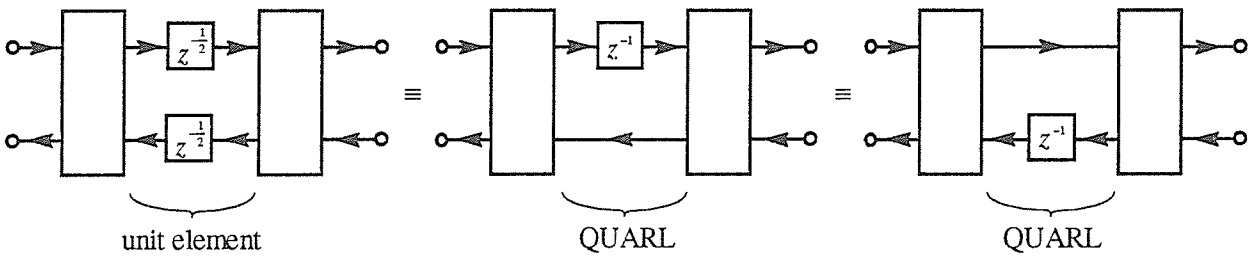

Figure 4.5 Three pipelineable cascades that are equivalent to within a constant group delay in the transmittance.

A given cascade of order m can be made pipelineable by introducing an additional delay of order m-1 (i.e. a factor of z^{-m+1} in the transmittance) at the output port, and then shifting a unit delay to a location between every two original sections, as shown in Fig. 4.6.

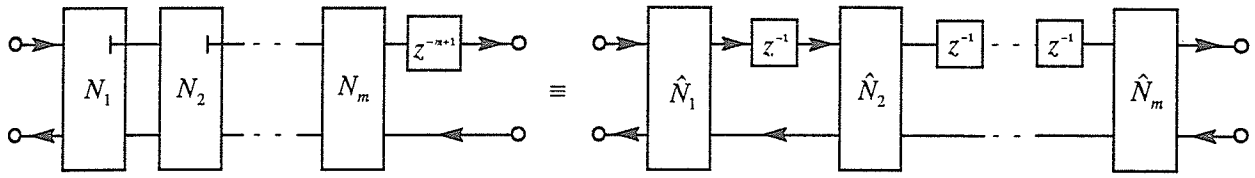

Figure 4.6 Partitioning of a delay block to effect pipelineability.

The shifting process is non-trivial and in practice requires Kuroda's and Levy's transformations [19]. We propose a much simpler solution: we simply treat the additional delay block as a transmission zero at $z^{-1}=0$ of multiplicity $m-1$ and resynthesize the resulting higher-order cascade, i.e., the order of the filter is increased to $2m-1$ and the original f_0 polynomial is replaced with

$$f = z^{-m+1} f_0 \tag{4.23}$$

The h and g polynomials are unchanged. Since the actual sequence of transmission zeros in the final cascade can be chosen arbitrarily, selecting every other zero at $z^{-1}=0$ produces a pipelineable cascade. In this way, no special treatment is necessary to effect pipelineability.

Canonic polynomials for a section that realizes a transmission zero at $z^{-1}=0$ are obtained by substituting $k=\omega_0=0$ into Eq. (3.19), i.e.,

$$f_0 = -\gamma_0 z^{-1} \quad , \quad h_0 = e^{j\alpha_0}\sqrt{1-\gamma_0^2} \quad , \quad g_0 = 1 \quad , \quad \sigma_0 = -e^{j\alpha_0} \tag{4.24}$$

which can be realized with a normalized 2-port adaptor ($\cos\theta_0=\gamma_0$ and $\sin\theta_0=\sqrt{1-\gamma_0^2}$) and a unit delay, as shown in Fig. 4.7.

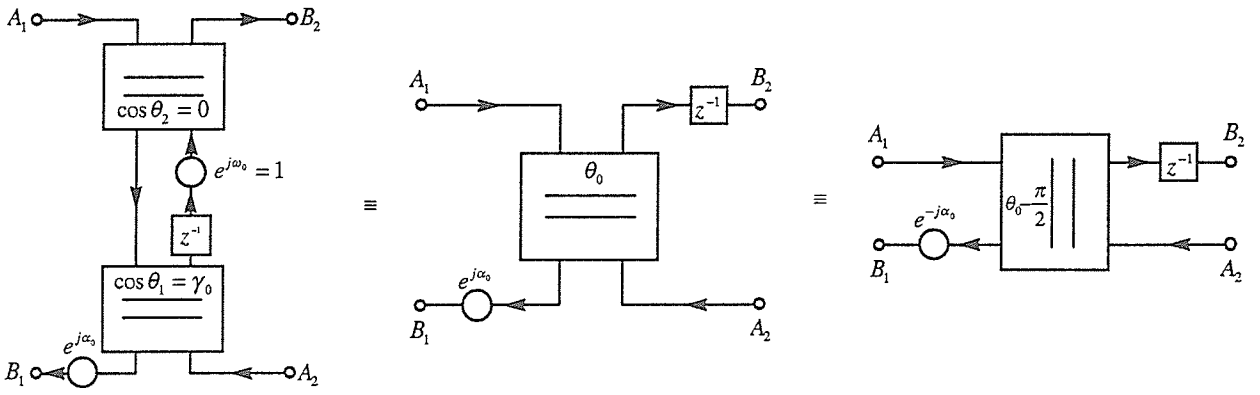

Figure 4.7 Three equivalent sections that realize a transmission zero at $z^{-1}=0$ with $\cos\theta_0=\gamma_0$.

Note that the sections introduced to realize pipelineabe structures do not affect the magnitudes of both scattering coefficients (see Eq. (4.23)) and therefore do not contribute towards the overall attenuation. For this reason, it is preferable to impose the conditions for pipelineability in Eq. (4.23) at the approximation stage so that original sections with transmission zeros at $z^{-1}=0$ do contribute towards filtering.

4.4 Synthesis of Real Circuits using 1st-order Complex Sections

The 1st-order complex section in Fig. 3.19a can be used in the synthesis of real filters by constraining the unimodular multipliers to the four possible real values $e^{j\alpha}=\pm 1$ and $e^{j\omega_0}=\pm 1$. For the case $k=1$, these cover the four possible 1st-order real sections that in the analog domain correspond to a series or parallel connection of a capacitance or an inductance ([13], Table I); if $k\neq 1$, the 1st-order section is nonreciprocal ($\sigma f_* \neq f$) and in the analog domain requires a gyrator ([13], Table IV). For transfer functions with 2nd-order factors comprised of a pair of complex conjugate transmission zeros, the decomposition is performed such that the section with a transmission zero at $ke^{j\omega_0}$ is followed by the section with a conjugate transmission zero $ke^{-j\omega_0}$. The two sections can be replaced with an equivalent real circuit shown in Fig. 4.8, where the additional unimodular multiplier $e^{-j(\alpha+\alpha_2)}$ must be borrowed from the section that comes next in order to make the overall $\sigma=1$. For real filters, after all the conjugate pairs have been grouped into 2nd-order real sections, only unimodular multipliers equal to ± 1 remain in the cascade.

The 2nd-order real circuit in Fig. 4.8 was derived using the same method as was used for the circuit in Fig. 3.19a and outlined in section 3.6, i.e., the derivation is a cascade decomposition problem based on the zeros of h_* which, for this case, are necessarily real and given by $h_* = cz^{-1}\left(z^{-1}+k_1\right)$. The known 1st-order solution in Fig. 3.19a is used in the extraction of the two 1st-order factors resulting in the following factored form of the scattering hybrid matrix:

$$\mathbf{H}=\frac{\begin{bmatrix}1 & z\cos\theta_0\\ \cos\theta_0 & z\end{bmatrix}}{\sin\theta_0}\frac{\begin{bmatrix}-\left(z^{-1}+\cos\theta_1\cos\theta_2\right) & \sin\theta_1\sin\theta_2\\ -z^{-1}\sin\theta_1\sin\theta_2 & z^{-1}\cos\theta_1\cos\theta_2+1\end{bmatrix}}{z^{-1}\cos\theta_1+\cos\theta_2}\frac{\begin{bmatrix}1 & -\cos\theta_3\\ -\cos\theta_3 & 1\end{bmatrix}}{\sin\theta_3} \tag{4.25}$$

The real circuit in Fig. 4.8 follows readily from the above factored **H**.

A 2nd-order real section with $f\left(ke^{\pm j\omega_0}\right)=0$ has the same four degrees of freedom $\{k,\ \omega_0,\ \alpha,\ \gamma\}$ as a 1st-order complex section in Fig. 3.19a. However, for the former, these cannot be chosen completely arbitrarily because the two auxiliary parameters $\cos\omega_1$ and $\cos\omega_2$ as defined in Fig. 4.8 must be bounded by one. There are of course no restrictions for a complex 2nd-order section.

For quantized designs, each 2-port adaptor in the real circuit in Fig. 4.8 is quantized passively according to Fig. 3.19. For $k=1$, there are two cases where this circuit can be converted to a structurally lossless voltage-wave circuit with transmission zeros that do not move away from the unit circle even for quantized multipliers:

1) case 1: $\sin\alpha=0 \Rightarrow \cos\theta_1=\pm1$ corresponds to a series or parallel resonant circuit section (Table II in [13]);

2) case 2: $\sin(\alpha-\omega_0)=0 \Rightarrow \cos\theta_2=\pm1$ corresponds to the matched 4-port adaptor (Fig. 5 in [13]), which was used extensively in the designs presented in [20].

For other cases, the 2-port adaptors corresponding to θ_1 and θ_2 must be quantized $\left(e^{j\theta_1}=a_1+jb_1\ ,\ e^{j\theta_2}=a_2+jb_2\right)$ passively, causing the pair of transmission zeros to move away from the unit circle; by substituting Eq. (3.23) for each factor of $\mathbf{H}$ in Eq. (4.25), it can be shown that the resulting radius of the pair of transmission zeros in the z-plane is given by $\sqrt{\left(a_1^2+b_1^2\right)\left(a_2^2+b_2^2\right)}<1$.

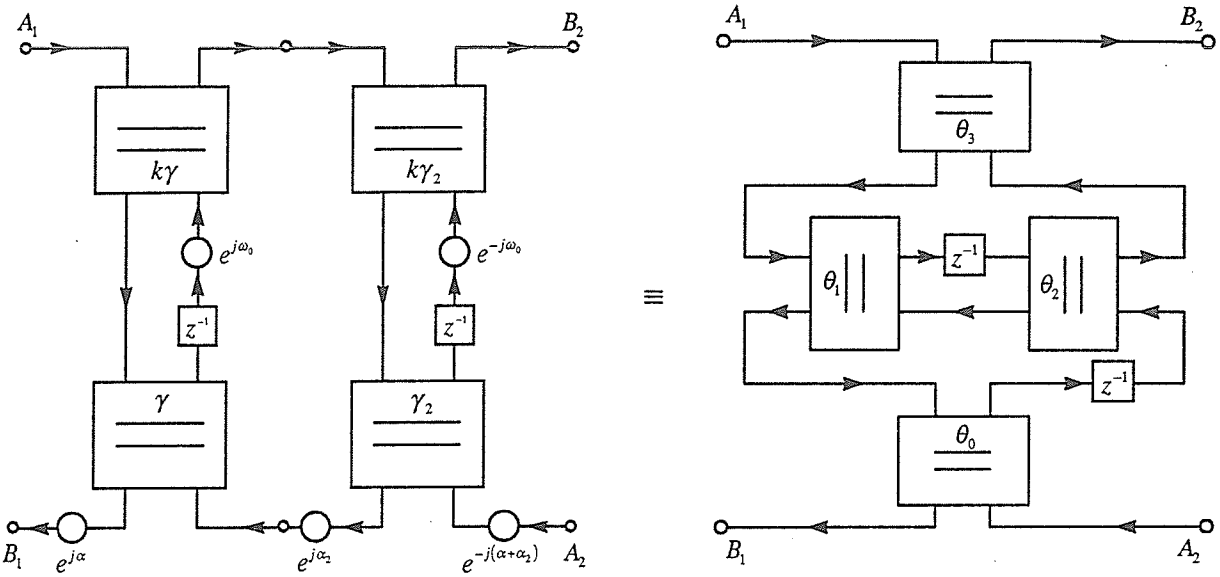

Degrees of Freedom: $\{k,\ \omega_0,\ \alpha,\ \gamma\}$

Transmittance: $\dfrac{f}{g}(ke^{\pm j\omega_0}) = 0$

Reflectance: $\dfrac{h}{g}(ke^{-j\omega_0}) = \dfrac{e^{j\alpha}\sqrt{1-\gamma^2}}{\sqrt{1-k^2\gamma^2}} \equiv \beta e^{j\alpha}$

Group Delay: $e^{-j\omega_0}\left(\dfrac{h'}{h}\left(e^{-j\omega_0}\right) - \dfrac{g'}{g}\left(e^{-j\omega_0}\right)\right) = \dfrac{\gamma^2}{1-\gamma^2} \equiv \delta$

Parameter: $(k \neq 1)\ \gamma = \sqrt{\dfrac{1-\beta^2}{1-k^2\beta^2}}$, $(k = \beta = 1)\ \gamma = \sqrt{\dfrac{\delta}{\delta+1}}$

Stability Relation: $\beta \gtreqless 1 \Leftrightarrow k \gtreqless 1 \Rightarrow \gamma^2 < 1$

$$f = z^{-2}\cos\theta_0 + \frac{(a-b)}{2}z^{-1} + \cos\theta_3$$

$$g = z^{-2}\cos\theta_0\cos\theta_3 + \frac{(a+b)}{2}z^{-1} + 1$$

$$h = -\sin\theta_0\sin\theta_3\left(z^{-1}\cos\theta_2 + \cos\theta_1\right)$$

$$\sigma = 1$$

$$a = \left(1+\cos\theta_0\right)\left(1+\cos\theta_3\right)\cos\left(\theta_1-\theta_2\right)$$

$$b = \left(1-\cos\theta_0\right)\left(1-\cos\theta_3\right)\cos\left(\theta_1+\theta_2\right)$$

Auxilliary Parameters:

$$\cos\omega_1 = \frac{\sqrt{\left(1-\gamma^2\right)\left(1-k^2\gamma^2\right)}}{k\gamma^2}\frac{\sin\alpha}{\sin\omega_0}$$

$$\cos\omega_2 = \sqrt{\left(1-\gamma^2\right)\left(1-k^2\gamma^2\right)}\frac{\sin\left(\alpha-\omega_0\right)}{\sin\omega_0}$$

$$\beta_0 = \gamma^2\frac{\sin\omega_1}{\sin\omega_2}, \qquad \beta_1 = -\frac{\tan\omega_2}{\tan\omega_1}$$

$$k_1 \equiv \frac{k_{1N}}{k_{1D}} = \frac{\left(1+k^2\right)\cos\omega_1 - 2k\cos\omega_0\cos\omega_2}{\left(1+k^2\right)\cos\omega_2 - 2k\cos\omega_0\cos\omega_1}$$

Circuit Parameters:

$$\cos\theta_0 = \beta_0, \qquad \sin\theta_0 = \sqrt{1-\beta_0^2}$$

$$\cos\theta_1 = sgn\left(k_{1D}\right)\sqrt{\frac{1-\beta_1^2}{1-k_1^2\beta_1^2}}, \qquad \sin\theta_1 = \beta_1\sin\theta_2$$

$$\cos\theta_2 = k_1\cos\theta_1, \qquad \sin\theta_2 = \sqrt{\frac{1-k_1^2}{1-k_1^2\beta_1^2}}$$

$$\cos\theta_3 = k^2\beta_0, \qquad \sin\theta_3 = \sqrt{1-k^4\beta_0^2}$$

$$\gamma_2 = \gamma\frac{\sin\omega_1}{\sin\omega_2}, \qquad \tan\left(\alpha+\alpha_2\right) = \frac{-\beta\sin\alpha\sin^2\omega_2}{\beta\cos\alpha\left(1+\cos^2\omega_2\right)+\left(1+\beta^2\right)\cos\omega_2}$$

Figure 4.8 An equivalence between a real 2nd-order section and a cascade of two 1st-order complex sections used in the synthesis of real two-ports.

CHAPTER V

DESIGN EXAMPLES

In this chapter, we present two design examples to show how the PU and the cascade structures derived in the previous chapters differ in their sensitivities to multiplier quantizations. Also the difference between transmittance and reflectance realizations for the two structures are examined.

5.1 The Computer Synthesis Programs

Two programs were written to implement the PU and cascade synthesis algorithm discussed in Chapter IV and V. The first version of the programs were developed with *THINK Pascal* using a *Macintosh* computer. Later, we translated all the programs to the more popular C++ compiler (Borland C++ 3.1) for use on IBM compatibles, which allowed more flexible coding and faster run time; note that the *Macintosh* does not yet have a good C++ compiler. The main features of the C++ compiler are object-oriented programming and the use of overriding operators (which in our case are ideal for complex number computations and polynomial operations). However, in order to be able to translate the programs so that they can be run under the *Macintosh* environment again, we tried to keep the structure of the C++ program more or less the same as the Pascal structure. In this way, we gave up some of the C++'s features, such as the object oriented data structure and memory management. A future version of the synthesis programs can be rewritten so that one can fully utilize the special features that the C++ offers. Appendix I shows the program listing and the required modules for each synthesis algorithm.

5.2 Example of a 3rd-order complex bandpass filter

The first example is a 3rd-order complex bandpass filter taken from [16] with the canonic polynomials given in Table 5.1, which satisfy the Feldkeller equation up to 7 decimal places.

f zeros	magnitude	angle / π
constant	0.001737179447817836	0.117376125505971182
1	1.239539805592213030	-0.352501728592457791
2	6.557134474620700520	-0.328283677132877787
3	0.973790267085636388	-0.381385815807027759

h zeros	magnitude	angle / π
constant	0.957560092196136287	0.0
1	1.0	-0.346153406900000000
2	1.0	-0.318835734100000000
3	1.0	-0.364351183000000000

g zeros	magnitude	angle / π
constant	0.916945088461950131	0.029341177711460338
1	1.034058128195634690	-0.315274223865586351
2	1.012472723813572680	-0.366322028770513232
3	1.041665754372504750	-0.347744925075360753

Table 5.1 Input data for Example 1 (3rd-order complex bandpass filter).

In this example, we synthesize the filter design using the PU, cascade, and pipeline cascade structure based on the transmittance and the reflectance, which behave differently for quantized multipliers (say 8 and 12-bit fixed-point multipliers). The cascade realization was made pipelineable by including a factor of z^{-2} in the transmittance polynomial (i.e. a zero at zero was inserted between the original transmission zeros). Since the order of this example is low, the DFT form synthesis for the PU structure gives satisfactory results immediately. The synthesis results for the transmittance realization are shown in Table 5.2-4, while the results for the reflectance realization are shown in Table 5.5-7, and the corresponding frequency responses are shown in Fig. 5.1 and Fig. 5.2. Note that the last $\cos\theta$ for the PU structure is set to one in order to obtain the frequency response.

i	$\cos\theta_i$	α_i/π
1	0.957560092196136284	-1.029340324000000000
2	0.047702365227116112	-0.944795096026392233
3	0.998252323578017612	-0.662120015435535012
4	0.101258976212685513	-0.219828231895825287

i	$\cos\theta_i$	α_i/π
5	0.994213470521244201	-0.657890528088391118
6	0.914671540879312931	-1.099229713497030090
7	0.314089092630529918	-0.856204400044218755
8	1.000052259810128780	-0.618772101296679698

Table 5.2 PU decomposition (DFT form) of the transmittance in Example 1.

i	k_i	ω_i/π	α_i/π	γ_i
1	1.239539805592213030	0.352501728592457791	-0.007554520086119123	0.702186819200128202
2	6.557134474620700520	0.328283677132877787	-0.034346625663405575	0.017397516345624240
3	0.973790267085636388	0.381385815807027759	0.014022008605176070	0.493353755831878257
4	0.000000000000000000	-0.000000000000000000	-0.034292388950355955	0.288234768028050422

Table 5.3 Cascade decomposition of the transmittance in Example 1.

i	k_i	ω_i/π	α_i/π	γ_i
1	1.239539805592213030	0.352501728592457791	-0.007554520086119123	0.702186819200128202
2	0.000000000000000000	-0.000000000000000000	-0.034334469553297889	0.097008412983706725
3	6.557134474620700520	0.328283677132877787	0.334466150955358439	0.026746097875690607
4	0.000000000000000000	-0.000000000000000000	-0.198164735784138883	0.993718832468785005
5	0.973790267085636388	0.381385815807027759	-0.618612584688495089	0.959510569853113821
6	0.000000000000000000	-0.000000000000000000	0.771458197438752087	0.999999999658423781

Table 5.4 Pipeline cascade decomposition of the transmittance in Example 1.

i	$\cos\theta_i$	α_i/π
1	0.013749429560620272	-0.944795096026392155
2	0.957650616873348732	-1.029340324000000000
3	0.044911105023321488	-1.703913039917487880
4	0.998266759706849972	-0.662034192868882767

i	$\cos\theta_i$	α_i/π
5	0.125031401481845955	-1.905102041047098000
6	0.999041925272336434	-0.661111605934160362
7	0.257799610181693932	-0.060694688027939839
8	1.000061695049873170	-0.647604579668720350

Table 5.5 PU decomposition (DFT form) of the reflectance in Example 1.

i	k_i	ω_i/π	α_i/π	γ_i
1	0.999999999999999999	0.346153406900000000	-0.437655461608194876	0.982002232690002730
2	1.000000000000000000	0.318835734100000000	-0.994411503132108745	0.981883899110585982
3	1.000000000000000000	0.364351183000000000	-0.490218658092795872	0.993102509757900023
4	0.000000000000000000	-0.000000000000000000	0.010321414550335327	0.999998491102605074

Table 5.6 Cascade decomposition of the reflectance in Example 1.

i	k_i	ω_i/π	α_i/π	γ_i
1	0.999999999999999999	0.346153406900000000	-0.437655461608194876	0.982002232690002730
2	0.000000000000000000	-0.000000000000000000	0.881991690073898222	0.999225710850659453
3	1.000000000000000000	0.318835734100000000	-0.547726739041740092	0.982527313002204999
4	0.000000000000000000	-0.000000000000000000	-0.454579847453955521	0.999908673582472656
5	1.000000000000000000	0.364351183000000000	-0.635648815150041211	0.993310427856011198
6	0.000000000000000000	-0.000000000000000000	-0.396600428027263030	1.000000000000000000

Table 5.7 Pipeline cascade decomposition of the reflectance in Example 1.

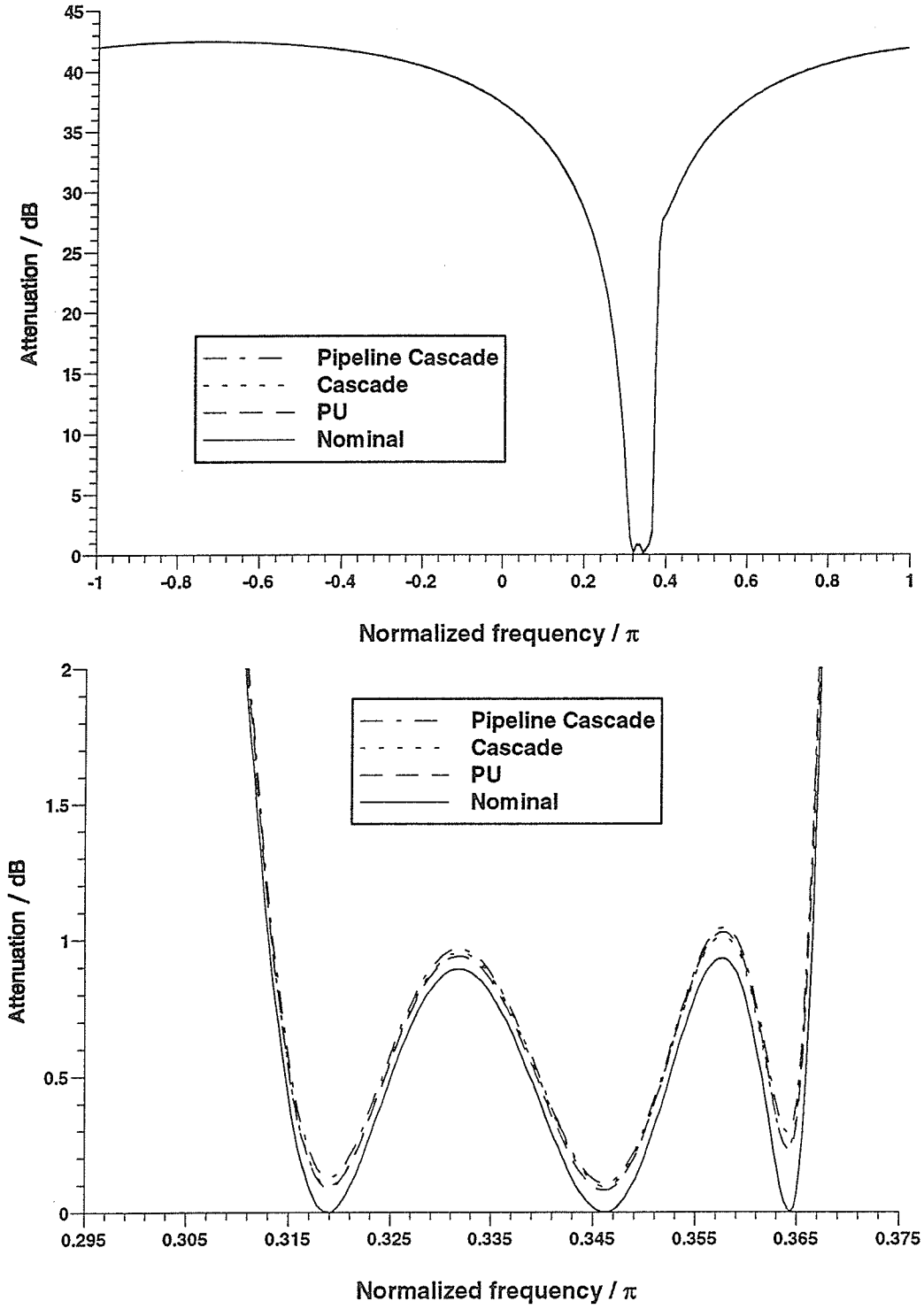

Figure 5.1 Frequency responses of the transmittance for Example 1 with 12-bit fixed-point multipliers; stopband (top) and passband (bottom).

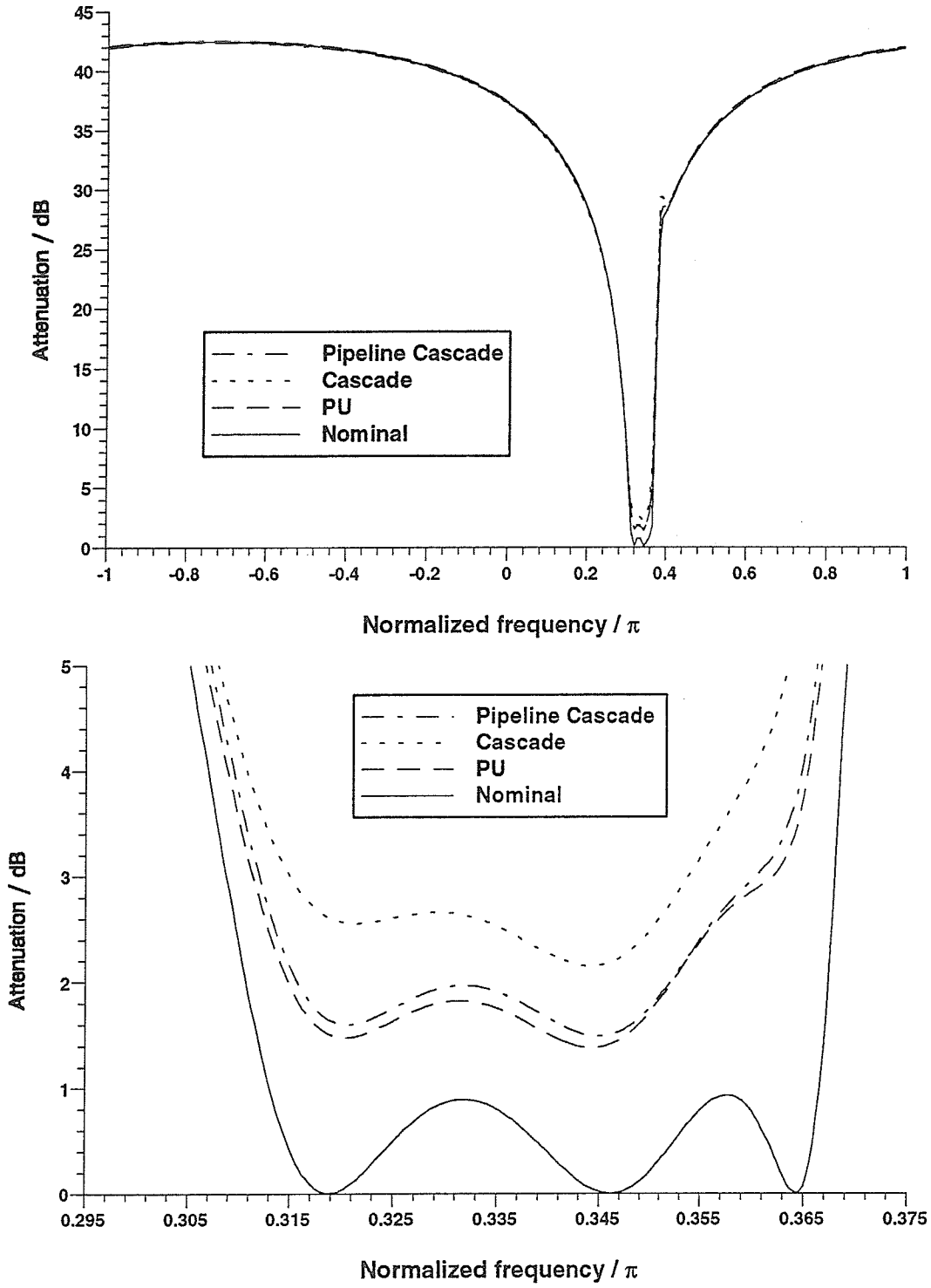

Figure 5.2 Frequency responses of the transmittance for Example 1 with 8-bit fixed-point multipliers; stopband (top) and passband (bottom).

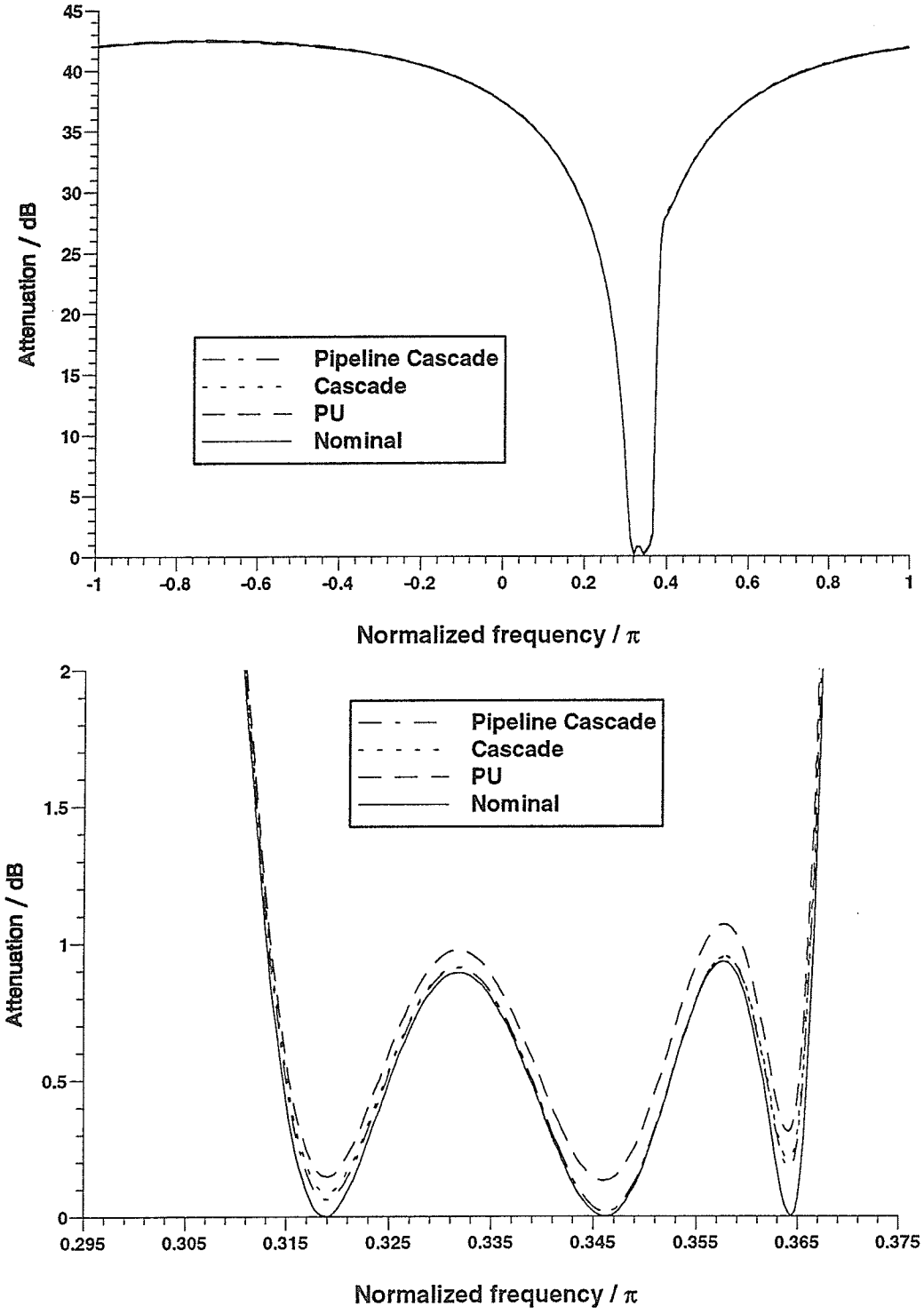

Figure 5.3 Frequency responses of the reflectance for Example 1 with 12-bit fixed-point multipliers; stopband (top) and passband (bottom).

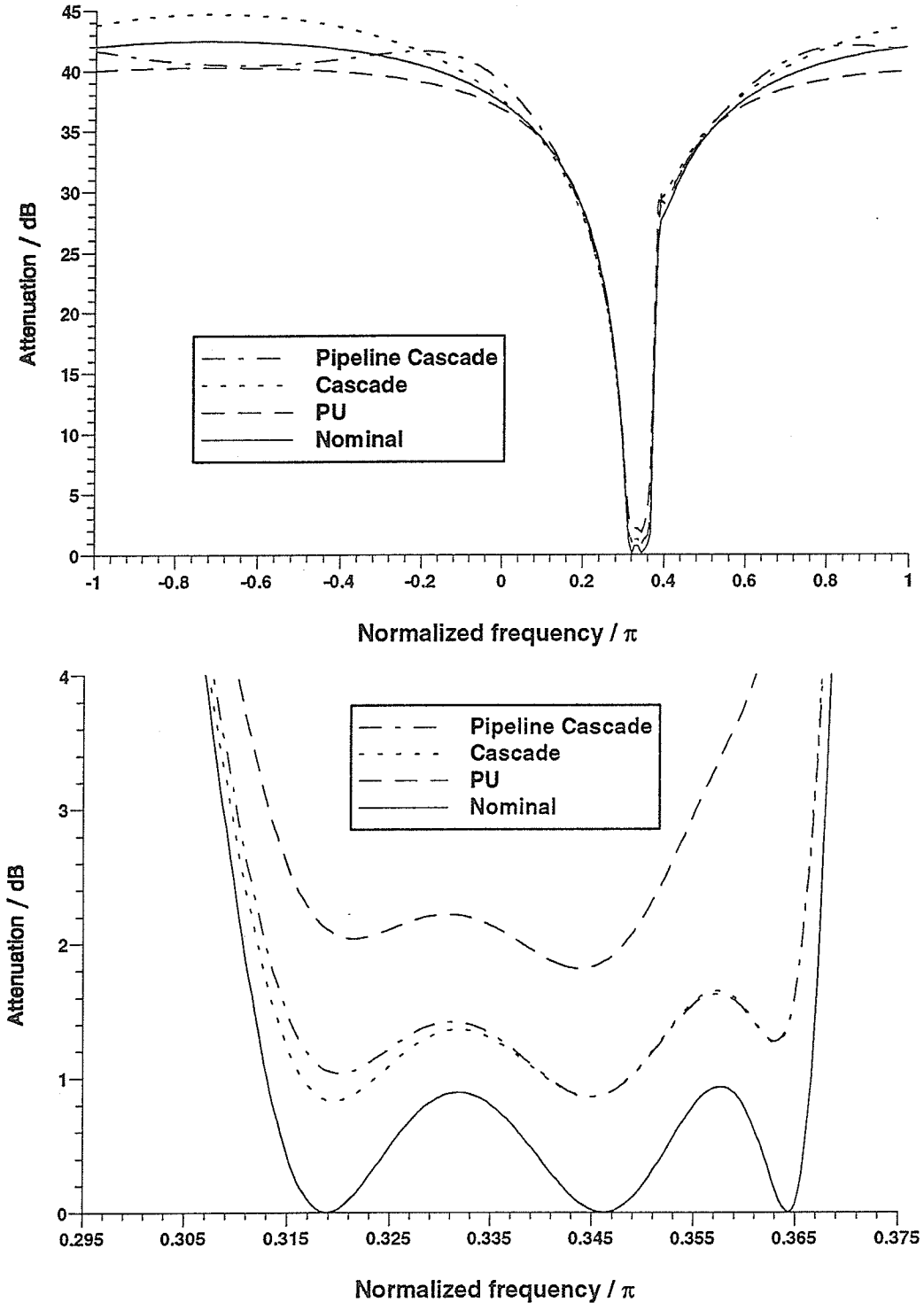

Figure 5.4 Frequency responses of the reflectance for Example 1 with 8-bit fixed-point multipliers; stopband (top) and passband (bottom).

5.3 Example of an 8th-order real bandpass filter

The second example is a real 8th-order bandpass filter taken from [21], and the canonic polynomials are recomputed to better satisfy the losslessness condition $gg_* = hh_* + ff_*$. The canonic polynomials are shown in Table 5.8, which satisfy the Feldkeller equation up to 15 decimal places.

f zeros	magnitude	angle / π
constant	0.00090521	0.0
1	1.0	0.430034232
2	0.0	0.0
3	1.0	-0.430034232
4	0.0	0.0
5	1.0	0.320538560
6	0.0	0.0
7	1.0	-0.320538560
8	0.0	0.0

h zeros	magnitude	angle / π
constant	0.938442111704	0.0
1	1.0	0.351732711368
2	1.0	-0.351732711368
3	1.0	0.365109796566
4	1.0	-0.365109796566
5	1.0	0.385182448776
6	1.0	-0.385182448776
7	1.0	0.398308216049
8	1.0	-0.398308216049

g zeros	magnitude	angle / π
constant	0.880673595637835194	0.0
1	1.008341527656365750	-0.399341528997245882
2	1.008341527656365750	0.399341528997245882
3	1.008545764020980650	-0.350675396462379855
4	1.008545764020980650	0.350675396462379855
5	1.023795851013025390	-0.364509517733878304
6	1.023795851013025390	0.364509517733878304
7	1.023471807530125960	-0.385806739150357242
8	1.023471807530125960	0.385806739150357242

Table 5.8 Input data for Example 2 (8th-order bandpass filter).

We can see that the input data for the transmittance is pipelineable from the outset for the cascade synthesis structure, where a factor of z^{-7} is introduced to make the reflectance pipelineable.

Transferring a factor of z^{-2} from the f to the f_* polynomial has no effect on the magnitude response and allows one to write $gg_* = h^2 + f^2 = (h + jf)(h - jf)$. It follows that a realization with a complex allpass section [22], [23], [24] of order four is also possible in this case. The

cascade synthesis is used to generate the required allpass section, and the input data is given in Table 5.9. Note that the zeros of h are reciprocal conjugates of those of g and the constants remain the same. The zeros of f can be chosen to be anywhere in the z^{-1}-plane but are normally chosen to be at $z^{-1}=0$ to generate a pipelineable cascade comprised of sections from Fig. 4.13 with the fewest number of rotations. The transmittance at frequency $z=e^{j\omega T}$ for the allpass section is given by $\frac{1}{2}\left(\frac{h}{g}(z)+\left(\frac{h}{g}(z^{-1})\right)^{*}\right)$ and the reflectance is $\frac{1}{2}\left(\frac{h}{g}(z)-\left(\frac{h}{g}(z^{-1})\right)^{*}\right)$.

f zeros	magnitude	angle / π
constant	0.0	0.0
1	0.0	0.0
2	0.0	0.0
3	0.0	0.0
4	0.0	0.0

h zeros	magnitude	angle / π
constant	0.938442111704000000	0.0
1	0.991727477816218162	0.399341528997245882
2	0.976757230467890762	0.364509517733878304
3	0.991526647252069689	-0.350675396462379855
4	0.977066483553886195	-0.385806739150357242

g zeros	magnitude	angle / π
constant	0.880673595637835194	0.0
1	1.00834152765636575	0.399341528997245882
2	1.00854576402098065	-0.350675396462379855
3	1.02379585101302539	0.364509517733878304
4	1.02347180753012596	-0.385806739150357242

Table 5.9 Input data for the 4th-order allpass section for Example 2.

Again, we synthesize the filter design using the PU, allpass, cascade, and pipeline cascade structure based on the transmittance and the reflectance. The synthesis results for the transmittance realization are shown in Table 5.10-13, whereas the results for the reflectance realization are shown in Table 5.14-16. The corresponding frequency responses for the 12-bit and 8-bit fixed-point multiplier quantizations are shown in Fig. 5.5-8.

i	$\cos\theta_i$	α_i/π
1	0.938442110231743405	-1.000000000000000000
2	0.000000000000000000	-1.000000000000000000
3	0.382034996637063172	-1.000000000000000000
4	0.000000000000000000	-1.000000000000000000
5	0.994879530326316629	-1.000000000000000000
6	0.000000000000000000	-1.000000000000000000
7	0.383096500999037531	-1.000000000000000000
8	0.000000000000000000	-1.000000000000000000
9	0.995858180702111374	-1.000000000000000000

i	$\cos\theta_i$	α_i/π
10	0.334065090668604390	-1.000000000000000000
11	0.360640861948289544	-1.000000000000000000
12	0.136479907865855847	-1.000000000000000000
13	0.932253262432831888	-1.000000000000000000
14	0.955467770404646774	-1.000000000000000000
15	0.140971139638418803	0.000000000000000000
16	0.402851064656629980	-1.000000000000000000
17	0.011855556196062364	0.000000000000000000
18	1.000000147786428040	-0.999999999978592176

Table 5.10 PU decomposition (DFT form) of the transmittance in Example 2.

i	k_i	ω_i/π	α_i/π	γ_i
1	1.000000000000000000	-0.430034232000000000	-0.129995225362160160	0.856902177327104619
2	1.000000000000000000	0.430034232000000000	0.329520485855107430	0.868905766082042025
3	0.000000000000000000	-0.000000000000000000	-0.199525260492946962	0.140573525501269946
4	0.000000000000000000	-0.000000000000000000	0.000000000000020977	0.921151940506531020
5	0.999999999999999999	-0.320538560000000000	0.007661338926213817	0.385108082381287339
6	0.999999999999999999	0.320538560000000000	-0.112061798322700076	0.755622704188970229
7	0.000000000000000000	-0.000000000000000000	0.104400459397340899	0.101067898652071465
8	0.000000000000000000	-0.000000000000000000	0.000000000102139107	0.924147856859237322
9	0.000000000000000000	-0.000000000000000000	-0.000000000101794639	0.345436543646600297

Table 5.11 Cascade decomposition of the transmittance in Example 2.

i	k_i	ω_i/π	α_i/π	γ_i
1	1.000000000000000000	-0.430034232000000000	-0.129995225362160160	0.856902177327104619
2	0.000000000000000000	-0.000000000000000000	0.177988575358195542	0.290809261580008262
3	1.000000000000000000	0.430034232000000000	0.372240496861656714	0.420018077150955863
4	0.000000000000000000	-0.000000000000000000	-0.420233846857810422	0.921151940506522988
5	0.999999999999999999	-0.320538560000000000	0.007661338926352295	0.385108082384979378
6	0.000000000000000000	-0.000000000000000000	-0.052519410605237151	0.178384822882619832
7	0.999999999999999999	0.320538560000000000	0.375270749327664280	0.428114894303120052
8	0.000000000000000000	-0.000000000000000000	-0.330412664510303397	0.924147856738074304
9	0.000000000000000000	-0.000000000000000000	-0.000000012492511568	0.345436540990829595

Table 5.12 Pipeline cascade decomposition of the transmittance in Example 2.

i	k_i	ω_i/π	α_i/π	γ_i
1	0.000000000000000000	-0.000000000000000000	-0.000000000000000000	0.345436543729513932
2	0.000000000000000000	-0.000000000000000000	-0.000000000000000009	0.924147856863023366
3	0.000000000000000000	-0.000000000000000000	0.002841829083873028	0.100676825918153140
4	0.000000000000000000	-0.000000000000000000	-0.020326334185806908	0.923464678888730942
5	0.000000000000000000	-0.000000000000000000	-0.009884406016452388	0.000000000000000000

Table 5.13 Allpass cascade decomposition in Example 2.

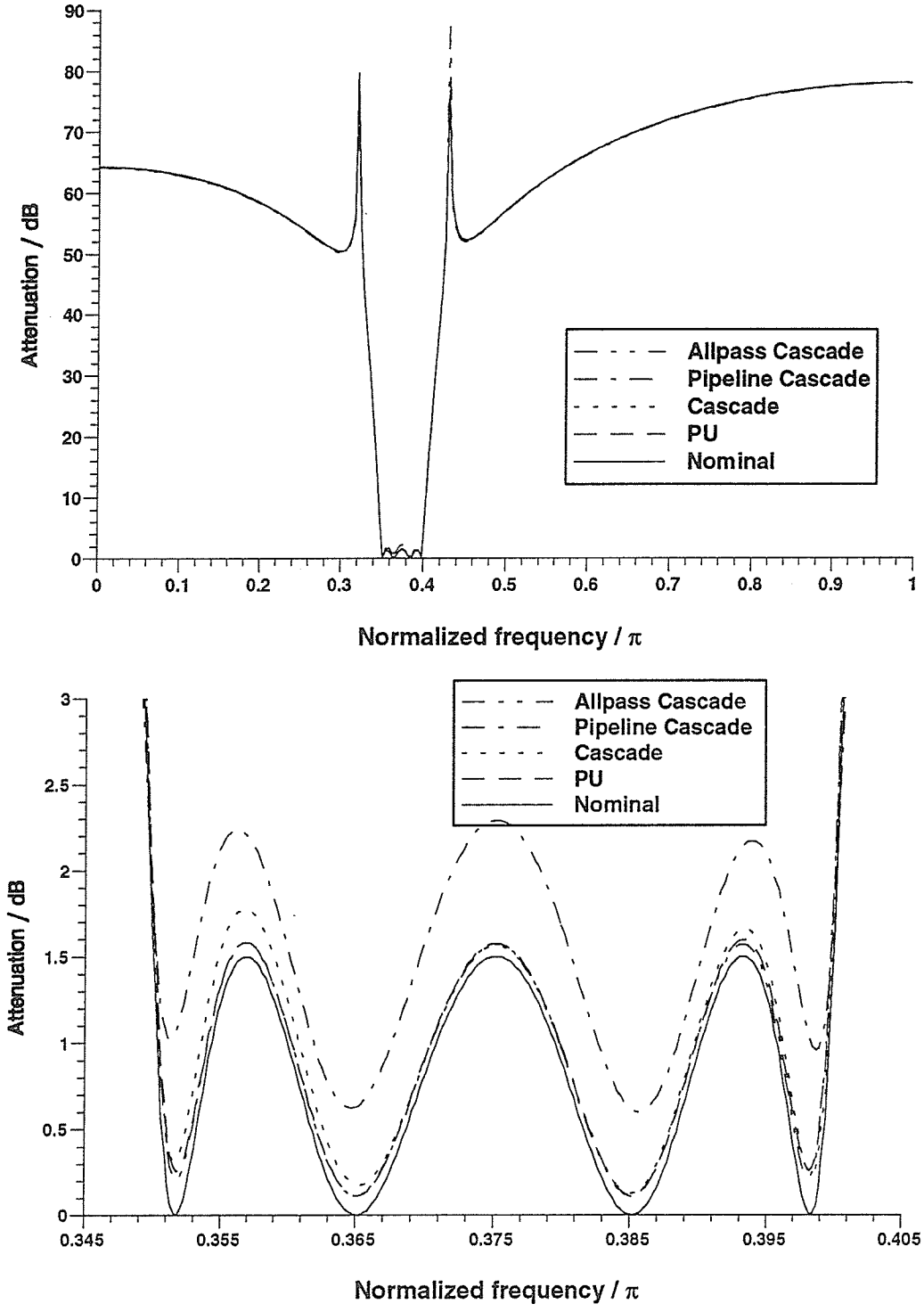

Figure 5.5 Frequency responses of the transmittance for Example 2 with 12-bit fixed-point multipliers; stopband (top) and passband (bottom).

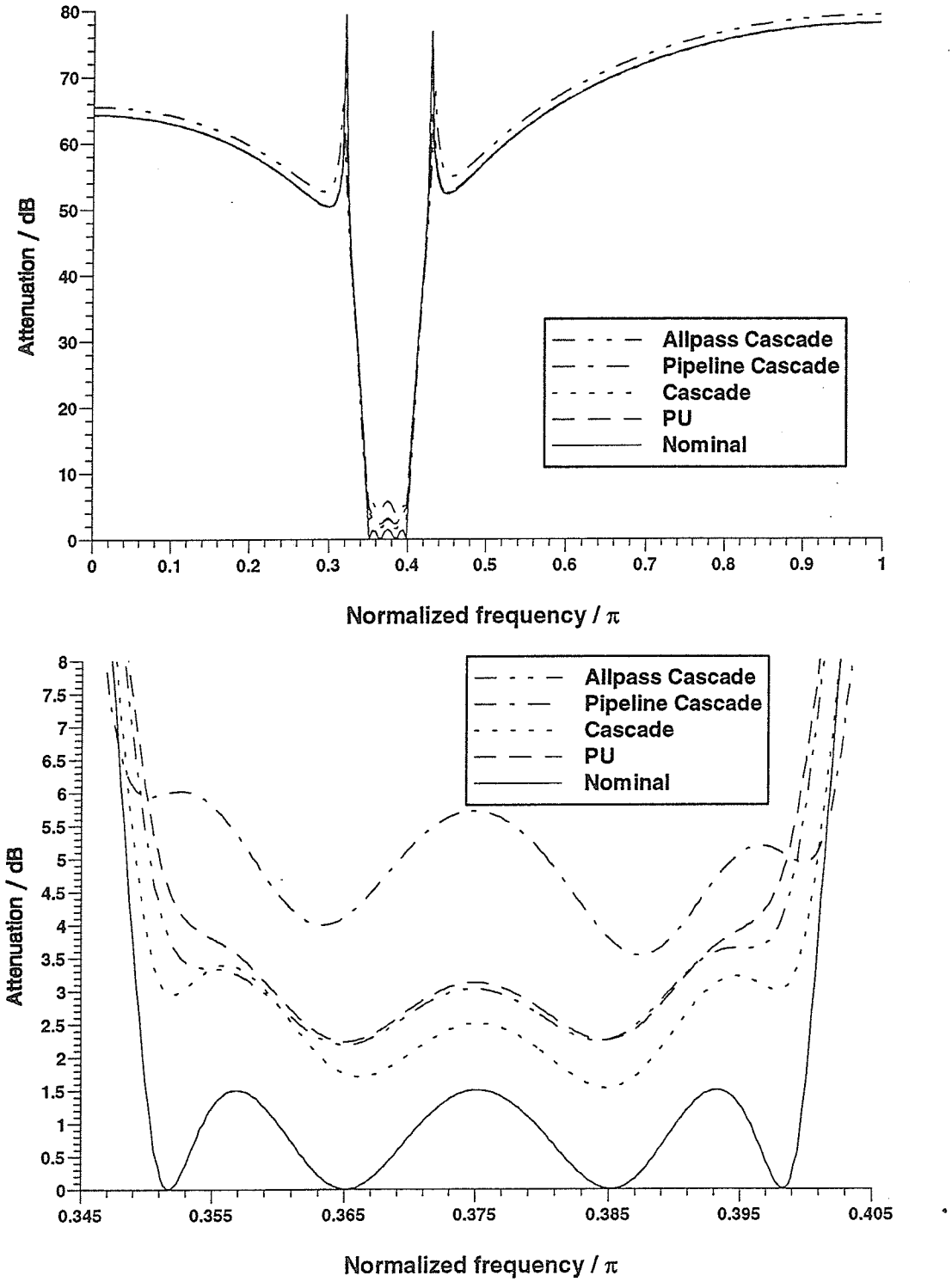

Figure 5.6 Frequency responses of the transmittance for Example 2 with 8-bit fixed-point multipliers; stopband (top) and passband (bottom).

i	$\cos\theta_i$	α_i/π
1	0.000000000000000000	-1.000000000000000000
2	0.938442110231743405	-1.000000000000000000
3	0.000000000000000000	-1.000000000000000000
4	0.382034996637063172	-1.000000000000000000
5	0.000000000000000000	-1.000000000000000000
6	0.994879530326316629	-1.000000000000000000
7	0.000000000000000000	-1.000000000000000000
8	0.383096500999037531	-1.000000000000000000
9	0.030373266988859827	-1.000000000000000000

i	$\cos\theta_i$	α_i/π
10	0.996317855963016627	-1.000000000000000000
11	0.000003812003936620	-1.000000000000000000
12	0.382447336695649320	-1.000000000000000000
13	0.009740966391351291	0.000000000000000000
14	0.994283478299853873	-1.000000000000000000
15	0.245457315725121985	0.000000000000000000
16	0.355382453718025351	-1.000000000000000000
17	0.248817858846223124	-1.000000000000000000
18	1.000000157517630890	-0.999999999977184076

Table 5.14 PU decomposition (DFT form) of the reflectance in Example 2.

i	k_i	ω_i/π	α_i/π	γ_i
1	1.000000000000000000	-0.351732711368000000	0.571467295401512715	0.995759910570240845
2	1.000000000000000000	0.351732711368000000	0.855661573467812382	0.995719283733996663
3	0.999999999999999999	-0.365109796566000000	0.145625268195202336	0.988687329369446869
4	0.999999999999999999	0.365109796566000000	0.851526571445161486	0.988399651228464212
5	1.000000000000000000	-0.385182448776000000	0.192538968231070712	0.988546956637328561
6	1.000000000000000000	0.385182448776000000	0.766451629213881752	0.988279747692755938
7	0.999999999999999999	-0.398308216049000000	0.294516982030966166	0.995702654610811803
8	0.999999999999999999	0.398308216049000000	0.645579536778435623	0.995675208687205493
9	0.000000000000000000	-0.000000000000000000	-0.323367824764013779	0.999999590297345307

Table 5.15 Cascade decomposition of the reflectance in Example 2.

i	k_i	ω_i/π	α_i/π	γ_i
1	1.000000000000000000	-0.351732711368000000	0.571467295401527639	0.995759910570241080
2	0.000000000000000000	-0.000000000000000000	-0.999999999999999792	0.999963581170383402
3	1.000000000000000000	0.351732711368000000	-0.795004228246988715	0.995748083873934500
4	0.000000000000000000	-0.000000000000000000	-0.776463067154461534	0.999912516975352343
5	0.999999999999999999	-0.365109796566000000	0.845246630861016261	0.988419605119843739
6	0.000000000000000000	-0.000000000000000000	0.779191309831084734	0.999929057318692151
7	0.999999999999999999	0.365109796566000000	0.892554605345273775	0.988221621614590118
8	0.000000000000000000	-0.000000000000000000	-0.516992546035456363	0.999991357125729693
9	1.000000000000000000	-0.385182448776000000	-0.922754932723995417	0.988469151747435729
10	0.000000000000000000	-0.000000000000000000	-0.319932271441926254	0.999966670048153334
11	1.000000000000000000	0.385182448776000000	-0.450642775036614698	0.988648490956818578
12	0.000000000000000000	-0.000000000000000000	0.693329979034896930	0.999959300186932423
13	0.999999999999999999	-0.398308216049000000	0.282678931410576393	0.995888661379942909
14	0.000000000000000000	-0.000000000000000000	-0.568971772410374962	0.999966391709661316
15	0.999999999999999999	0.398308216049000000	-0.601691400109065778	0.995925783415216364
16	0.000000000000000000	-0.000000000000000000	-0.369832210956248215	0.999999999999999988

Table 5.16 Pipeline cascade decomposition of the reflectance in Example 2.

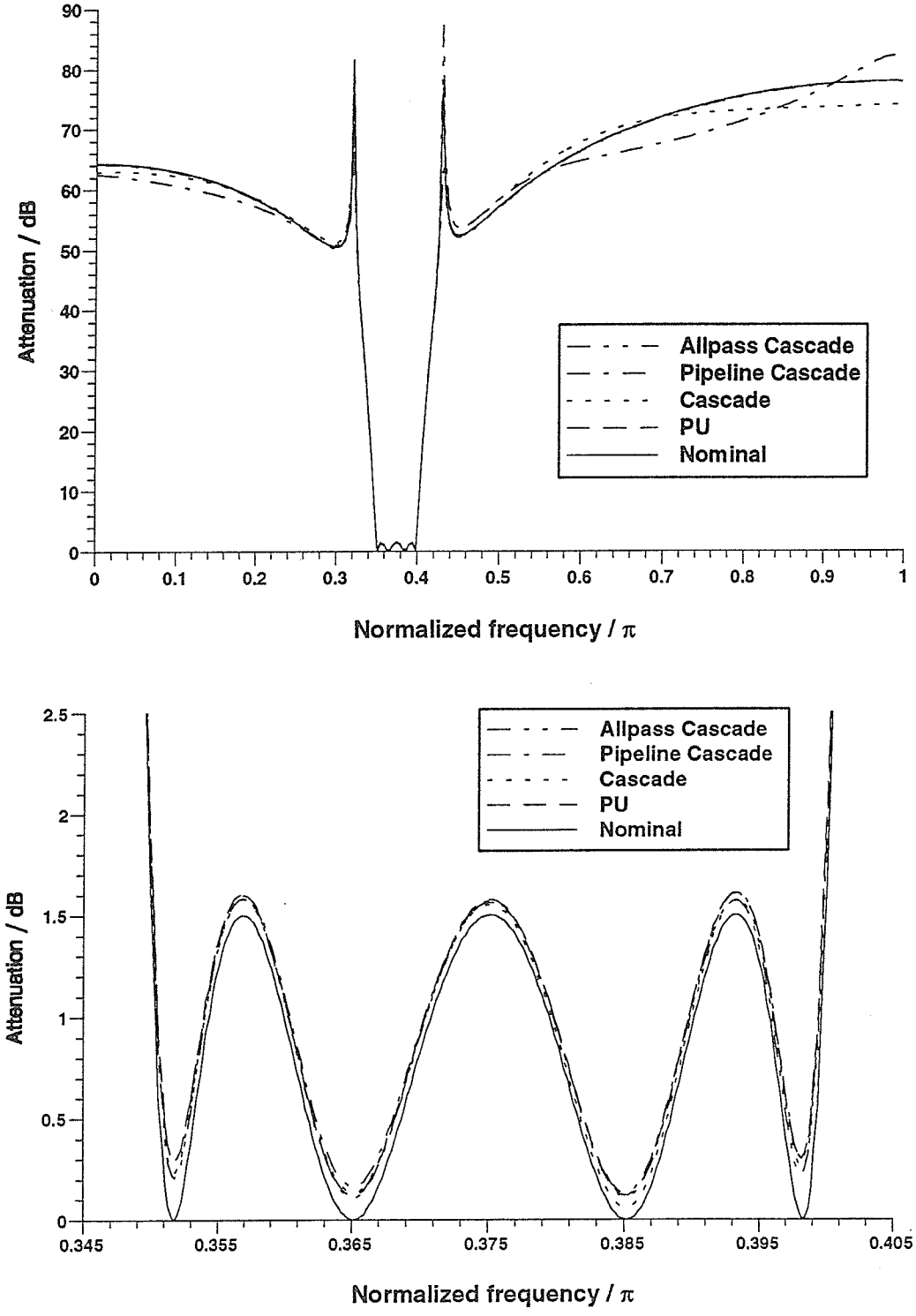

Figure 5.7 Frequency responses of the reflectance for Example 2 with 12-bit fixed-point multipliers; stopband (top) and passband (bottom).

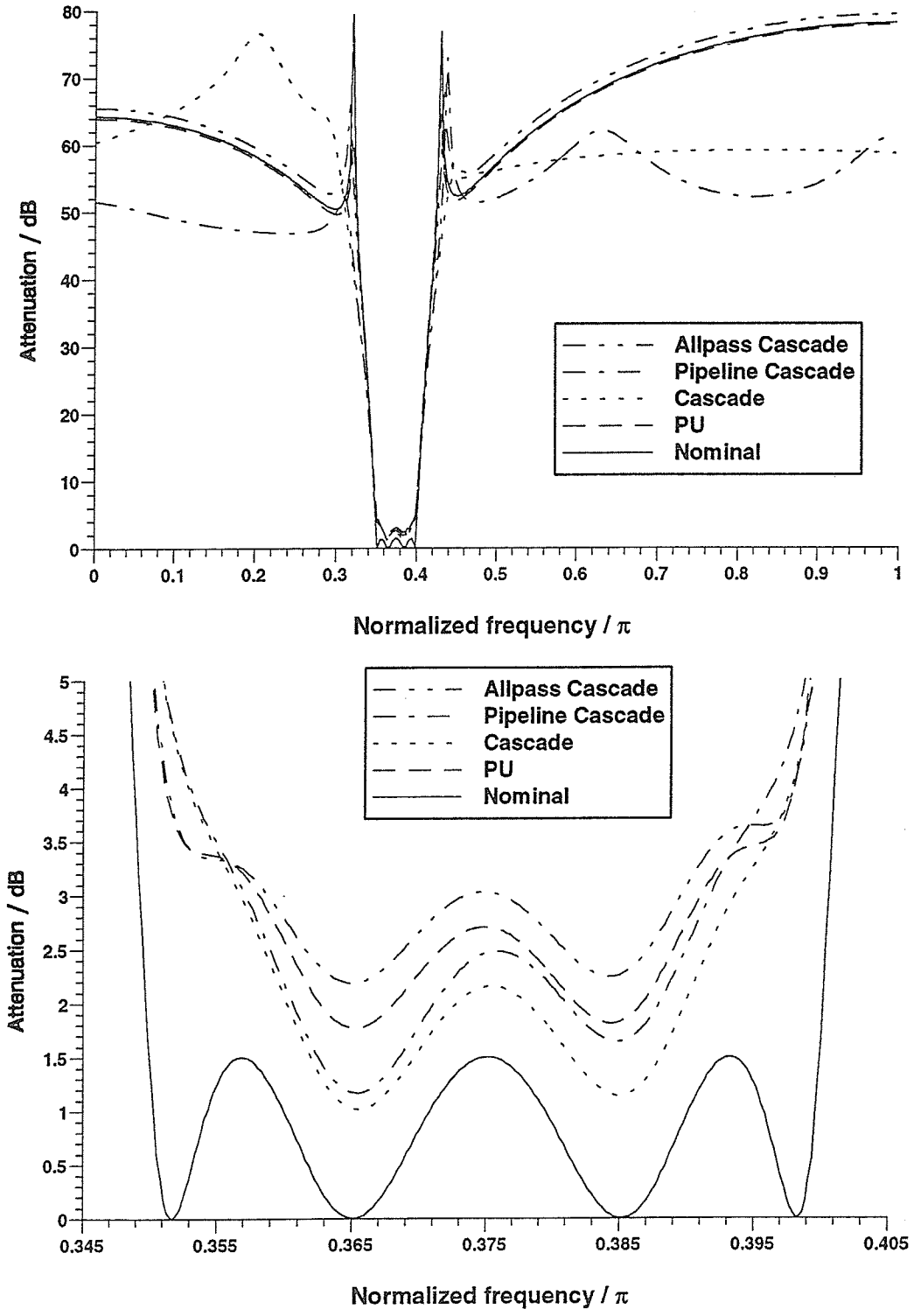

Figure 5.8 Frequency responses of the reflectance for Example 2 with 8-bit fixed-point multipliers; stopband (top) and passband (bottom).

5.4 General Observations on Examples 1 and 2

In Example 1, which is a low-order example, the Feldkeller equation is only satisfied up to 7 decimal places. However, the PU structure synthesized using the DFT form still gives satisfactory results. On the other hand, the Feldkeller-equation must be satisfied to a much higher accuracy in order to obtain an acceptable synthesis result for higher-order filters (see Section 3.5 for effects on input data inaccuracy). Also, the PU structure has no direct control of either a transmission or a reflection (attenuation) zero. This is shown by the 8-bit multiplier quantizations for both examples.

For the cascade decomposition structure, transfer functions with a narrow passband that have as many attenuation zeros as the order of the filter tend to have the poles located near those zeros. As a result, the return group delay evaluated at an attenuation zero can be approximated by $\delta \cong 1/(r_i - 1) >> 1$, where $r_i \cong 1$ but $r_i > 1$ is the radius of the nearest pole, and the corresponding filter parameter obtained using Eq. (3.23) is given by $\gamma_i \cong 1/\sqrt{r_i} \cong 1$. A single extraction step only removes one attenuation zero without significantly affecting the locations of the remaining poles with respect to the remaining attenuation zeros. It follows that transfer functions realized as the reflectance of a lossless two-port where the filter parameters are obtained from the return group delay values at the attenuation zeros, tend to have all the $\gamma_i \cong 1$ (see the γ column in Tables 5.6-7 and 5.15-16). Such values are hard to quantize and the filter response tends to be more sensitive (see stop band response on Fig. 5.4 and Fig. 5.8). On the other hand, transfer functions realized as the transmittance (see Table 5.3-4 and 5.13-14) do not have this problem because the γ_i are obtained from the return group delay values at the transmission zeros, and these locations are relatively much further away from the pole locations. This observation has been borne out by numerous examples.

The reflectance realization of the pipelineable cascade suffers most in the stop band (Fig. 5.8) because all $\gamma_i \cong 1$ and the multiplier quantizations in 7 additional sections.

CHAPTER VI

CONCLUSIONS

The synthesis of complex lossless two-port WD filters using the PU structure yields circuits that are inherent pipelineable, internally passive (hence wave digital), and easy to implement. Three different forms of polynomial representation are available for the synthesis process, namely the coefficient form, DFT-sample form, and the zero form, with the second one being the easiest to implement. The zero form requires zero-finding routines that are relatively slow. However, numerous examples show that the zero form gives acceptable results with input data inaccuracy for which the other two forms give totally unreliable results. One should obtain a set of input data that satisfy the losslessness condition with acceptable accuracy, especially for the synthesis of higher-order filters. A convenient consistency check of the PU synthesis results is the last $\cos\theta$ being one, which is the losslessness condition for the PU structure.

We have also shown that it is possible to generate complex lossless two-port cascades that are also restriction-free, internally passive, and that can easily be made pipelineable. The accompanying synthesis algorithm is a simple two-step procedure that is easily programmed and can also generate real two-port cascades and allpass circuits. The noncanonic "sample" representation of polynomials is very convenient for it circumvents the numerical problems encountered when forcing exact cancellations between either coefficient or zero-form polynomials. Numerous examples have shown that the roundoff error generated during synthesis is negligible and that it is more important to have the input data satisfy $gg_* = hh_* + ff_*$ with acceptable accuracy. A convenient consistency check of the synthesis results is available from the observation that after $N = m+1$ iterations, all the "sample" sets must correspond to a simple "feed-through" two-port. We conclude that narrow-band transfer functions should be realized as the transmittance of a lossless two-port.

Finally, both cascade and PU structures can realize allpass sections. In the PU synthesis algorithm we set $h = 0$ and $f = \pm g_*$, and for the cascade synthesis algorithm, we let $f = z^{-m}$ where m is the order of the allpass section and $h = \pm g_*$.

The following table gives a comparison between properties of the PU structure and the cascade structure.

PU Structure	Cascade Structure
- pipelineability is inherent.	- pipelineable cascades are generated by choosing all even-indexed sections with their transmission zeros at $z^{-1} = 0$.
- no direct control over the transmission zeros or reflection ones, each section contributes to the overall filtering.	- each section directly controls either a transmission or reflection zero.
- 6 basic rotations per filter order.	- 6 basic rotations per filter order for non-pipelineable cascade synthesis. - 9 basic rotations per filter order for pipelineable cascades.

If one wants to have direct control of either the transmission or reflection zeros together with pipelineability, the pipelineable cascade is the only choice and the three additional rotations per filter order are necessary.

REFERENCES

[1] A. Fettweis, "Wave digital filters: theory and practice," *Proc. IEEE*, vol. 74, pp. 270-327, Feb. 1986.

[2] K. Meerkötter, "Complex Passive Networks and Wave Digital Filters," *Proc. Eur. Conf. on Circuit Theory and Design* (Warsaw, Poland, Sept. 1980), vol. 2, pp. 24-35.

[3] M. R. Jarmasz, "A simplified synthesis of lossless two-port wave digital and analog filters", Ph.D. Thesis, University of Manitoba, Winnipeg, Canada, 1990.

[4] A. Fettweis, "Principles of complex wave digital filters," *Int. J. Circuit Theory Appl.*, vol. 9, pp. 119-134, Apr. 1981.

[5] V. Belevitch, *Classical Network Theory*, San Francisco, CA: Holden-Day, 1968.

[6] H. Baher, *Synthesis of Electrical Networks*, Chichester, Sussex, England: John Wiley, 1984.

[7] A. Fettweis, "Scattering properties of real and complex lossless two-ports," *Proc. IEE*, vol. 128, Pt. G, No. 4, Aug. 1981.

[8] M. R. Jarmasz, V. Cheng and G. O. Martens, "Synthesis of pipelineable complex wave digital filters", in review process.

[9] A. Fettweis, "Design of Orthogonal and related digital filters by network-theory approach", *Arch. Elec. Übertragung.*, vol. 44, pp. 65-74, Apr. 1990.

[10] S. K. Rao and T. Kailath, "Orthogonal Digital Filters for VLSI Implementation", *IEEE Trans. Circuits Syst.*, vol. CAS-31, no. 11, pp. 933-945, Nov. 1984.

[11] A. Fettweis, "Digital Filter Sturctures Related to Classical Filter Networks", *Arch. Elec. Übertragung.*, vol. AEU-25, pp. 79-89, 1971.

[12] A. Sedlmeyer, A. Fettweis, "Digital filters with true ladder configuration", *Circuit Theory Appl.*, vol. 1, pp. 5-10, 1973.

[13] M. Jarmasz and G. O. Martens, "A simplified synthesis of lossless cascade analog and digital two-port networks," *IEEE Trans. Circuit Syst.*, vol. 38, no. 12, pp. 1501-1516, 1991.

[14] A. Fettweis, "Factorization of transfer matrices of lossless two-ports," *IEEE Trans. Circuit Theory*, vol. CT-17, pp. 86-94, Feb. 1970.

[15] P. P. Vaidyanathan, "A General Theorem for Degree-Reduction of a Digital BR Function," *IEEE Trans. Circuits Syst.*, vol. CAS-32, no. 4, pp. 414-415, Apr. 1985.

[16] J. I. Acha and F. Torres, "Realization of Complex Digital Filters Based on the LBC Two-Pair Extraction Procedure", *International Journal of circuit theory and applications,*, vol. 18, pp. 563-575, Mar. 1990.

[17] A. Fettweis, "Passivity and Losslessness in Digital Filtering," *Arch. Elec. Übertragung.*, vol. 42, no. 1, pp. 1-8, Jan./Feb. 1988.

[18] P. DeWilde, E. Deprettere, and R. Nouta, "Parallel and piplined VLSI implementation of signal processing algorithms," in *VLSI and Modern Signal Processing*, S. Y. Kung, H. J. Whitehouse, and T. Kailath, Prentice-Hall, Eds. Englewood Cliffs, NJ: 1985.

[19] R. Unbehauen and A. Cichocki, *MOS Switched-Capacitor and Continuous-Time Integrated Circuits and Systems - Analysis and Design*, Springer-Verlag, Berlin, Heidelberg, New York, 1989.

[20] M. Jarmasz and G. O. Martens, "Design of canonic wave digital filters using Brune and matched 4-port adaptors," *IEEE Trans. Circuit Syst.*, vol. CAS-34, pp. 480-496, May. 1987.

[21] P. P. Vaidyanathan and S. K. Mitra, "Low passband sensitivity digital filters: A generalized viewpoint and synthesis procedures," *Proc. IEEE*, pp. 404-423, Apr. 1984.

[22] A. Fettweis, "Multidimensional digital filters with closed loss behavior designed by complex network theory approach," *IEEE Trans. Circuits Syst.*, vol. CAS-34, no. 4, pp. 338-344, Apr. 1987.

[23] P. P. Vaidyanathan, P. A. Regalia and S. K. Mitra, "Design of doubly-complementary IIR digital filters using a single complex allpass filter, with multirate applications", *IEEE Trans. Circuits Syst.*, vol. CAS-34, no. 4, pp. 378-389, Apr. 1987.

[24] K. Meerkötter, "Antimetric wave digital filters derived from complex reference filters," *Proc. Eur. Conf. on Circuit Theory and Design* (Stuttgart, W. Germany, Sept. 1983), pp. 217-220.

[25] H. V. Jagadish, R. G. Mathews, T. Kailath and J. A. Newkirk, "A Study of Pipelining in Computing Arrays," *IEEE Trans. on Computers*, vol. C-35, no. 5, pp. 431-440, May 1986.